

Doctoral Dissertation

Development of Newly Amorphous Zirconium (Hydr)oxide/MgFe Layered Double Hydroxide Composite for Phosphate Recovery

(リン回収のための新規アモルファス水酸化ジルコニウム/マグネシウム-鉄系層状複水酸化物複合材料の開発)

September 2021

ATIN NURYADIN

Graduate School of Sciences and Technology for Innovation,
Yamaguchi University

ABSTRACT

Phosphorus is an indispensable nutrient to sustain the daily life of all living things on Earth. However, the over-enrichment of the aquatic ecosystem with phosphorus leads to eutrophication, which is still a global environmental problem. More stringent regulations have been put in place for the limit of phosphorus discharge to address this problem and resulted in the removal of phosphorus removal becomes exceptionally crucial. Furthermore, phosphorus deposits are a non-renewable resource and forecasted to deplete until 2170, given the current usage and global population growth. Thus, the removal of phosphorus coupled with the recovery and reuse of phosphorus offer the best strategies to meet the future phosphorus demand.

Accordingly, adsorption represents a fascinating separation technique for phosphate from water because of the possibility of phosphorus recovery. Moreover, this approach has many advantages, such as efficient, easy operating conditions, low sludge production, and the possibility of regenerating the adsorbent. Numerous attractive low-cost adsorbents have been studied for phosphate removal, one of which is layered double hydroxides (LDH). Unfortunately, a high phosphate adsorption capacity of LDH can generally be achieved by calcination, which increases the preparation cost of LDH. In this study, LDH is functionalized with amorphous zirconium (hydr)oxide to obtain enhanced adsorption capacity and eliminate the high-temperature requirement during the synthesis process.

Although different treatment techniques have been developed to eliminate phosphorus contamination, including for wastewater treatment, treated water often fails to meet quality regulations. Amorphous zirconium (hydr)oxide/MgFe layered double hydroxides composites (am-Zr/MgFe-LDH) with different molar ratios ($Zr/Fe = 1.5-2$) were prepared in two-stage synthesis by the combination of coprecipitation and hydrothermal methods. The synthesis of the composite could eliminate the requirement of high-temperature calcination in the LDH for phosphate adsorption. Moreover, the phosphate adsorption ability of the composite was higher than that of the individual LDH and amorphous zirconium (hydr)oxide. The presence of amorphous zirconium (hydr)oxide increased the phosphate adsorption ability of composite at low pH. The adsorption capacity was increased by decreasing the pH and increasing the temperature (from 290 to 324 K). The bicarbonate (HCO_3^-) was the most competitive anion for phosphate adsorption. The pseudo-second-order model provided the best description of the kinetic adsorption data. Furthermore, the adsorbed phosphate was easily desorbed by 1 N and reused 2 N of NaOH solutions. The results suggest that the am-Zr/MgFe-LDH composite is a promising material for phosphate removal and recovery from wastewater.

A Fixed-bed column has been considered an industrially feasible technique for phosphate removal from water. Besides the adsorption capacity, the effectiveness of an adsorbent is also determined by its reusability efficiency. In this study, phosphate removal by a synthesized am-Zr/MgFe-LDH in a fixed-bed column system was examined. The results showed that the increased bed height and phosphate concentration, and reduced flow rate, pH, and adsorbent particle size were found to increase the column adsorption capacity. The optimum adsorption capacity of 25.15 mg-P g⁻¹ was obtained at pH 4. The coexistence of seawater ions had a positive effect on the phosphate adsorption capacity of the composite. Nearly complete phosphate desorption, with a desorption efficiency of 91.7%, could be effectively achieved by 0.1 N NaOH for an hour. Moreover, the initial adsorption capacity was maintained at approximately 83% even after eight adsorption-desorption cycles, indicating that the composite is economically feasible. The am-Zr/MgFe-LDH, with its high adsorption capacity and superior reusability, has the potential to be utilized as an adsorbent for phosphorus removal in practical wastewater treatment.

The possible adsorption mechanisms of phosphate by am-Zr/MgFe-LDH were investigated via X-ray diffraction (XRD), Fourier transform infrared (FTIR), X-ray photoelectron spectroscopy (XPS), and pH at the point of zero charge (pH_{PZC}) analyses. It was suggested that the high phosphate adsorption capacity of the composite involves three main adsorption mechanisms, which are the electrostatic attraction, inner-sphere complexation, and anion exchange, where the amorphous zirconium (hydr)oxide on the surface of the layered double hydroxides likely increased the number of active binding sites and surface area for adsorption. This study provides insights into the design of am-Zr/MgFe-LDH for phosphorus removal and recovery in a practical system.

ACKNOWLEDGEMENT

I would like to extend my sincere and deepest gratitude to my supervisor, Professor Tsuyoshi Imai, who has always guided and supported me during this research with his kindness. I thank him for giving me the opportunity to work in his laboratory. I have learned so many things during the time I studied under his supervision.

My most profound appreciation to my graduate committee, Professor Masahiko Sekine, Professor Masakazu Niinae, Professor Takaya Higuchi, and Professor Eiichi Toorisaka, who have helped me so much to improve the quality of my work with their constructive suggestions.

I was glad to have Associate Professor Koichi Yamamoto and Associate Professor Ariyo Kanno in Environmental Symbiosis Seminar in the EISEI laboratory, who have helped to shape my critical thinking during the seminar.

I gratefully acknowledge The Indonesian Ministry of Research, Technology, and Higher Education (RISTEK-DIKTI), as well as the Project Implementation Unit (PIU) of the Islamic Development Bank (IsDB) 4in1 Project of Mulawarman University for providing the scholarship.

I owed so much to Miss Toshimi Yamamoto, who has patiently helped me in the preparation of experiments, and I also thank Associate Professor Tasuma Suzuki for his valuable assistance with FTIR analysis.

My special thanks to Rafitah Hasanah and Masato Fukushima, who have supported me greatly during my study life in Japan.

I'm not lonely in this doctoral endeavor with the support and friendship of the members of the EISEI lab: Nguyen Kim Diem Mai, Gde Yudha Partama, Natha Okajima, Sativandi Riza, Dyah Asri Handayani Taroepratjeka, Passaworn Warunyuwong, Jitrera Buates, Riku Motohashi, Hideya Saeki, Enamul Kabir, Ganjar Samudro, and all the master and B4 students. Thank you all very much for creating a special atmosphere that makes working in the laboratory very enjoyable.

I would also like to thank all my colleagues in the Department of Physics Education, Mulawarman University, especially Dr. Zeni Haryanto and Nurul Fitriyah Sulaeman, Ph.D., who have always supported me with their valuable discussion.

I would also like to thank all my friends in Japan who make my life more colorful during my stay in Japan.

Finally, I would like to express my heartfelt gratitude to my family in Indonesia, who have supported me during my study.

TABLE OF CONTENTS

ABSTRACT	i
ACKNOWLEDGEMENT	iii
TABLE OF CONTENTS	v
LIST OF FIGURES	viii
LIST OF TABLES	xi
LIST OF ABBREVIATIONS	xii
CHAPTER 1: INTRODUCTION	1
1.1. Rationale and background	1
1.2. Dissertation objectives	2
1.3. Structure of the dissertation	2
CHAPTER 2: LITERATURE REVIEW	
2.1. Phosphorus and its environmental relevance	5
2.1.1 Chemistry of phosphorus	5
2.1.2 Significance of phosphorus	7
2.1.3 Eutrophication	9
2.2. Phosphorus removal technologies	11
2.2.1. Chemical precipitation	11
2.2.2. Biological phosphorus removal	13
2.2.3. Crystallization technology	14
2.2.4. Adsorption	16
2.3. Zirconium-functionalized LDH as phosphate adsorbents	18
2.3.1 Zirconium-based phosphate adsorbent	18
2.3.2 LDH as phosphate adsorbent	19
2.3.3 Synthesis of zirconium-functionalized LDH as phosphate adsorbent	20
2.3.4 The current state of research	21
2.4. Mathematical models for phosphate adsorption	21
2.4.1. Adsorption kinetics	21
2.4.2. Adsorption isotherm	22
2.4.3. Adsorption thermodynamics	24
2.4.4. Breakthrough prediction of fixed-bed column adsorption	24

CHAPTER 3: PHOSPHATE ADSORPTION AND DESORPTION ON TWO-STAGE SYNTHESIZED AMORPHOUS-ZIRCONIUM (HYDR)OXIDE/MgFe LAYERED DOUBLE HYDROXIDES COMPOSITE

3.1. Introduction.....	35
3.2. Material and methods.....	37
3.2.1. Materials	37
3.2.2. Preparation of am-Zr/MgFe-LDH	37
3.2.3. Characterization of am-Zr/MgFe-LDH.....	37
3.2.4. Batch adsorption experiments.....	38
3.2.5. Desorption experiments	38
3.3. Results and discussion.....	39
3.3.1. Effect of Zr molar ratio and calcination	39
3.3.2. Characterization	40
3.3.3. Effect of solution pH	43
3.3.4. Effect of competing anions	45
3.3.5. Adsorption kinetics	45
3.3.6. Adsorption isotherm	47
3.3.7. Adsorption thermodynamics	49
3.3.8. Phosphate desorption and adsorbent reusability	50
3.4. Summary.....	52

CHAPTER 4: APPLICATION OF AMORPHOUS ZIRCONIUM (HYDR)OXIDE/MgFe LAYERED DOUBLE HYDROXIDES COMPOSITE IN FIXED-BED COLUMN FOR PHOSPHATE REMOVAL FROM WATER

4.1. Introduction.....	60
4.2. Materials and methods	61
4.2.1. Adsorbent and adsorbate preparation	61
4.2.2. Adsorption experiments	62
4.2.3. Regeneration and reusability experiments.....	63
4.3. Results and discussion.....	64
4.3.1. Fixed-bed column adsorption	64
4.3.2. Breakthrough curve modelling	68
4.3.3. Phosphate adsorption from real municipal anaerobic sludge filtrate and synthetic seawater	70
4.3.4. Column regeneration and reusability	72
4.4. Summary.....	74

CHAPTER 5: MECHANISM STUDY OF PHOSPHATE ADSORPTION AND DESORPTION ON AMORPHOUS ZIRCONIUM (HYDR)OXIDE/MgFe LAYERED DOUBLE HYDROXIDES COMPOSITE

5.1. Introduction.....	79
5.2. Materials and Methods	80
5.2.1. Materials	80
5.2.2. X-ray diffraction (XRD) analysis.....	80
5.2.3. Fourier transform infrared (FTIR) analysis	80
5.2.4. X-ray photoelectron spectroscopy (XPS) analysis.....	81
5.2.5. pH at the point charge (pH _{pzc}) analysis	81
5.3. Results and discussions	81
5.3.1. FTIR spectra and XRD patterns analysis	81
5.3.2. XPS spectra analysis	82
5.3.3. pH _{pzc} analysis.....	83
5.3.4. Proposed phosphate adsorption and desorption mechanisms.....	84
5.4. Summary.....	87

CHAPTER 6: CONCLUSIONS AND FUTURE WORKS

6.1. Conclusions.....	91
6.2. Future works.....	92

APPENDIX

LIST OF PUBLICATIONS	93
LIST OF PRESENTATIONS.....	93

LIST OF FIGURES

Figure 2.1	– Element properties of phosphorus.....	5
Figure 2.2	– Distribution of phosphate species in aqueous solution as a function of pH.....	6
Figure 2.3	– Geological and biological phosphorus cycle.....	7
Figure 2.4	– The strategy of chemical precipitation process addition in biological phosphorus removal process, (1) pre-precipitation, (2) coprecipitation, and (3) post-precipitation	12
Figure 2.5	– Typical configuration of biological phosphorus removal process.....	14
Figure 2.6	– Typical configuration of phosphorus crystallization by continuous stirred reactors.....	16
Figure 2.7	– Phosphate adsorption mechanisms of zirconium (hydr)oxides.....	19
Figure 2.8	– (a) Schematic structure of layered double hydroxides and (b) mechanism of phosphate anion exchange and surface adsorption on LDH.....	20
Figure 2.9	– Mass transfer zone and breakthrough curve of adsorption process in a fixed-bed column in different stages	25
Figure 3.1	– (a) Phosphate adsorption on LDH, composites, and am-Zr, before and after calcination, and (b) Comparative cost for the removal of 1 mg-P of phosphate using studied adsorbents.....	40
Figure 3.2	– X-ray powder diffraction patterns of LDH, composites, and am-Zr (a) before calcination, and (b) after calcination	41
Figure 3.3	– FTIR spectra of LDH, composite (Zr(1.5)/LDH), and am-Zr before calcination in the range of (a) 4000–600 cm ⁻¹ , and (b) 550–350 cm ⁻¹ ...	42
Figure 3.4	– Scanning electron micrographs of (a) LDH, (b) am-Zr, (c) composite before adsorption and (d) composite after adsorption, and (e) XPS spectra of composite before and after phosphate adsorption	43
Figure 3.5	– Effect initial pH on phosphate adsorption	44

Figure 3.6	– Effect of common competing anions Cl^- , NO_3^- , SO_4^{2-} , and HCO_3^- on the phosphate removal efficiency.....	45
Figure 3.7	– The plots of: (a) phosphate adsorption capacity of LDH, composite, and am-Zr vs. contact time, (b) pseudo-first-order model of composite, and (c) pseudo-second-order model of composite	46
Figure 3.8	– The non-linear fitting plots of adsorption using the (a) Langmuir, (b) Freundlich, (c) Temkin, and (d) D-R isotherm equations at different treatment temperatures.....	48
Figure 3.9	– The plot of the relationship between $\ln K_d$ and T^{-1} for the calculation of thermodynamic parameters of phosphate adsorption	50
Figure 3.10	– (a) Phosphate desorption by different concentrations of NaOH solution, and (b) the reusability of composite for phosphate adsorption with desorption solution of 1 N of NaOH and reused 2 N NaOH	51
Figure 4.1	– Schematic diagram of lab-scale fixed-bed column adsorption system..	62
Figure 4.2	– The Effect of (a) flow rate, (b) bed height, (c) influent phosphate concentration, (d) solution pH, and (e) composite particle size, on the fixed-bed column studies.....	65
Figure 4.3	– Breakthrough curves for phosphate adsorption from anaerobic sludge filtrate, synthetic P water, and synthetic P seawater.....	72
Figure 4.4	– Continuous phosphate desorption curve on am-Zr/MgFe-LDH column by 0.1 N NaOH.....	72
Figure 4.5	– Column reusability study: (a) phosphate adsorption breakthrough curve on am-Zr/MgFe-LDH for each consecutive eight adsorption-desorption cycles at a flow rate 2.5 mL/min, and (b) column adsorption capacity calculated for each adsorption cycle.....	73
Figure 5.1	– (a) FTIR spectra and (b) XRD patterns of am-Zr/MgFe-LDH composite before and after adsorption.....	82
Figure 5.2	– XPS analysis of am-Zr/MgFe-LDH composite before and after phosphate adsorption: (a) Mg 1s, (b) Fe 2p, (c) Zr 3d, and (d) C 1s	83

Figure 5.3 – Potentiometric mass titration curves of am-Zr/MgFe-LDH composite samples using 0.1 M HNO₃..... 84

Figure 5.4 – Proposed mechanism of phosphate adsorption on am-Zr/MgFe-LDH.. 85

Figure 5.5 – Proposed mechanism of phosphate desorption from am-Zr/MgFe-LDH by NaOH solution..... 86

LIST OF TABLES

Table 2.1 – Comparison of various technologies for phosphorus removal	17
Table 3.1 – Kinetic model parameters for phosphate adsorption by am-Zr/MgFe-LDH	47
Table 3.2 – Isotherm relative parameters for phosphate adsorption by am-Zr/Mg Fe-LDH	49
Table 3.3 – Thermodynamic parameters for phosphate adsorption by am-Zr/MgFe-LDH	50
Table 4.1 – Fixed-bed column parameters for phosphate adsorption on am-Zr/MgFe-LDH	66
Table 4.2 – Comparison of the phosphate adsorption capacity of am-Zr/MgFe-LDH with various	68
Table 4.3 – Yoon-Nelson, Thomas, and MDR model parameters for phosphate adsorption by am-Zr/MgFe-LDH in fixed-bed column at various experimental conditions.....	69
Table 4.4 – The details of anaerobic sludge filtrate, synthetic P water, and synthetic P seawater used in fixed-bed column phosphate adsorption...	71

LIST OF ABBREVIATIONS

%	percent
Å	angstrom
ΔG^0	Gibbs energy change
ΔH^0	enthalpy change
ΔS^0	entropy change
μm	Micrometer
θ	angel
τ	Time required for 50% adsorption breakthrough
$^{\circ}\text{C}$	degree Celsius
a	a modified dose-response model parameter
A-Zr-NP	alginate-/zirconium-grafted newspaper pellets
am-Zr	amorphous zirconium (hydr)oxide
am-Zr/MgFe-LDH	amorphous zirconium (hydr)oxide/MgFe layered double hydroxides
b_t	a constant related to the heat of adsorption
C	carbon
C	effluent concentration
C_0	influent concentration
C_e	phosphate equilibrium concentration
Ca^{2+}	calcium ion
CaCl_2	calcium chloride
CaCO_3	calcium carbonate
Cl^-	chloride ion
cm	centimeter
CO_3^{2-}	carbonate ion

COD	chemical oxygen demand
CS-Zr-PEPA	polyethylene polyamine grafted chitosan-Zr composite beads
Cu-K α	copper K-alpha
<i>d</i>	particle size
D-R	Dubinin–Radushkevich
DI	Deionized
<i>E</i>	mean free energy of adsorption
<i>EAP</i>	eluted amount of phosphorus
eV	electron volt
Fe	iron
FeCl ₃ ·6H ₂ O	iron(III) chloride hexahydrate
FTIR	Fourier transform infrared
<i>g</i>	gram
<i>h</i>	hour
<i>h</i>	bed height
H ₂ PO ₄ ⁻	dihydrogen phosphate
HCl	hydrochloric acid
HCO ₃	nitric acid
HNO ₃ ⁻	bicarbonate ion
K	kelvin
<i>k</i> ₁	the rate constant of the pseudo-first-order model
<i>k</i> ₂	the rate constant of the pseudo-second-order model
K ⁺	potassium ion
K ₂ HPO ₄	dipotassium hydrogen phosphate
KCl	potassium chloride

K_d	distribution coefficient
k_f	Freundlich adsorption constant
k_l	Langmuir adsorption constant
k_t	an equilibrium binding constant
KNO_3	potassium nitrate
KOH	potassium hydroxide
k_{Th}	Thomas kinetic coefficient
kV	kilovolt
k_{YN}	Yoon-Nelson kinetic coefficient
L	liter
LDH	layered double hydroxides
M	molar
m	mass
MDR	modified dose-response
Mg	magnesium
mg	milligram
mg-P	milligram as phosphorus
Mg^{2+}	magnesium ion
MgCl_2	magnesium chloride
$\text{MgCl}_2 \cdot 6\text{H}_2\text{O}$	magnesium chloride hexahydrate
MgFe-LDH	magnesium iron layered double hydroxides
min	minute
mL	milliliter
mm	millimeter
N	normal

n	a constant related to adsorption intensity or surface heterogeneity
N_2	nitrogen
n_2	number of the last fraction in the desorption operation
Na^+	sodium ion
Na_2CO_3	sodium carbonate
Na_2SO_4	sodium sulfate
$NaCl$	sodium chloride
$NaOH$	sodium Hydroxide
nm	nanometer
NO_3^-	nitrate ion
$NO_3^- - N$	nitrate as nitrogen
O	oxygen
OH	hydroxyl
OH^-	hydroxyl ion
OH_2^+	protonated hydroxyl ion
P	phosphorus
P seawater	synthetic phosphate-containing seawater
P water	synthetic phosphate-containing water
$PAOs$	polyphosphate-accumulating organisms
pH_{pzc}	pH at the point of zero charge
PMT	potentiometric mass titration
PO_4-P	phosphate as phosphorus
PSU	practical salinity unit
PZC	point of zero charge
Q	flow rate

$q_{adsorbed}$	total amount of adsorbed phosphate
$q_{desorbed}$	total amount of desorbed phosphate
q_e	equilibrium adsorption capacity
q_m	theoretical maximum adsorption capacity
q_{mdr}	predicted adsorption capacity of modified dose-response model
q_t	adsorbed phosphate at time t
q_{Th}	predicted adsorption capacity of Thomas model
R	universal gas constant ($8.314 \text{ J K}^{-1} \text{ mol}^{-1}$)
R^2	coefficient of determination
rpm	rotation per minute
SEM	scanning electron microscopy
SO_4^{2-}	sulfate ion
T	temperature
t	time
$t\text{-ZrO}_2$	tetragonal zirconia
t_b	breakthrough time
t_e	time required to reach exhaustion time
TSS	total suspended solid
V	volume
V_q	effluent volume of the q-th fraction
XPS	X-ray photoelectron spectroscopy
XRD	X-ray diffraction
Zr	Zirconium
Zr(1.5)/LDH	synthesized composite with Zr:Fe of 1.5
Zr-loaded okara	Soybean residue (okara) loaded with zirconium(IV)

Zr-loaded SOW gel	Saponified orange waste gel loaded with zirconium(IV)
Zr-FPS	Fiber containing phosphonate and sulfonate (FPS) loaded with Zr
ZrO ₂	zirconium oxide
ZrOCl ₂ · 8H ₂ O	Zirconyl chloride octahydrate

CHAPTER 1

INTRODUCTION

1.1 Rationale and background

Eutrophication is still being known as a global aquatic environmental problem, and even more stringent regulations are made for phosphorus discharge to cope with this problem since phosphorus is considered as the main responsible for the eutrophication process [1]. Standard biological treatment and chemical precipitation processes frequently fail to achieve the near to zero levels of phosphorus removal to fulfill the regulations. For this reason, some study has been sparked in the exploration of alternative wastewater treatment technologies for phosphorus removal. Adsorption is considered an attractive alternative in wastewater treatment because of its simplicity, low cost, and superior removal ability [2].

On the other hand, in considering the growing concern about global phosphorus scarcity and the demand for this element is undergoing rapid growth, it is essential to deal with not only phosphorus removal but also phosphorus recovery. The adsorption becomes a more fascinating separation technique of phosphorus from water because of the possibility of phosphorus recovery while adsorbent recycling [3]. The increase in sludge volume generated from wastewater treatment plants and stringent restriction on landfilling of the sludge makes the adsorbent techniques have gained particular interest because of less sludge production and repetitive usability [4].

Layered double hydroxide (LDH) materials are suggested to be potential phosphate adsorbents because of their ability to remove phosphate from a solution by interlayer anion exchange and surface adsorption [5]. LDH materials naturally show excellent adsorption toward various anions, including phosphate, due to their positively charged layers and weak interlayer binding [6]. Furthermore, the functionalization of amorphous zirconia (am-Zr) on phosphate adsorbents is increasingly attracting attention because it can enhance the adsorption capacity of some adsorbents [7–9]. Moreover, it is crucial to determine the appropriate methods for the composite preparation considering it is not easy to control their structures accurately. In this study, the composite of amorphous zirconium (hydr)oxide/MgFe layered double hydroxides (am-Zr/MgFe-LDH) was synthesized by the combination of coprecipitation and hydrothermal methods in two-stage synthesis. The phosphate adsorption ability of the composite was investigated via both batch and fixed-bed column studies. The combination is expected to not only enhance the phosphate

adsorption ability of magnesium iron layered double hydroxide (MgFe-LDH) but also the adsorption capacity of am-Zr itself.

1.2 Dissertation objectives

The aim of this research to:

1. Develop the am-Zr/MgFe-LDH with a novel two-stage synthesis to increase the adsorption capacity for phosphate adsorption.
2. Investigate the effects of the solution pH and competing anions on the phosphate adsorption of the composite under batch tests, and study the adsorption kinetics, isotherm, and thermodynamic to explain the properties of phosphate adsorption.
3. Investigate the effects of some essential design parameters for practical application such as bed height, flow rate, influent phosphate concentration, solution pH, and adsorbent particle size on the phosphate adsorption of the composite under fixed-bed column tests and apply the widely used breakthrough curve models to interpret the experimental breakthrough data.
4. Evaluate the composite applicability as phosphate adsorbent for real anaerobic sludge filtrate and phosphorus enriched seawater.
5. Investigate the reusability of the composite as phosphate adsorbent.
6. Study the mechanism of phosphate adsorption and desorption on the composite.

1.3 Structure of the dissertation

Chapter 1 states the rationale and background, objectives, and structure of the dissertation.

Chapter 2 presents the literature reviews on phosphorus and its environmental relevance, alternative phosphorus removal technologies, previous study about zirconium-functionalized LDH as phosphate adsorbents, and mathematical models for phosphate adsorption.

Chapter 3 describes the process of the am-Zr/MgFe-LDH synthesis and characterization, the effect of Zr molar ratio and calcination process on phosphate adsorption, and the effect of pH and competing anions on the phosphate adsorption ability. Also, this chapter explains the adsorption kinetics, isotherm, and thermodynamic, as well as the reusability of the composite.

Chapter 4 examines the phosphate adsorption performance and reusability of a fixed-bed column filled with am-Zr/MgFe-LDH. This chapter outlines the effect of several design

parameters on phosphate adsorption, the interpretation of adsorption breakthrough data by using some column adsorption models, and the actual applicability of the composite.

Chapter 5 discusses the possible mechanisms of phosphate adsorption and desorption on am-Zr/MgFe-LDH.

Chapter 6 recapitulates the results of the study and offers suggestions for future studies.

References

- [1] M. Le Moal, C. Gascuel-Oudou, A. Ménesguen, Y. Souchon, C. Étrillard, A. Levain, F. Moatar, A. Pannard, P. Souchu, A. Lefebvre, G. Pinay, Eutrophication: A new wine in an old bottle?, *Sci. Total Environ.* 651 (2019) 1–11. <https://doi.org/10.1016/j.scitotenv.2018.09.139>.
- [2] H. Bacelo, A.M.A. Pintor, S.C.R. Santos, R.A.R. Boaventura, C.M.S. Botelho, Performance and prospects of different adsorbents for phosphorus uptake and recovery from water, *Chem. Eng. J.* 381 (2020) 122566. <https://doi.org/10.1016/j.cej.2019.122566>.
- [3] W. Huang, Y. Zhang, D. Li, Adsorptive removal of phosphate from water using mesoporous materials: A review, *J. Environ. Manage.* 193 (2017) 470–482. <https://doi.org/https://doi.org/10.1016/j.jenvman.2017.02.030>.
- [4] H. Qiu, W. Ni, H. Zhang, K. Chen, J. Yu, Fabrication and evaluation of a regenerable HFO-doped agricultural waste for enhanced adsorption affinity towards phosphate, *Sci. Total Environ.* 703 (2020) 135493. <https://doi.org/https://doi.org/10.1016/j.scitotenv.2019.135493>.
- [5] K.H. Goh, T.T. Lim, Z. Dong, Application of layered double hydroxides for removal of oxyanions: A review, *Water Res.* 42 (2008) 1343–1368. <https://doi.org/10.1016/j.watres.2007.10.043>.
- [6] F. Peng, T. Luo, Y. Yuan, Controllable synthesis of Mg-Fe layered double hydroxide nanoplates with specific Mg/Fe ratios and their effect on adsorption of As(v) from water, *New J. Chem.* 38 (2014) 4427–4433. <https://doi.org/10.1039/c4nj00548a>.
- [7] W. Wang, H. Zhang, L. Zhang, H. Wan, S. Zheng, Z. Xu, Adsorptive removal of phosphate by magnetic Fe₃O₄@C@ZrO₂, *Colloids Surfaces A Physicochem. Eng. Asp.* 469 (2015) 100–106. <https://doi.org/10.1016/j.colsurfa.2015.01.002>.
- [8] F. Long, J.L. Gong, G.M. Zeng, L. Chen, X.Y. Wang, J.H. Deng, Q.Y. Niu, H.Y. Zhang, X.R. Zhang, Removal of phosphate from aqueous solution by magnetic Fe-Zr binary oxide, *Chem. Eng. J.* 171 (2011) 448–455. <https://doi.org/10.1016/j.cej.2011.03.102>.

- [9] X. Luo, X. Wang, S. Bao, X. Liu, W. Zhang, T. Fang, Adsorption of phosphate in water using one-step synthesized zirconium-loaded reduced graphene oxide, *Sci. Rep.* 6 (2016) 39108. <https://doi.org/10.1038/srep39108>.

CHAPTER 2

LITERATURE REVIEW

2.1 Phosphorus and its environmental relevance

2.1.1 Chemistry of Phosphorus

Phosphorus (P) is a nonmetallic chemical element with an atomic number of 15 and an atomic weight of $30.97376 \text{ g}\cdot\text{mol}^{-1}$, which belongs to the “nitrogen family” in the periodic table. It has a melting point of $44.1 \text{ }^\circ\text{C}$, boiling point of $280 \text{ }^\circ\text{C}$, and density of 1.82 gram/cm^3 (at $20 \text{ }^\circ\text{C}$) [1]. Phosphorus can appear in different valency states, +3 (phosphorous), +5 (phosphoric), or empty *d* orbitals [2]. It has three main allotropic forms differentiated based on their colors: white, red, and black phosphorus. The summary of phosphorus (white) properties can be seen in Figure 2.1.

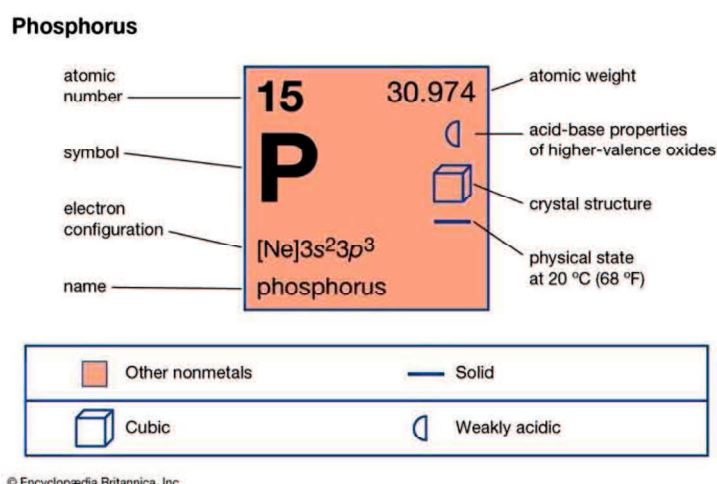


Figure 2.1 – Element properties of phosphorus [1].

Phosphorus is a pentavalent element with its natural oxide of phosphorus pentoxide (P_2O_5), which is highly hygroscopic and exothermically high reactive with water to form phosphoric acid (H_3PO_4) [3]. This acid forms phosphates when it reacts with varying alkaline compounds. The phosphorus compounds can be linear or chain, cyclic or ring, and branched-chain polymers or crystals. The formula of linear or chain polymers can be described by $\text{M}_{(n+2)}(\text{P}_n\text{O}_{(3n+1)})_x$, where M is a cation with *x* valence and *n* is an integer. The prefix “ortho” is used when the *n* = 1 and “pyro” is used if the *n* = 2. This formula can be modified to $\text{A}_m\text{B}_n(\text{PO}_4)_{(mx+ny)/3}$ if it has two cations in the chain, A and B, with valences of *x* and *y*, respectively. However, the formula of phosphate polymers with ring or chain

structures is represented by $[M(PO_3)_x]_n$, where $n > 2$. The prefix “meta” is used for ring or chain phosphate polymers [3]. For the crystal form of phosphates, the individual atom or oxygen-bonded unit of phosphorus, such as PO_4 and PO_3 , can be arranged in various configurations of the crystal structure [4].

Phosphorus is the 12th most common element on Earth’s crust of about one gram per kilogram, and its atomic abundance in the cosmos is about 1/100 of silicon atoms [1]. Phosphorus, however, cannot be found as a free element on Earth due to its high reactivity, and it has no stable gaseous form. In soil, it is widely distributed as soluble, mineral, organic, and adsorbed materials, and it generally occurs as orthophosphates PO_4^{3-} (or referred to as phosphates). The free form of PO_4^{3-} anions, which is soluble and the only form that plants can use for growth, only accounts for a small fraction of total phosphorus in soil [5]. In water, phosphorus is most frequently found as soluble reactive PO_4^{3-} as a released material from various sources, such as ocean and freshwater sediments, plant and animal fragments, human and animal wastes, soil erosion, etc. Several hundred of natural crystalline phosphate minerals that have been described are mainly found as apatites. The apatite minerals can be formulated as $M_5(PO_4)_3Z$, where M is a divalent metal and Z is an anion (F^- , OH^- , Cl^- , and CO_3^{2-}). Phosphorus compounds are mainly dominated by phosphorus linkages to oxygen (oxyphosphorus), carbon (organophosphorus), nitrogen (azaphosphorus), and metals (metallophosphorus) [6].

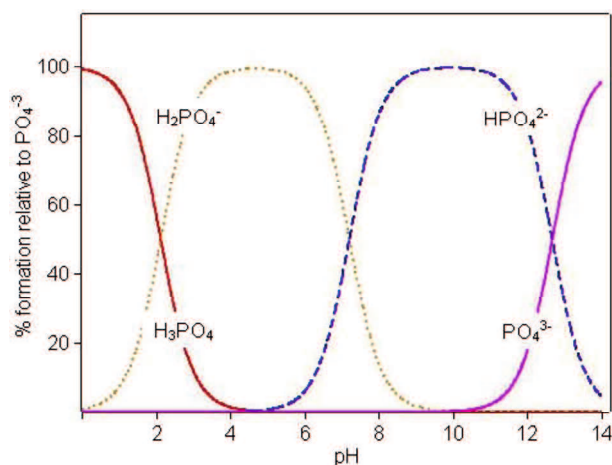


Figure 2.2 – Distribution of phosphate species in aqueous solution as a function of pH.

In water, phosphate can appear in different species based on the pH. Figure 2.2 recalls the influence of pH (in the range 0–14) on the distribution of phosphate species in solution. In extreme conditions, Orthophosphoric acid (H_3PO_4) is the main species at $pH < 2$, whereas

PO_4^{3-} is dominant at $\text{pH} > 13$. Phosphates mainly appear in H_2PO_4^- and HPO_4^{2-} under natural pH conditions.

2.1.2 Significance of phosphorus resource

Phosphorus is one of the fundamental nutrients to sustain daily life, affecting every organism on Earth. It is an indispensable nutrient for the animal's body since it takes its essential role in the structural stability of bones and teeth, development of cell membranes and nucleic acid molecules for genetic substances, energy metabolism activity (including ATP, ATP), and photosynthesis process for plants [7]. Animal adsorbs phosphorus through plant-eating animals (herbivores), which in turn comes from soil or the phosphorus fertilizers applied to plants. In industrial activity, phosphorus (in the form of high-purity phosphoric acid) is mainly used for additives in food processing and doping donors in semiconductors [8,9]. In the state of red phosphorus, it is used in pyrotechnic, matches, and effective flame retardants for accidental fires in organic polymer materials [1,10].

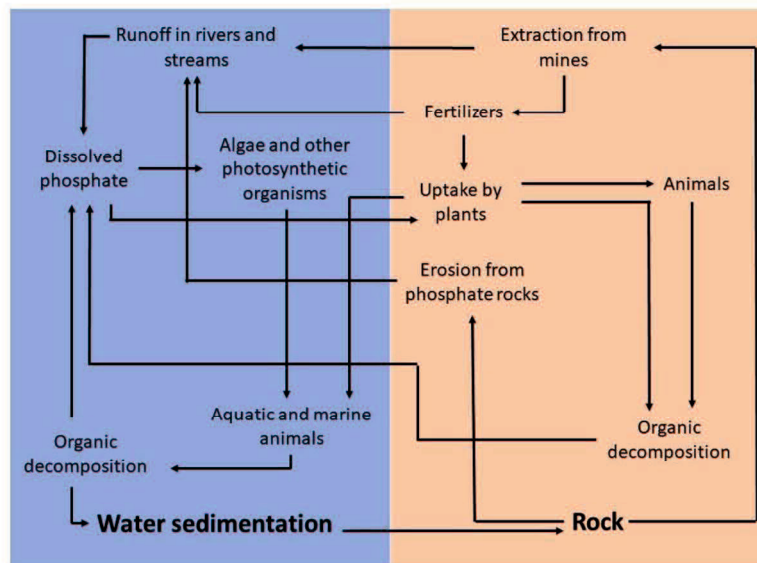


Figure 2.3 – Geological and biological phosphorus cycle. Image reproduced from The Editors of Encyclopaedia Britannica, 2020.

Phosphorus becomes a main growth-limiting factor for plants because of its low concentration in soil and low solubility. Consequently, in the soil with a low phosphorus concentration or an insufficient phosphorus release rate, the external phosphorus input must be presented as fertilizers. Agriculture is still the dominant user of global phosphorus, accounting for about 80% of the total annually mined phosphorus deposits are mainly used

to produce agricultural fertilizers [12]. In phosphorus fertilizers, the high purity of phosphoric acid is not required, and the direct production from mined phosphate ores is lower in cost. Global phosphorus demand for fertilizer use is forecasted to increase from 4.6 million tons in 1961 to approximately 49 million tons in 2022 [13]. To secure food production sustainability in the future, the demand for these fertilizers is expected to increase continuously since the population is projected to grow by about 1.9 billion inhabitants from 2020 to 2050 [14]. The world's commercial phosphorus fertilizers are mainly produced from mined phosphorus rock, which is a non-renewable, limited, and geographically nonhomogeneous resource [15]. Moreover, the natural phosphorus cycle is much slower than those of hydrogen, carbon, nitrogen, and oxygen cycles, which can take millions of years to complete the cycle. Figure 2.3 illustrates the geographical and biological phosphorus cycle in nature. Human activities have ruined this cycle, which sped up phosphate extraction during the past several centuries. This makes the scarcity of phosphorus and access to its supplies are recently becoming a significant concern.

The significance of phosphorus as a limited natural resource has been emphasized by The International Conference on Sustainable Phosphorus Chemistry (SUSPHOS) series, established in 2015 [16]. Experts stated that the phosphorus reserves are decreasing, even though its availability estimates are still quite diverse. As first introduced by Hubbert in 1949 to describe the period of oil reserves reaching their maximum rate before depletion [17], the Hubbert linearization was also applied to estimate the peak of phosphorus production. By using industry data, the Hubbert linearization analysis shows that the peak of global phosphorus production may occur by 2033 [18]. After the peak, the demand would exceed supply which will lead to scarcity of global phosphorus resources. Another assessment, based on the present and future phosphorus consumption, the increase of meat consumption, and the rise in biofuel and bioenergy crops, the exploitable phosphorus resources are estimated to be depleted in 2084, and the total reserves of phosphorus (including currently inaccessible phosphorus resources) will only last until 2179 [19]. Furthermore, based on the decrease of annual population growth rate as estimated by the United Nations (UN), the current phosphate rock production will last until 2315; however, if the growth rate keeps continuing at about the current rate, the production will be depleted in 2170 [5]. Although the exact timeline might be unpredictable, phosphate rock is still the primary source of phosphorus in the global market. Management of phosphorus usage is essential for sustaining future food production since the world's population is continuously growing.

The negative expectations of future phosphorus resources affect the price of global phosphate rock and its products. The increase in demand for phosphorus products and the

requirement of high cost for the extraction of phosphate rocks, which are increasingly difficult to reach and declining in quality, tend to increase the price of phosphate rock. The price increase seemingly will occur even without the depletion of phosphorus resources [20]. This would undoubtedly increase the amount of agricultural land that is not nourished by fertilizer. Consequently, escalating the efficiency of the phosphorus resources usage and promoting the phosphorus recovery from wastes are worthwhile, although the phosphorus exhaustion is not imminent.

Throughout the past few centuries, anthropogenic activities, such as agricultural and wastewater disposal practices, have ruptured the geographical and biological phosphorus cycle characterized by high losses and low use efficiency [21]. Especially in agriculture, a large amount of phosphorus has been discharged into water bodies by human activities. Only a tiny proportion of external phosphorus applied to soil (about 10–20%) is absorbed by the plants, where the rest remained in the soil due to the fixation by the reactive soil components to form insoluble compounds [22]. The phosphorus is likely to bind to soil particles and then be carried away into water bodies by runoff, leaching, and erosion. Since the use of phosphorus fertilizer in agriculture is inefficient and phosphorus is a non-renewable and non-substitutable resource, the recovery and reuse of phosphorus are significant. The recovery method is considered to be able to save less than half of the imported phosphorus [23]. The recovery and reuse of phosphorus can be made along the entire phosphorus cycle, redistribution of phosphorus from phosphorus-rich wastes such as sewage sludge, manure, offal, and water bodies, to the areas that require more phosphorus [24]. However, phosphorus-containing wastes are increasingly contaminated by heavy metals and toxic substances and harmful for direct redistribution to crops. Consequently, various technologies of phosphorus recovery are needed.

2.1.3 Eutrophication

The accumulation of phosphorus and nitrogen is the main factor of eutrophication in surface waters. Eutrophication has been identified as the most fundamental global environmental problem relating to water bodies and is causing deterioration of water quality and disruption of aquatic ecosystems [25]. Eutrophication is an ecological response to the progressive enrichment of water by nutrients, especially nitrogen and/or phosphorus compounds, accelerating the growth of algae and phytoplankton to create aquatic ecosystems imbalance and reduce the water quality [26]. It is mainly recognized that eutrophication is linked to the increase of harmful algal blooms and depletion of dissolved oxygen (hypoxia) which in turn destroy the aquatic life in affected areas [27].

In freshwater, phosphorus is the primary limiting factor of algal growth where nitrogen is highly in excess [28]. Before anthropogenic interference, nutrients (especially phosphorus) accumulation in water bodies is a slow natural process determined by mineral degradation and solution as an effect of decomposer organisms in rocks [29]. Intensive agricultural practices, industrial activities, and population growth have triggered the accelerated mobilization of phosphorus into the environment and accumulated mainly in water bodies [30]. By the year 2000, it was reported that human activities have roughly tripled the phosphorus flows to the environment in comparison to natural rates [31]. A statistical analysis from Water Research Commission, South Africa, shows that 54%, 53%, 48%, 41%, and 28 % of lakes/reservoirs in Asia, Europe, North America, South America, and Africa deal with eutrophication problems, respectively [32].

A study in periphyton (algal) growth in global freshwater systems analyzed from 1990 to 2016 has found that 31% of international catchment areas show alarming periphyton growth levels. Nearly 76% of the undesirable periphyton growth was triggered by phosphorus pollution, which is dominated by agricultural land in North and South America and Europe [33]. There are various sources of phosphorus-inducing eutrophication. Point sources (e.g., municipal wastewater treatment plants and industrial discharge) are easier to be identified and managed than diffuse sources since diffuse sources have varied nature [34]. The primary diffuse sources of phosphorus are phosphorus accumulation in soils by the inefficient use of fertilizer or manure on the farm.

Most studies assume that a concentration above $100 \mu\text{g P L}^{-1}$ is too high and potential to cause eutrophication, even though there is still no explicit agreement yet on the acceptable phosphorus concentration to prevent eutrophication [35]. Policy implementation in phosphorus discharge is one of the possible options to reduce the phosphorus release and improve the ecological state of surface waters. The European Union (EU) via The Council Directive of May 21, 1991 (91/271/EEC) concerning urban wastewater treatment requires phosphate removal from wastewater discharge by introducing the limitations on the released pollutant loads [26]. From 2010 to 2020, the noticeable reduction of eutrophication risk has been managed to achieve by a few countries. However, some other countries such as Greece, Spain, Lithuania, Luxembourg, Denmark, Portugal, and Cyprus still have over 90% of the ecosystems region in danger of eutrophication [36]. The requirements for treated wastewater are varied for each EU Member States, depending on agglomeration size (in Population Equivalent, PE), wastewater receiver type, and the sensitivity of the receiver to eutrophication. Denmark is the most restrictive in EU countries that set 0.4 mg/L total phosphorus (TP) as a limit of dischargeable treated wastewater, while Germany and Sweden specify the limit of TP in

treated wastewater at a level not more than 1 mg/L ($BOD_5 < 6000 \text{ kg/d}; >100,000 \text{ PE}$) and 0.5 mg/L (every category), respectively [36]. Similar measures have been applied in non-EU countries, such as the USA, China, and Japan, by different approaches. The USA and China have established a maximum permissible value for TP in areas sensitive to eutrophication at 1.0–0.1 mg/L and 0.5 mg/L, respectively [36]. While the Ministry of the Environment in Japan sets the quality standard for total phosphorus for the living environment in lakes is varied from 0.005 mg/L to 0.1 mg/L based on the designation of the water [37].

Although the nutrients (phosphorus and nitrogen) removal by wastewater treatment plants is forecasted to increase by 10%–40% from 2010 to 2050, the phosphorus discharge to the environment will continue to increase by 7%–60% [38]. Phosphorus pollution is still an essential issue in developed countries, despite enhancements in wastewater nutrients removal and surface water quality. The discharge of untreated wastewater remains everyday activity, especially in developing countries, due to the lack of budget, infrastructure, and technical capacity. The fact that a small fraction of wastewater treated in developing countries offers investment opportunities for water and wastewater treatment and recovery of valuable byproducts, such as phosphorus, in developing countries. However, the removal and recovery of phosphorus from sewage which are still in the development stage, demand high technologies.

2.2 Phosphorus removal technologies

The removal of phosphorus from domestic wastewater before discharge is essential to reduce the risk of eutrophication in natural waters. In many countries, phosphorus removal has become obligatory and common. However, the rate of phosphorus removal of a wastewater treatment plant depends on the composition of total phosphorus, regulation of phosphorus discharge limit, and applied technology of phosphorus removal [39]. Various technologies can be used for phosphorus removal from wastewater, such as chemical precipitation, biological phosphorus removal, crystallization, and adsorption. Each technology has its advantages and disadvantages, as can be seen in Table 2.1.

2.2.1 Chemical precipitation

Chemical precipitation is one of the most widely applied phosphorus removal technologies besides the biological method because of its easy operation. Chemical precipitation removes inorganic phosphates in wastewater by adding coagulant and flocculant to precipitate slightly soluble phosphate compounds and then removing the sedimentation by either gravitational settling or filtration. A coagulant is added to transform

the stable phosphates to the unstable phase by neutralizing the negative charge on phosphates and form small clumps of particles (micro flocs). The multivalent metals are usually used as the coagulant, such as ferric, ferrous, aluminum, or calcium salts. While flocculant merges destabilized phosphates together into big flocs and drops them out of solution. The most widely used flocculants are synthetic polymers with molecular weights range from 1000 to 30×10^6 [40]. The coagulation process requires rapid mixing of wastewater and coagulant, while a gentle mixing is performed in the flocculation process to avoid the big flocs destruction.

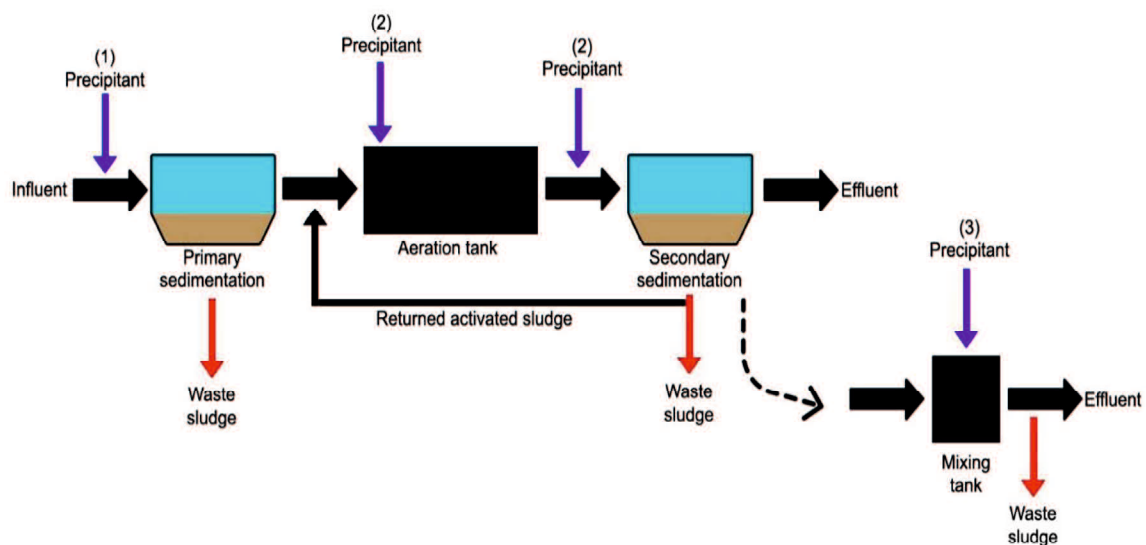


Figure 2.4 – The strategy of chemical precipitation process addition in the biological phosphorus removal process, (1) pre-precipitation, (2) coprecipitation, and (3) post-precipitation.

In biological phosphorus removal processes, the chemical phosphorus removal is usually applied for the supplemental process. In this case, the precipitants (coagulant and flocculant) are added to either pre-treated wastewater (pre-precipitation), activated sludge aeration basin (coprecipitation), or to the separate tertiary treatment process before discharge (post-precipitation) [41], as illustrated in Figure 2.4. Pre-precipitation involves the addition of precipitants to raw wastewater in primary sedimentation influent. Pre-precipitation is applied to reduce the loading to the subsequent biological treatment stage, decreasing energy and hydraulic retention time consumption. While in coprecipitation, the phosphorus precipitation by coagulant is performed simultaneously with the biological treatment in the aeration tank. The precipitants can be added to the biological treatment tank or the effluent of biological treatment before secondary sedimentation. Post-precipitation involves the addition of precipitants in the effluent secondary sedimentation

installation. The chemical precipitation in post-precipitation becomes stronger since anaerobic biological treatment transforms some organic phosphates into orthophosphates. Besides that, chemical precipitation technology requires high cost for the chemicals, treatment of resulted sludge, and neutralization of effluent, and it is susceptible to environmental factors, such as pH and temperature [42,43].

2.2.2 Biological phosphorus removal

Biological phosphorus removal (BPR) promotes a lower-cost alternative to chemical precipitation methods for phosphate removal. BPR, especially enhanced biological phosphorus removal (EBPR), has been extensively studied in recent years because it reduces chemical use and is an environmentally friendly phosphorus removal method [44]. EBPR utilizes a group of heterotrophic bacteria, called phosphorus-accumulating organisms (PAOs), primarily responsible for phosphorus removal. These organisms can absorb dissolved phosphorus from wastewater as intracellular polyphosphate in their energy storage mechanism, resulting in phosphorus removal from wastewater.

Regardless of how phosphorus is removed by the microorganisms is still not clearly understood, the biological phosphorus removal in wastewater treatment systems has three main proposed mechanisms [45]. The first is the normal uptake mechanism, which involves the uptake of phosphorus by organisms as it is an essential element required for their energy metabolism activity and cell membranes development. In aerobic, phosphorus accumulation always occurs since organisms are growing and multiplying. However, this mechanism can only remove about 15-25% of phosphorus in many municipal wastewaters [46]. The second mechanism is the luxury uptake mechanism. In this mechanism, the organisms in a treatment system are exposed to a nutrient deficiency (other than phosphorus) stress where phosphorus is available in excessive amounts than required for growth [47]. As a result, the available energy is used by the organisms for storing excess phosphorus within the biomass as polyphosphates, leading to enhanced phosphorus uptake from wastewater. The third mechanism is overplus accumulation, which is based on the rapid phosphorus accumulation by phosphorus-starved organisms. Phosphorus-starved organisms are obtained by exposing the activated sludge to anaerobic conditions, where aerobic organisms release large amounts of phosphorus in anaerobic conditions. In anaerobic conditions, the organisms consume carbon sources and store them as polyhydroxyalkanoates (PHA) simultaneously with the hydrolyze of stored polyphosphates and the release of orthophosphate [48]. Rapid phosphorus uptake by organisms occurs in subsequent aerobic conditions to reclaim the released phosphorus in an anaerobic process and to absorb additional phosphorus for energy storage as polyphosphate. This phosphorus

accumulation uses stored PHA as an energy source to absorb orthophosphate from a liquid medium. This process results in enhanced biological phosphorus removal from wastewater.

In BPR, PAOs are enriched in the bacterial community within activated sludge. The activated sludge process in EBPR is operated by recirculating sludge through anaerobic and aerobic conditions[49]. The most basic configuration of biological phosphorus removal is shown in Figure 2.5. The configuration consists of an arrangement of anaerobic and aerobic tanks for stimulating carbon oxidation and phosphorus removal. However, in most EBPR configurations, an anoxic process is added between anaerobic and aerobic processes to minimize the amount of nitrate fed (in returned activated sludge) to the anaerobic tank by recycling mixed liquor from the aerobic tank to anoxic tank. Since the existence of nitrate in the anaerobic tank inhibits biological phosphorus removal. Under ideal conditions, EBPR can reduce total phosphorus to 0.1–0.2 mg-P/L. However, in the actual application, EBPR has low stability because its performance depends on many factors (such as influent flow and pollution loading variations), resulting in the requirement of high skilled operators for complex process control [43]. The effective EBPR is also determined by local environmental conditions as the conditions affect the microbial diversity and metabolic behavior of the community [50]. This makes the ideal conditions for EBPR relatively narrow. Moreover, this method is not suitable for phosphorus removal at trace levels because the bacterial metabolism would be decreased simultaneously.

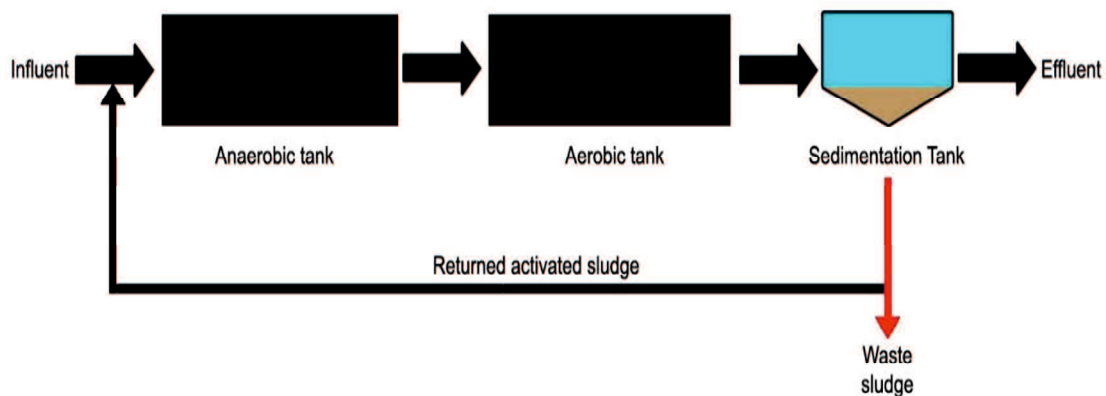


Figure 2.5 – Typical configuration of the biological phosphorus removal process.

2.2.3 Crystallization technology

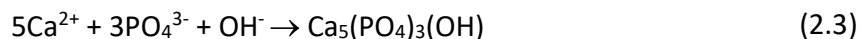
Crystallization has been recognized as a useful method that is not only for phosphorus removal but also for phosphorus recovery at the same time. The phosphorus crystallization technology involves seed crystals as the medium for transforming liquid phase phosphorus

to solid-phase under metastable conditions. This method is based on the final product solubility of phosphorus-containing salts, such as magnesium ammonium phosphate (MAP), magnesium potassium phosphate (MPP), and hydroxyapatite (HAP). The selection of salts in the crystallization process depends on the relative concentrations of ammonium or potassium and phosphate in the wastewater [51].

A high concentration of ammonia and potassium are required to precipitate phosphorus to MAP and MPP, respectively, and phosphorus compounds are precipitated when the solubility of products surpassed by adding magnesium and adjusting pH. However, wastewaters that meet these conditions are limited. The chemical reaction for phosphorus precipitation to MAP and MPP are presented in Equation 2.1 [52] and Equation 2.2 [53], respectively:



The reaction for the precipitation of HAP is shown in Eq. 2.3 [54]:



The crystallization to HAP is effectively performed at low phosphorus concentration, and there is concern toward the effluent at high phosphorus concentration.

Seed crystals are loaded into a crystallization reactor, and pH is adjusted to an appropriate value for promoting the phosphorus deposition on seed crystals. The efficiency of phosphorus removal by crystallization technology is highly affected by the pH of the reaction. The pH of the crystallization system needs to be kept below the phosphorus chemical precipitation limit because the precipitation of phosphate would take place at a high pH in addition to crystallization. This makes skilled operators are required for the crystallization method. In the final stage in this method, an increase in sludge production can be prevented, and the final product can be easily dewatered [55]. The final outcome of the crystallization method has the potential to be reused as fertilizer as it has phosphorus content that is comparable to phosphorus rock. Some reactors, such as continuous stirred tank reactors (CSTRs), fluidized bed reactors, and bubble column-type reactors, can be applied for the crystallization process, where continuous stable flow is preferred for a large wastewater volume [51]. The basic scheme for phosphorus crystallization by CSTRs is shown in Figure 2.6.

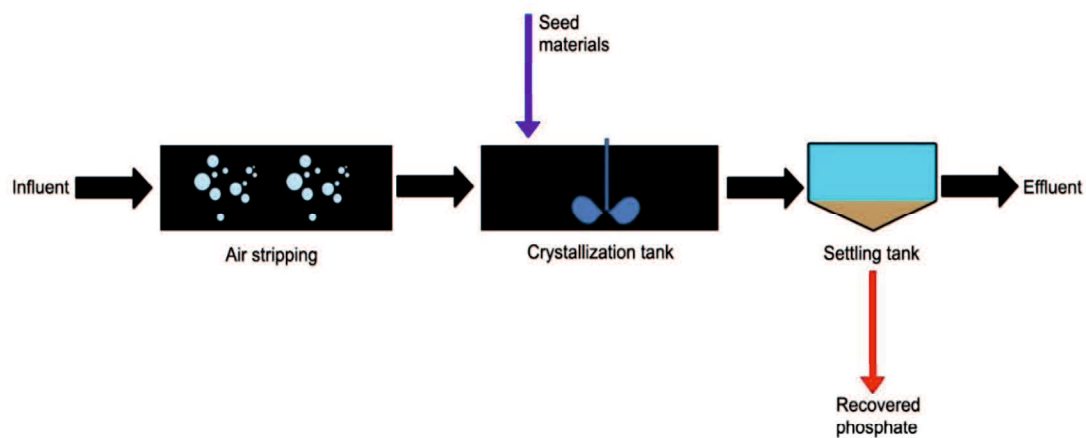


Figure 2.6 – Typical configuration of phosphorus crystallization by continuous stirred reactors.

2.2.4 Adsorption

Although adsorption is less commonly employed in large-scale phosphorus removal from wastewater, there has been a lot of works dealing with phosphorus removal improvement using this method in the past few years. Adsorption is recognized as a method that is simple, convenient, low cost, highly selective, and low amounts of sludge production, compared to other phosphorus removal methods [56]. The adsorption method has become a more promising method since it can remove phosphorus at low contents over a wide pH range [57]. Adsorption is a method to remove phosphorus via molecule transfer from a liquid bulk to the surface of solid material. Phosphorus removal by adsorption depends on the phosphorus adsorption behaviors of specific materials to remove phosphorus from wastewater. Besides that, adsorbent is reusable by using an appropriate desorption technique. Until now, numerous adsorbents have been investigated to examine the ability to remove and recover phosphorus from water.

Oxides/hydroxides-based adsorbents have been recognized as the most successful and attractive candidates as adsorbents to remove phosphorus and other oxyanions from water [56]. The removal efficiency of adsorbents is varying based on their chemical and physical characteristics and environmental conditions of the adsorption. Therefore, the unique adsorption mechanisms of specific metal oxides/hydroxides determine the adsorption efficiency of different adsorbents. Many studied adsorbents have the potential for phosphorus removal. The selection of adsorbents depends on their criteria for the target application, such as adsorption capacity, cost, chemical stability, and application method (powder or fixed-bed column). Several practical applications require near-zero phosphorus removals, such as eutrophic surface water restoration, wastewater reuse in artificial lakes,

and effluent polishing after chemical or biological phosphorus removal due to more stringent regulation phosphorus discharge [58]. In contrast with traditional biological and chemical precipitation methods, adsorption in a fixed-bed column method can reduce dissolved phosphorus to very low concentration, especially for polishing treated wastewater [35,59]. Table 2.1 shows the comparison of different types of phosphorus removal technology.

Table 2.1 – Comparison of various technologies for phosphorus removal.

Technology	Advantages	Disadvantages	Reference
Chemical precipitation	<ul style="list-style-type: none"> • Easy to use. 	<ul style="list-style-type: none"> • High cost for chemicals. 	[42]
	<ul style="list-style-type: none"> • Reliable and well-established. • Usable for treating a large volume of wastewater. 	<ul style="list-style-type: none"> • Low effectiveness at low phosphorus concentration. • High sludge production that requires treatment. • Effluent neutralization requirement. • Susceptible to many environmental factors (pH, chemical concentration, etc.), resulting in a complex control system. • Subsequent biological treatment may be affected by chemicals. • Phosphorus recovery is relatively difficult. 	[60] [43]
Biological phosphorus removal	<ul style="list-style-type: none"> • Low operational cost, except for infrastructural investment. • Environmentally friendly. • No chemicals required. • Simultaneous removal of phosphorus and nitrogen. 	<ul style="list-style-type: none"> • Low reliability and stability. • Low effectiveness at low phosphorus concentration. • High sludge production. • Uncontrolled bacterial growth. • Susceptible to inhibiting substances, especially to the coexistence of glycogen accumulating organisms. • High skilled operators are required. 	[61] [50] [43] [44]
Crystallization technology	<ul style="list-style-type: none"> • Simultaneous phosphorus removal and recovery. 	<ul style="list-style-type: none"> • High cost for chemicals. 	[62]
	<ul style="list-style-type: none"> • No sludge production. 	<ul style="list-style-type: none"> • Increase effluent salinity. • Influenced by many factors (pH, temperature, etc.), resulting in a complex control system. • High skilled operators are required. 	[55] [63]

Adsorption	<ul style="list-style-type: none"> • High efficiency. • Great potential for P recovery. • Wide pH range operation. • Simplicity of design. • Ease of operation. • Fast adsorption rate. • No sludge production. • Robust and cost-effective. • Effective in low phosphorus contents. 	<ul style="list-style-type: none"> • Can be costly for pretreatment and sorbent regeneration. • Low selectivity against competing ions. • Downstream processes are needed to recover phosphate. 	<p>[43] [64]</p>
------------	---	--	----------------------

2.3 Zirconium-functionalized LDH as phosphate adsorbents

2.3.1 Zirconium-based phosphate adsorbent

Many metal (hydr)oxides adsorbents were reported to be effective for phosphate adsorption, such as iron, aluminum, manganese, and zirconium [65]. Among these metal (hydr)oxides, zirconium (hydr)oxide is an excellent adsorbent due to its nontoxicity, insolubility, strong affinity for phosphate, and superior chemical stability under acidic and basic conditions [64]. Besides, zirconium (hydr)oxide as phosphate adsorbent was found to have good desorption efficiency for reuse. The oxides of zirconium are classified into three major types of structure (polymorph): cubic, tetragonal, and monoclinic. Each type can be obtained at a different temperature range, and a high-temperature structure can be stabilized at room temperature by adding additives (stabilizer). However, an amorphous form of zirconium (zirconium (hydr)oxide) is preferred to be a phosphate adsorbent because of its simplicity of synthesis, large specific surface areas, high active binding sites, and strong affinity for phosphate [66]. The phosphate adsorption onto zirconium (hydr)oxides mainly involves the electrostatic, ion exchange, and Lewis acid-base interactions between the functional groups on the adsorbent surface and the phosphate anions in solution (Figure 2.7), depending on the pH solution.

A significant number of researches have focused on removing phosphate by zirconium-based materials, such as amorphous zirconium hydroxide, mesoporous zirconium oxide, amorphous zirconium oxide nanoparticles, and hydrated zirconium oxide [67–70]. It has been reported that the functionalization of zirconium noticeably enhanced the phosphate adsorption capacity of adsorbents. This enhancement can be associated with the fact that zirconium is readily hydrolyzed to produce abundant hydroxyl ions and water molecules by forming tetranuclear ions or octanuclear species, where hydroxyl bonds in the metal surfaces are involved in the ligand exchange reaction with phosphate ions in solution [71].

Moreover, the chemical inertness of zirconia is envisaged to enhance the chemical stability of modified adsorbents, considering that the sensitivity of some adsorbents towards pH changes becomes a significant issue for real wastewater treatment applications.

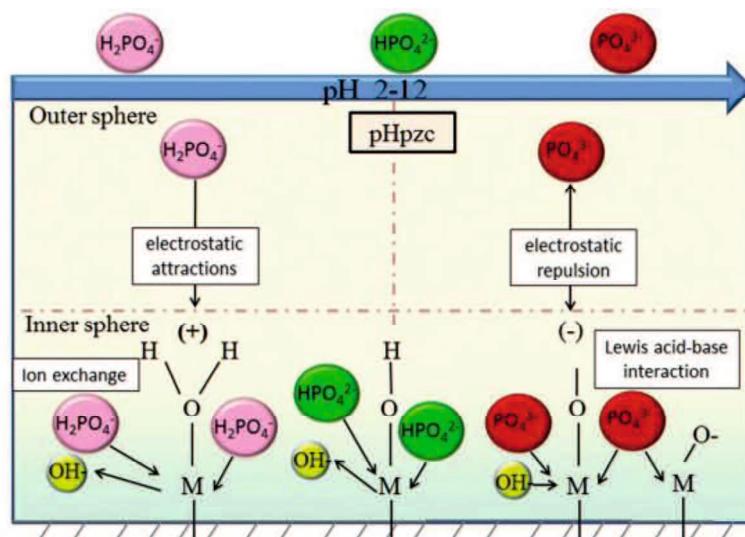


Figure 2.7 – Phosphate adsorption mechanisms of zirconium (hydr)oxides [65].

2.3.2 LDH as phosphate adsorbent

Layered double hydroxide (LDH) materials, also known as hydrotalcite-like compounds, are layered material with hydroxide sheets, where a net positive charge is developed on the brucite-like octahedral layers because trivalent cations substitute divalent cations partially. The net positively charged layers are compensated by anions in the interlayer region, such as NO_3^- and CO_3^{2-} , along with hydrogen-bonded water molecule. The typical formula of LDH structures can be expressed as can be represented as $[M_{1-x}^{2+} M_x^{3+} (\text{OH})_2]^{x+} (A^{n-})_{x/n} \cdot m\text{H}_2\text{O}$, where M^{2+} and M^{3+} are divalent (e.g., Mg^{2+} , Zn^{2+} , etc.) and trivalent cations (e.g., Fe^{3+} , Al^{3+} , etc.), respectively; A^{n-} is the interlayer anion of valence n , and x is the molar ratio of $M^{3+}/(M^{2+} + M_x^{3+})$ that typically ranges from 0.18 to 0.33 [72]. The structure of LDH can be described in Figure 2.8a.

LDH materials have been reported to be promising selective ion exchangers for phosphate [72]. LDH materials capture phosphate from aqueous solution by surface adsorption and anion exchange, as shown in Figure 2.8b. Anion exchangeability of LDH is due to the relatively weak interlayer bonding. Therefore, it can be easily replaced by organic and inorganic anions. Recently, some studies have been dedicated to the design and application of LDH as an adsorbent for phosphate removal in an aqueous solution. These

include Mg-Fe LDH, Mg-Al LDH, Ca-Al LDH, chloride-Zn-Al LDH, chloride-Zn-Al-Fe LDH, and so on [72,73]. Moreover, the modification of LDH with different metal cations of valence +2, +3, and even +4 was carried out to engineer the selectivity of LDH as adsorbents. Besides being recognized as naturally occurring minerals, LDH materials are also relatively simple and economical to synthesize [73]. One of the significant advantages of LDH materials is that they are composed of hydroxides of metals abundant on Earth. Nevertheless, LDH materials have several drawbacks that are still becoming problems for their large-scale phosphate treatment applications. First, potential dissolution of LDH constituent metals, especially at an acidic solution. Second, regeneration LDH adsorbents can be costly due to the involvement of the calcination process. Third, adsorption by using calcined LDH significantly increased the basicity of treated water [73].

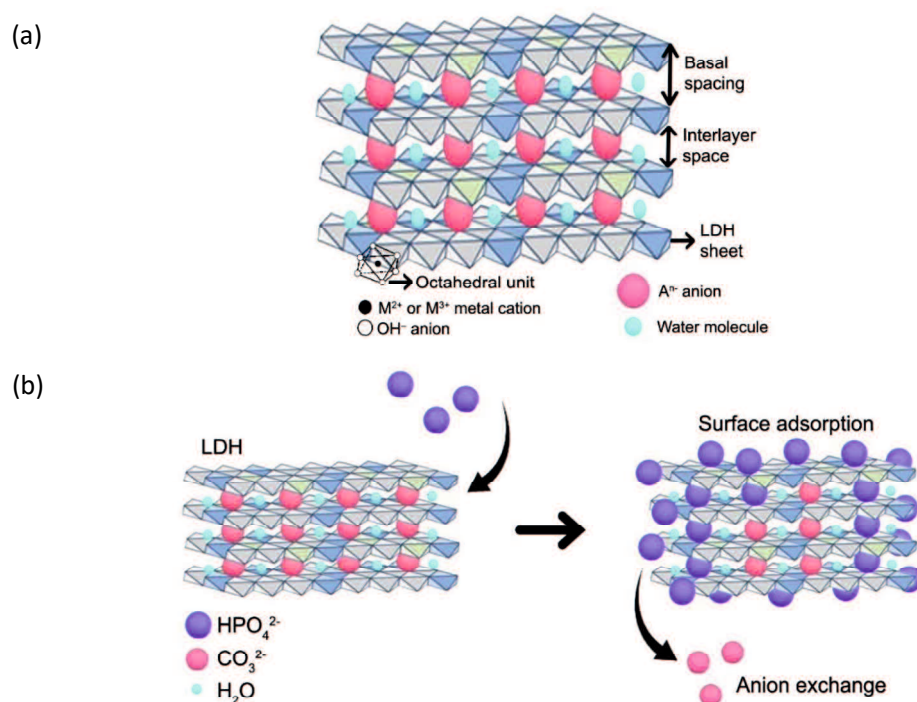


Figure 2.8 – (a) Schematic structure of layered double hydroxides and (b) mechanism of phosphate anion exchange and surface adsorption on LDH.

2.3.3 Synthesis of zirconium-functionalized LDH as phosphate adsorbent

Since zirconium is a pretty expensive material, the full use of zirconium in phosphorus removal is relatively high cost. To reduce the cost of zirconium usage as an adsorbent, it is necessary to combine zirconium with other low-cost materials to make it more cost-effective. In addition to reducing the production costs, the zirconium-modified adsorbents

are also supposed to have better phosphate adsorption performance. Several studies have been carried out to combine zirconium with other cheap materials, such as zirconium-loaded okara and zirconium-modified chitosan beads [74,75].

Because of the large surface area and high amounts of hydroxyl groups on zirconium (hydroxides), the modified LDH materials by zirconium (hydr)oxides are envisaged to have a better ability to remove phosphate from water than single LDH adsorbents. Besides that, the LDH materials are economical to synthesize, which can reduce the preparation cost. The interaction mechanisms between zirconium-LDH-based adsorbents and phosphate are the combination of ligand exchange reaction and anion exchange mechanisms. In addition, it was reported that zirconium introduction to LDH materials enhanced phosphate adsorption in seawater, which contains plenty of other anions, although most of LDH adsorbents are not suitable for phosphate adsorption in seawater [76].

2.3.4 The current state of research

Several zirconium-modified LDH adsorbents have been studied, and most of them for phosphate removal. For example, zirconium ion modified MgAl-LDH was found to consist of binary MgAl-LDH and amorphous zirconium oxide, which provides a superior phosphate adsorption property [76]. Superparamagnetic microparticles modified MgFe-Zr LDH was reported to have high phosphate adsorption capacity and excellent reusability for 15 adsorption/desorption cycles [77]. Zirconium-modified Mg-Fe LDH showed an enhanced phosphate removal, which has been associated with the presence of zirconium hydroxides on the LDH sheets [78]. These adsorbents were synthesized by conventional coprecipitation method. However, several studies reported that the coprecipitation method in zirconium-modified LDH synthesis involved the distribution of Zr ions in the octahedral sites of the brucite-like layers of LDH, instead of producing pure composite materials [79,80], which may affect the phosphate adsorption of modified materials.

2.4 Mathematical models for phosphate adsorption

2.4.1 Adsorption kinetics

Adsorption kinetics is the most vital parameter to examine when designing an adsorption system. Adsorption kinetics is the measure of the rate of adsorption uptake with respect to a constant concentration and is applied for studying the diffusion of adsorbate in the adsorbent surface. Typical kinetics models frequently used to simulate the adsorbent-adsorbate interaction are pseudo-first-order, pseudo-second-order, Elovich, and Intra-particle diffusion models. Pseudo-first-order kinetic model (or Lagergren model) assumes

that adsorption occurs via diffusion through the adsorbent surface, while the pseudo-second-order kinetic model assumes the adsorption process is controlled by adsorption reaction at the adsorbent surface. Pseudo-first-order and pseudo-second-order can be determined by Equation 2.1 and 2.2 [75], respectively:

$$\ln(q_e - q_t) = \ln(q_e) - k_1 t \quad (2.1)$$

$$\frac{t}{q_t} = \frac{1}{k_2 q_e^2} + \frac{1}{q_e} t \quad (2.2)$$

where q_e and q_t (mg g^{-1}) are the amount of adsorbed phosphate at equilibrium and time t , respectively; k_1 (h^{-1}) and k_2 ($\text{g mg}^{-1} \cdot \text{h}^{-1}$) are the rate constant of the pseudo-first-order model and pseudo-second-order model, respectively.

Elovich kinetics model assumes that the adsorption rate exponentially decreases as the amount of adsorbed solute increases on the adsorbent surface without any interaction among adsorbed species. The Elovich kinetic model is represented as Equation 3.3 [75]:

$$q_t = \frac{\ln a_e b_e}{b_e} + \frac{1}{b_e} \ln t \quad (2.3)$$

where a_e is the initial adsorption rate ($\text{mg g}^{-1} \text{h}^{-1}$) and b_e is related to the extent of surface coverage and activation energy for chemisorption (g mg^{-1}).

The intra-particle diffusion model is widely employed to examine the rate-limiting step during adsorption, where the adsorption in solution involves film diffusion, surface diffusion, and pore diffusion. Intra-particle diffusion can be determined by Equation 2.4 [75]:

$$q_t = k_3 t^{0.5} \quad (2.4)$$

where k_3 is the intraparticle diffusion rate constant ($\text{mg g}^{-1} \text{h}^{-0.5}$).

Among the models mentioned above, pseudo-first-order and pseudo-second-order are widely employed in almost every adsorption process. The compatibility of the kinetics model is determined by correlation coefficient (R^2) or Sum of Squared Errors (SSE). To examine the suitability of adsorption kinetics, linear forms have been applied.

2.4.2 Adsorption isotherm

The information about adsorption mechanisms is essential to design the adsorbents and the adsorption systems. The adsorption mechanisms have been widely explored by the modelling of adsorption data by isotherm models. Moreover, the adsorption isotherm models can be used to obtain the data of maximum adsorption capacity, which is essential

in the estimation of the adsorbent performance. The adsorption isotherms explain the relation between the adsorbate concentration and its degree of accumulation onto an adsorbent surface at a constant temperature. Several isotherms models have been widely applied in adsorption systems, such as the Langmuir model, Freundlich model, Temkin model, and Dubinin–Radushkevich (D-R).

At first, the most widely used applied Langmuir isotherm was developed to represent the gas-solid adsorption. It assumes that the adsorption is monolayer, the distribution of adsorption sites is homogeneous, the adsorption energy is constant, and the interaction between adsorbed species is negligible. The Langmuir isotherm is presented by Equation 2.5:

$$q_e = \frac{q_m k_l C_e}{1 + k_l C_e} \quad (2.5)$$

where C_e (mg-P L⁻¹) is the phosphate equilibrium concentration, q_e (mg-P g⁻¹) is the equilibrium adsorption capacity of the adsorbent, q_m (mg g⁻¹) is the theoretical maximum adsorption capacity of the adsorbent, k_l (L g⁻¹) is the Langmuir adsorption constant associated with the adsorption energy.

The Freundlich model is applied to represent the nonlinear adsorption phenomenon. The Freundlich model has been considered an empirical equation without physical meaning and represents the multi-layer adsorption on heterogamous surfaces. The Freundlich model is defined by Equation 2.6 [81]:

$$q_e = k_f C_e^{\frac{1}{n}} \quad (2.6)$$

where k_f (mg g⁻¹) is the Freundlich adsorption constant associated with the adsorption capacity, and n is a constant related to adsorption intensity or surface heterogeneity.

The Temkin model presumes that adsorption is a multi-layer process, where extremely high and low adsorbate concentrations in the liquid phase are ignored. The Temkin model is described by Equation 2.7 [81]:

$$q_e = \frac{RT}{b_t} \ln(k_t C_e) \quad (2.7)$$

where k_t (L mg⁻¹) and b_t (J mol⁻¹) are an equilibrium binding constant and a constant related to the heat of adsorption, respectively; R is the universal gas constant (8.314 J K⁻¹ mol⁻¹), and T (K) is the absolute temperature.

The D-R model was proposed to represent the adsorption of vapors on solids, based on the assumption that the distribution of pores in adsorbent follows the Gaussian energy distribution. The D-R model is described by Equation 2.8 [81]:

$$q_e = q_m e^{-[RT \ln(1+1/C_e)]^2 / 2E^2} \quad (2.8)$$

where E (kJ mol⁻¹) is the mean free energy of adsorption.

2.4.3 Adsorption thermodynamics

The temperature has a significant influence on the adsorption process. Thermodynamic parameters are essential to examine the spontaneity and feasibility of the adsorption process. Some thermodynamic parameters of adsorption, which are standard free energy change, enthalpy, and entropy, can be calculated from the adsorption isotherm at different temperatures by using Equation 2.9 and 2.10 [75]:

$$\Delta G^0 = -RT \ln K_d \quad (2.9)$$

$$\ln K_d = \frac{\Delta S^0}{R} - \frac{\Delta H^0}{RT} \quad (2.10)$$

where K_d is the distribution coefficient, ΔG^0 (kJ mol⁻¹) is the change of Gibbs energy, and ΔS^0 (kJ mol⁻¹ K⁻¹) and ΔH^0 (kJ mol⁻¹) are the change of entropy and enthalpy, respectively. The values of ΔS^0 and ΔH^0 were determined by the plot of $\ln k_d$ and $1/T$, where the intercept and the slope of the plot correspond to $\Delta S^0/R$ and $\Delta H^0/R$, respectively. The thermodynamic parameters of ΔS^0 and ΔH^0 can be determined from the slope and intercept of $\ln K_d$ versus $1/T$ linear plotting, where K_d is obtained from the slope of the plot $\ln(q_e/C_e)$ against C_e at different temperatures and extrapolating to zero C_e [75].

2.4.4 Breakthrough prediction of fixed-bed column adsorption

In practical application, adsorbents are usually applied in fixed-bed columns. A Fixed-bed column has been considered as an industrially feasible technique for phosphate removal from wastewater. The performance of fixed-bed columns is commonly studied through breakthrough curves. Breakthrough curves represent the function of the effluent concentration of pollutants versus time in a fixed-bed column process. The dynamic behavior of a fixed-bed column can be explained in terms of the mass transfer zone (MTZ) that travels through the bed as a function of mass loading and saturation of the adsorbent, as shown in Figure 2.10. MTZ can be defined as the length of the region where the adsorption takes place. The time when the front of MTZ just reaches the end of the bed is called breakthrough time. Exhaustion time is when effluent concentration is about equal to influent concentration, and the bed is unable to remove adsorbate further.

Breakthrough curves of adsorption commonly exhibit a characteristic 'S' shape, as shown in Figure 2.9, but with varying steepness [82]. This steepness depends on several factors, including the adsorbate's physical and chemical properties, the adsorbent, the particular rate-limiting mechanisms involved, the depth of the bed, and the velocity of flow [59]. Slow mass transfer results in flat curves, whereas fast mass transfer leads to sharp step curves.

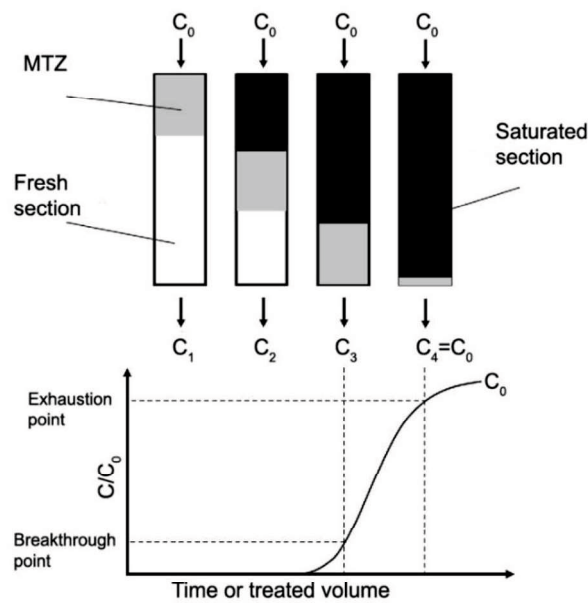


Figure 2.9 – Mass transfer zone and breakthrough curve of adsorption process in a fixed-bed column in different stages.

Several mathematical mass transfer models have been developed to predict the behavior of dynamic adsorption onto a fixed-bed column adsorption system. The modeling of breakthrough curves is significant for designing a column adsorption system for practical applications. In this study, three nonlinear mathematical model equations, Yoon-Nelson, Thomas, and modified-dose-response (MDR) models, were used. The Yoon-Nelson model is developed based on the assumption that the decrease in the adsorption probability of each molecule is proportional to the adsorption probability of the molecule and the probability of the molecule breakthrough on the adsorbent. The Yoon-Nelson model can be expressed by Equation 2.11 [74]:

$$\ln\left(\frac{C}{C_0 - C}\right) = k_{YN}t - \tau k_{YN} \quad (2.11)$$

where C_0 and C are the influent and effluent phosphate concentrations (mg/L), respectively, t is the time required to reach exhaustion time (min), k_{YN} is the Yoon-Nelson kinetic coefficient (1/min), and τ is the time required for 50% phosphate adsorption breakthrough (min).

The Thomas model is one of the most general and widely used theoretical methods to describe column performance. It assumes that the adsorption is only controlled by the surface reaction between adsorbate and adsorbent surface, where the effects of intraparticle diffusion and external film resistances are neglected. Thomas model is presented by Equation 2.11 [74]:

$$\ln\left(\frac{C_0}{C} - 1\right) = \frac{k_{Th}q_{Th}m}{Q} - k_{Th}C_0t \quad (2.12)$$

where Q is the flow rate (mL min^{-1}), q_{Th} is the predicted adsorption capacity of the Thomas model (mg/g), and k_{Th} is the Thomas kinetic coefficient (L/mg min).

A model initially developed for pharmacological studies, the MDR model, was developed based on mathematical issues to reduce the error resulting from the Thomas model. The MDR model can be expressed by Equation 2.13 [83]:

$$\ln\left(\frac{C}{C_0 - C}\right) = a \ln\left(\frac{C_0Qt}{1000}\right) - a \ln q_{mdr}m \quad (2.13)$$

where m is the weight of adsorbent packed inside the column (g), q_{mdr} is the predicted adsorption capacity of the MDR model (mg/g), and a is an MDR model parameter.

References

- [1] The Editors of Encyclopaedia Britannica, Phosphorus, *Encycl. Br.* (2019). <https://www.britannica.com/science/phosphorus-chemical-element>.
- [2] V. Ji Ram, A. Sethi, M. Nath, R. Pratap, Phosphorous-Based Heterocycles, in: V. Ji Ram, A. Sethi, M. Nath, R.B.T.-T.C. of H. Pratap (Eds.), *Chem. Heterocycles Chem. Six to Eight Membered N,O, S, P Se Heterocycles*, Elsevier, 2019: pp. 457–468. <https://doi.org/https://doi.org/10.1016/B978-0-12-819210-8.00005-9>.
- [3] A.S. Wagh, Chapter 4 - Phosphate Chemistry, in: A.S.B.T.-C.B.P.C. (Second E. Wagh (Ed.), Elsevier, 2016: pp. 51–60. <https://doi.org/https://doi.org/10.1016/B978-0-08-100380-0.00004-X>.
- [4] A.S. Wagh, Chapter 8 - Crystal Structure, Mineralogy of Orthophosphates, in: A.S.B.T.-C.B.P.C. (Second E. Wagh (Ed.), Elsevier, 2016: pp. 99–113. <https://doi.org/https://doi.org/10.1016/B978-0-08-100380-0.00008-7>.
- [5] S. Daneshgar, A. Callegari, A. Capodaglio, D. Vaccari, The Potential Phosphorus Crisis:

- Resource Conservation and Possible Escape Technologies: A Review, *Resources*. 7 (2018) 37. <https://doi.org/10.3390/resources7020037>.
- [6] D.E.C. Corbridge, *Phosphorus: An Outline of its Chemistry, Biochemistry and Uses*, Elsevier Science B.V., Netherlands, 1995. <https://doi.org/https://doi.org/10.1016/B978-0-444-89307-9.50006-4>.
- [7] Z. Tang, N. Kong, J. Ouyang, C. Feng, N.Y. Kim, X. Ji, C. Wang, O.C. Farokhzad, H. Zhang, W. Tao, *Phosphorus Science-Oriented Design and Synthesis of Multifunctional Nanomaterials for Biomedical Applications*, *Matter*. 2 (2020) 297–322. <https://doi.org/https://doi.org/10.1016/j.matt.2019.12.007>.
- [8] M. Lee, H.-Y. Ryu, E. Ko, D.-H. Ko, *Effects of Phosphorus Doping and Postgrowth Laser Annealing on the Structural, Electrical, and Chemical Properties of Phosphorus-Doped Silicon Films*, *ACS Appl. Electron. Mater.* 1 (2019) 288–301. <https://doi.org/10.1021/acsaelm.8b00057>.
- [9] L.E. Lampila, K.W. McMillin, *Phosphorus Additives in Food Processing*, in: O. Gutiérrez, K. Kalantar-Zadeh, R. Mehrotra (Eds.), *Clin. Asp. Nat. Added Phosphorus Foods*. Nutr. Heal., Springer New York, New York, NY, 2017: pp. 99–110. https://doi.org/10.1007/978-1-4939-6566-3_6.
- [10] M.M. Velencoso, A. Battig, J.C. Markwart, B. Schartel, F.R. Wurm, *Molecular Firefighting—How Modern Phosphorus Chemistry Can Help Solve the Challenge of Flame Retardancy*, *Angew. Chemie Int. Ed.* 57 (2018) 10450–10467. <https://doi.org/10.1002/anie.201711735>.
- [11] The Editors of *Encyclopaedia Britannica*, *Phosphorus cycle*, *Encycl. Br.* (2020). <https://www.britannica.com/science/phosphorus-cycle>.
- [12] T.L. Roberts, A.E. Johnston, *Phosphorus use efficiency and management in agriculture*, *Resour. Conserv. Recycl.* 105 (2015) 275–281. <https://doi.org/10.1016/j.resconrec.2015.09.013>.
- [13] FAO, *World fertilizer trends and outlook to 2022*, Rome, 2019.
- [14] UN, *World Population Prospects: the 2019 Revision*, New York, 2019. <https://esa.un.org/unpd/wpp/>.
- [15] R.B. Chowdhury, G.A. Moore, A.J. Weatherley, M. Arora, *Key sustainability challenges for the global phosphorus resource, their implications for global food security, and options for mitigation*, *J. Clean. Prod.* 140 (2017) 945–963. <https://doi.org/https://doi.org/10.1016/j.jclepro.2016.07.012>.
- [16] R. Waterman, *Phosphorus chemistry: discoveries and advances*, *Dalt. Trans.* 45 (2016) 1801–1803. <https://doi.org/10.1039/C6DT90013E>.

- [17] M.K. Hubbert, Energy from Fossil Fuels, *Science* (80-.). 109 (1949) 103–109. <http://www.jstor.org/stable/1676618>.
- [18] D. Cordell, J.-O. Drangert, S. White, The story of phosphorus: Global food security and food for thought, *Glob. Environ. Chang.* 19 (2009) 292–305. <https://doi.org/https://doi.org/10.1016/j.gloenvcha.2008.10.009>.
- [19] A.L. Smit, P.S. Bindraban, J.J. Shroeder, J.G. Conijin, V.D.M.H. G, Phosphorus in agriculture: global resources, trends and developments, Wageningen, The Netherlands, 2009. <http://www.pri.wur.nl/>.
- [20] E. Desmidt, K. Ghyselbrecht, Y. Zhang, L. Pinoy, B. Van der Bruggen, W. Verstraete, K. Rabaey, B. Meesschaert, Global Phosphorus Scarcity and Full-Scale P-Recovery Techniques: A Review, *Crit. Rev. Environ. Sci. Technol.* 45 (2015) 336–384. <https://doi.org/10.1080/10643389.2013.866531>.
- [21] R. Scholz, F.-W. Wellmer, Cycling and Anthropogenic Use of Phosphorus in the 21st Century: Geoscientific and Geosocial Foundations of Agriculture, *Better Crop. with Plant Food.* 103 (2019) 9–12. <http://bettercrops.org/10.24047/BC10319>.
- [22] M.Z. Aziz, M. Yaseen, M. Naveed, X. Wang, K. Fatima, Q. Saeed, A. Mustafa, Polymer-Paraburkholderia phytofirmans PsJN Coated Diammonium Phosphate Enhanced Microbial Survival, Phosphorous Use Efficiency, and Production of Wheat, *Agronomy.* 10 (2020) 1344. <https://doi.org/10.3390/agronomy10091344>.
- [23] C. Sartorius, J. von Horn, F. Tettenborn, Phosphorus Recovery from Wastewater—Expert Survey on Present Use and Future Potential, *Water Environ. Res.* 84 (2012) 313–322. <https://doi.org/https://doi.org/10.2175/106143012X13347678384440>.
- [24] P.S. Bindraban, C.O. Dimkpa, R. Pandey, Exploring phosphorus fertilizers and fertilization strategies for improved human and environmental health, *Biol. Fertil. Soils.* 56 (2020) 299–317. <https://doi.org/10.1007/s00374-019-01430-2>.
- [25] Y. Ding, F. Dong, J. Zhao, W. Peng, Q. Chen, B. Ma, Non-Point Source Pollution Simulation and Best Management Practices Analysis Based on Control Units in Northern China, *Int. J. Environ. Res. Public Health.* 17 (2020) 868. <https://doi.org/10.3390/ijerph17030868>.
- [26] The Council of The European Communities (CEC), Council Directive of 21 May 1991 concerning urban wastewater treatment (91/271/EEC), *Off. J. Eur. Communities.* L135 (1991) 40–52.
- [27] S.S. Rathore, P. Chandravanshi, A. Chandravanshi, K. Jaiswal, Eutrophication: Impacts of Excess Nutrient Inputs on Aquatic Ecosystem, *IOSR J. Agric. Vet. Sci.* 09 (2016) 89–96. <https://doi.org/10.9790/2380-0910018996>.

- [28] J. Pu, S. Wang, Z. Ni, Y. Wu, X. Liu, T. Wu, H. Wu, Implications of phosphorus partitioning at the suspended particle-water interface for lake eutrophication in China's largest freshwater lake, Poyang Lake, *Chemosphere*. 263 (2021) 128334. <https://doi.org/10.1016/j.chemosphere.2020.128334>.
- [29] C.N. Sawyer, Basic Concepts of Eutrophication, *J. (Water Pollut. Control Fed.* 38 (1966) 737–744. <http://www.jstor.org/stable/25035549>.
- [30] M. Nanda, D. Cordell, A. Kansal, Assessing national vulnerability to phosphorus scarcity to build food system resilience: The case of India, *J. Environ. Manage.* 240 (2019) 511–517. <https://doi.org/https://doi.org/10.1016/j.jenvman.2019.03.115>.
- [31] V. Smil, PHOSPHORUS IN THE ENVIRONMENT: Natural Flows and Human Interferences, *Annu. Rev. Energy Environ.* 25 (2000) 53–88. <https://doi.org/10.1146/annurev.energy.25.1.53>.
- [32] P.M. Nyenje, J.W. Foppen, S. Uhlenbrook, R. Kulabako, A. Muwanga, Eutrophication and nutrient release in urban areas of sub-Saharan Africa — A review, *Sci. Total Environ.* 408 (2010) 447–455. <https://doi.org/10.1016/j.scitotenv.2009.10.020>.
- [33] R.W. McDowell, A. Noble, P. Pletnyakov, B.E. Haggard, L.M. Mosley, Global mapping of freshwater nutrient enrichment and periphyton growth potential, *Sci. Rep.* 10 (2020) 3568. <https://doi.org/10.1038/s41598-020-60279-w>.
- [34] R.W. McDowell, D.P. Hamilton, Nutrients and eutrophication: introduction, *Mar. Freshw. Res.* 64 (2013) iii. <https://doi.org/10.1071/MF13059>.
- [35] P.S. Kumar, L. Korving, M.C.M. van Loosdrecht, G.J. Witkamp, Adsorption as a technology to achieve ultra-low concentrations of phosphate: Research gaps and economic analysis, *Water Res.* X. 4 (2019) 100029. <https://doi.org/10.1016/j.wroa.2019.100029>.
- [36] M. Preisner, E. Neverova-Dziopak, Z. Kowalewski, An Analytical Review of Different Approaches to Wastewater Discharge Standards with Particular Emphasis on Nutrients, *Environ. Manage.* 66 (2020) 694–708. <https://doi.org/10.1007/s00267-020-01344-y>.
- [37] Ministry of Environment, Environmental standards for water pollution (in Japanese), *Minist. Environ. Gov. Japan.* (1971). <http://www.env.go.jp/kijun/mizu.html> (accessed February 24, 2021).
- [38] P.J.T.M. van Puijenbroek, A.H.W. Beusen, A.F. Bouwman, Global nitrogen and phosphorus in urban waste water based on the Shared Socio-economic pathways, *J. Environ. Manage.* 231 (2019) 446–456. <https://doi.org/10.1016/j.jenvman.2018.10.048>.

- [39] M. Huber, K. Athanasiadis, B. Helmreich, Phosphorus removal potential at sewage treatment plants in Bavaria – a case study, *Environ. Challenges*. 1 (2020) 100008. <https://doi.org/10.1016/j.envc.2020.100008>.
- [40] E.S. Tarleton, R.J. Wakeman, Pretreatment of suspensions, in: *Solid/Liquid Sep.*, Elsevier, 2007: pp. 126–151. <https://doi.org/10.1016/B978-185617421-3/50003-1>.
- [41] J. Derco, R. Kuffa, B. Urminská, J. Dudáš, J. Kušnierová, Influence of Phosphorus Precipitation on Wastewater Treatment Processes, in: K. Jian (Ed.), *Oper. Res. Art Mak. Good Decis., InTech*, 2016. <https://doi.org/10.5772/65492>.
- [42] H. Helness, Biological phosphorus removal in a moving bed biofilm reactor, Norwegian University of Science and Technology, 2007.
- [43] Q. Wang, Z. Liao, D. Yao, Z. Yang, Y. Wu, C. Tang, Phosphorus immobilization in water and sediment using iron-based materials: A review, *Sci. Total Environ.* 767 (2021) 144246. <https://doi.org/10.1016/j.scitotenv.2020.144246>.
- [44] J. Zhao, Q. Yuan, Y. Sun, J. Zhang, D. Zhang, R. Bian, Effect of fluoxetine on enhanced biological phosphorus removal using a sequencing batch reactor, *Bioresour. Technol.* 320 (2021) 124396. <https://doi.org/10.1016/j.biortech.2020.124396>.
- [45] J.C. Lamb III, Biological phosphorus removal: current status and future prospects, The Soap and Detergent Association, New York, NY, 1984.
- [46] G.A. Ekama, Biological Nutrient Removal, in: P.B.T.-T. on W.S. Wilderer (Ed.), *Treatise Water Sci.*, Elsevier, Oxford, 2011: pp. 409–526. <https://doi.org/10.1016/B978-0-444-53199-5.00094-4>.
- [47] N. Powell, A.N. Shilton, S. Pratt, Y. Chisti, Factors Influencing Luxury Uptake of Phosphorus by Microalgae in Waste Stabilization Ponds, *Environ. Sci. Technol.* 42 (2008) 5958–5962. <https://doi.org/10.1021/es703118s>.
- [48] A. Khoshmanesh, B.T. Hart, A. Duncan, R. Beckett, Luxury uptake of phosphorus by sediment bacteria, *Water Res.* 36 (2002) 774–778. [https://doi.org/10.1016/S0043-1354\(01\)00272-X](https://doi.org/10.1016/S0043-1354(01)00272-X).
- [49] A. Oehmen, P. Lemos, G. Carvalho, Z. Yuan, J. Keller, L. Blackall, M. Reis, Advances in enhanced biological phosphorus removal: From micro to macro scale, *Water Res.* 41 (2007) 2271–2300. <https://doi.org/10.1016/j.watres.2007.02.030>.
- [50] J.T. Bunce, E. Ndam, I.D. Ofiteru, A. Moore, D.W. Graham, A Review of Phosphorus Removal Technologies and Their Applicability to Small-Scale Domestic Wastewater Treatment Systems, *Front. Environ. Sci.* 6 (2018). <https://doi.org/10.3389/fenvs.2018.00008>.

- [51] H. Hiroyuki, I. Katsutoshi, Phosphorus Recovery by Crystallization, in: T. Zhang (Ed.), Phosphorus - Recover. Recycl., IntechOpen, 2018. <https://doi.org/10.5772/intechopen.81549>.
- [52] F. Ulu, M. Kobya, Ammonia removal from wastewater by air stripping and recovery struvite and calcium sulphate precipitations from anesthetic gases manufacturing wastewater, J. Water Process Eng. 38 (2020) 101641. <https://doi.org/10.1016/j.jwpe.2020.101641>.
- [53] Y. Gao, B. Liang, H. Chen, P. Yin, An experimental study on the recovery of potassium (K) and phosphorous (P) from synthetic urine by crystallization of magnesium potassium phosphate, Chem. Eng. J. 337 (2018) 19–29. <https://doi.org/10.1016/j.cej.2017.12.077>.
- [54] H. Jang, S.-H. Kang, Phosphorus removal using cow bone in hydroxyapatite crystallization, Water Res. 36 (2002) 1324–1330. [https://doi.org/10.1016/S0043-1354\(01\)00329-3](https://doi.org/10.1016/S0043-1354(01)00329-3).
- [55] X. Chen, H. Kong, D. Wu, X. Wsng, Y. Lin, Phosphate removal and recovery through crystallization of hydroxyapatite using xonotlite as seed crystal, J. Environ. Sci. 21 (2009) 575–580. [https://doi.org/10.1016/S1001-0742\(08\)62310-4](https://doi.org/10.1016/S1001-0742(08)62310-4).
- [56] H. Bacelo, A.M.A. Pintor, S.C.R. Santos, R.A.R. Boaventura, C.M.S. Botelho, Performance and prospects of different adsorbents for phosphorus uptake and recovery from water, Chem. Eng. J. 381 (2020) 122566. <https://doi.org/10.1016/j.cej.2019.122566>.
- [57] R. Liu, L. Chi, X. Wang, Y. Sui, Y. Wang, H. Arandiyan, Review of metal (hydr)oxide and other adsorptive materials for phosphate removal from water, J. Environ. Chem. Eng. 6 (2018) 5269–5286. <https://doi.org/10.1016/j.jece.2018.08.008>.
- [58] A. Sperlich, Phosphate Adsorption onto Granular Ferric Hydroxide (GFH) for Wastewater Reuse, Technische Universität Berlin, 2010. <https://doi.org/10.14279/depositonce-2573>.
- [59] A. Sperlich, Phosphate Adsorption onto Granular Ferric Hydroxide (GFH) for Wastewater Reuse, Technische Universität Berlin, 2010. <https://doi.org/10.14279/depositonce-2573>.
- [60] M. Bilal, J.A. Shah, T. Ashfaq, S.M.H. Gardazi, A.A. Tahir, A. Pervez, H. Haroon, Q. Mahmood, Waste biomass adsorbents for copper removal from industrial wastewater—A review, J. Hazard. Mater. 263 (2013) 322–333. <https://doi.org/10.1016/j.jhazmat.2013.07.071>.
- [61] O. Panasiuk, Phosphorus Removal and Recovery from Wastewater using Magnetite, KTH Royal Institute of Technology, 2010. <http://kth.diva->

portal.org/smash/get/diva2:473397/FULLTEXT01.pdf.

- [62] L.E. de-Bashan, Y. Bashan, Recent advances in removing phosphorus from wastewater and its future use as fertilizer (1997–2003), *Water Res.* 38 (2004) 4222–4246. <https://doi.org/10.1016/j.watres.2004.07.014>.
- [63] B. Li, H.M. Huang, I. Boiarkina, W. Yu, Y.F. Huang, G.Q. Wang, B.R. Young, Phosphorus recovery through struvite crystallisation: Recent developments in the understanding of operational factors, *J. Environ. Manage.* 248 (2019) 109254. <https://doi.org/https://doi.org/10.1016/j.jenvman.2019.07.025>.
- [64] N. Pitakteeratham, A. Hafuka, H. Satoh, Y. Watanabe, High efficiency removal of phosphate from water by zirconium sulfate-surfactant micelle mesostructure immobilized on polymer matrix, *Water Res.* 47 (2013) 3583–3590. <https://doi.org/10.1016/j.watres.2013.04.006>.
- [65] M. Li, J. Liu, Y. Xu, G. Qian, Phosphate adsorption on metal oxides and metal hydroxides: A comparative review, *Environ. Rev.* 24 (2016) 319–332. <https://doi.org/10.1139/er-2015-0080>.
- [66] R. Chitrakar, S. Tezuka, A. Sonoda, K. Sakane, K. Ooi, T. Hirotsu, Selective adsorption of phosphate from seawater and wastewater by amorphous zirconium hydroxide, *J. Colloid Interface Sci.* 297 (2006) 426–433. <https://doi.org/https://doi.org/10.1016/j.jcis.2005.11.011>.
- [67] M.A.H. Johir, M. Pradhan, P. Loganathan, J. Kandasamy, S. Vigneswaran, Phosphate adsorption from wastewater using zirconium (IV) hydroxide: Kinetics, thermodynamics and membrane filtration adsorption hybrid system studies, *J. Environ. Manage.* 167 (2016) 167–174. <https://doi.org/10.1016/j.jenvman.2015.11.048>.
- [68] Y. Su, H. Cui, Q. Li, S. Gao, J.K. Shang, Strong adsorption of phosphate by amorphous zirconium oxide nanoparticles, *Water Res.* 47 (2013) 5018–5026. <https://doi.org/10.1016/j.watres.2013.05.044>.
- [69] H. Liu, X. Sun, C. Yin, C. Hu, Removal of phosphate by mesoporous ZrO₂, *J. Hazard. Mater.* 151 (2008) 616–622. <https://doi.org/10.1016/j.jhazmat.2007.06.033>.
- [70] L.A. Rodrigues, L.J. Maschio, L. de S.C. Coppio, G.P. Thim, M.L.C. Pinto da Silva, Adsorption of phosphate from aqueous solution by hydrous zirconium oxide, *Environ. Technol.* 33 (2012) 1345–1351. <https://doi.org/10.1080/09593330.2011.632651>.
- [71] J. Wang, Y. Liu, P. Hu, R. Huang, Adsorption of phosphate from aqueous solution by Zr(IV)-crosslinked quaternized chitosan/bentonite composite, *Environ. Prog. Sustain. Energy.* 37 (2018) 267–275. <https://doi.org/10.1002/ep.12667>.

- [72] J.-Q. Jiang, S.M. Ashekuzaman, Preparation and evaluation of layered double hydroxides (LDHs) for phosphate removal, *Desalin. Water Treat.* 55 (2015) 836–843. <https://doi.org/10.1080/19443994.2014.934734>.
- [73] K.H. Goh, T.T. Lim, Z. Dong, Application of layered double hydroxides for removal of oxyanions: A review, *Water Res.* 42 (2008) 1343–1368. <https://doi.org/10.1016/j.watres.2007.10.043>.
- [74] T.A.H. Nguyen, H.H. Ngo, W.S. Guo, T.Q. Pham, F.M. Li, T. V Nguyen, X.T. Bui, Adsorption of phosphate from aqueous solutions and sewage using zirconium loaded okara (ZLO): Fixed-bed column study, *Sci. Total Environ.* 523 (2015) 40–49. <https://doi.org/https://doi.org/10.1016/j.scitotenv.2015.03.126>.
- [75] X. Liu, L. Zhang, Removal of phosphate anions using the modified chitosan beads: Adsorption kinetic, isotherm and mechanism studies, *Powder Technol.* 277 (2015) 112–119. <https://doi.org/https://doi.org/10.1016/j.powtec.2015.02.055>.
- [76] H. Miyauchi, T. Yamamoto, R. Chitrakar, Y. Makita, Z. Wang, J. Kawai, T. Hirotsu, Phosphate adsorption site on zirconium ion modified MgAl-layered double hydroxides, *Top. Catal.* 52 (2009) 714–723. <https://doi.org/10.1007/s11244-009-9209-1>.
- [77] K. Mandel, A. Drenkova-Tuhtan, F. Hutter, C. Gellermann, H. Steinmetz, G. SEXTL, Layered double hydroxide ion exchangers on superparamagnetic microparticles for recovery of phosphate from waste water, *J. Mater. Chem. A.* 1 (2013) 1840–1848. <https://doi.org/10.1039/c2ta00571a>.
- [78] R. Chitrakar, S. Tezuka, J. Hosokawa, Y. Makita, A. Sonoda, K. Ooi, T. Hirotsu, Uptake properties of phosphate on a novel Zr-modified MgFe-LDH(CO₃), *J. Colloid Interface Sci.* 349 (2010) 314–320. <https://doi.org/10.1016/j.jcis.2010.05.068>.
- [79] R. Chitrakar, S. Tezuka, A. Sonoda, K. Sakane, K. Ooi, T. Hirotsu, Synthesis and phosphate uptake behavior of Zr⁴⁺ incorporated MgAl-layered double hydroxides, *J. Colloid Interface Sci.* 313 (2007) 53–63. <https://doi.org/10.1016/j.jcis.2007.04.004>.
- [80] D. Tichit, N. Das, B. Coq, R. Durand, Preparation of Zr-Containing Layered Double Hydroxides and Characterization of the Acido-Basic Properties of Their Mixed Oxides, *Chem. Mater.* 14 (2002) 1530–1538. <https://doi.org/10.1021/cm011125l>.
- [81] J. Wang, X. Guo, Adsorption isotherm models: Classification, physical meaning, application and solving method, *Chemosphere.* 258 (2020) 127279. <https://doi.org/10.1016/j.chemosphere.2020.127279>.
- [82] H. Patel, Fixed-bed column adsorption study: a comprehensive review, *Appl. Water Sci.* 9 (2019) 45. <https://doi.org/10.1007/s13201-019-0927-7>.

- [83] G. Yan, T. Viraraghavan, M. Chen, A New Model for Heavy Metal Removal in a Biosorption Column, *Adsorpt. Sci. Technol.* 19 (2001) 25–43. <https://doi.org/10.1260/0263617011493953>.

CHAPTER 3

PHOSPHATE ADSORPTION AND DESORPTION ON TWO-STAGE SYNTHESIZED AMORPHOUS-ZIRCONIUM (HYDR)OXIDE/MgFe LAYERED DOUBLE HYDROXIDES COMPOSITE

3.1. Introduction

Phosphorus is imperative for the growth of all living things and is also used in food production [1]. However, excessive discharge of phosphorus in water bodies often causes serious eutrophication problems, which leads to algal blooms, the disruption of aquatic ecosystems, and water quality deterioration [2]. Different treatment techniques have been developed to eliminate phosphorus (usually existing as phosphate in water) contamination, including biological and chemical methods, which have been widely used in wastewater treatment [3]. However, these methods have some limitations, such as the high cost of neutralizing products and handling the produced sludge for chemical methods [4], and inefficient elimination of trace levels of phosphate for biological methods [5]. Moreover, the resultant treated water often fails to meet the strict regulatory quality standard for phosphorus, which has recently become more stringent for wastewater treatment in some countries [6]. For example, the standard has been revised from 1.0 to 0.5 mg-P L⁻¹ in China, and from 2.0 to 0.2 mg-P L⁻¹ in some areas of Korea [7]. The concentration of phosphorus must be maintained as low as possible—even in waterbodies that are assessed as having a ‘good’ environmental condition—in order to conserve the water environment for the next generation, especially considering the difficulty of restoring eutrophic waterbodies.

Phosphate rock deposits are a non-renewable resource, and experts estimate that reserves will only last until 2170, given the present usage and population growth rate [8]. Hence, the recovery and reuse of phosphorus offer the best strategies to meet the future phosphorus demand. Accordingly, adsorption represents a fascinating separation technique for phosphate from water because of the possibility of phosphorus recovery [5]. Moreover, this approach has many advantages, such as efficient, easy operating conditions, low sludge production, and the possibility of regenerating the adsorbent [9].

In recent decades, layered double hydroxides (LDH) materials have become very attractive as an inorganic anion adsorbent for deterring pollution in nature by anion exchange in the interlayer [10]. LDH is a layered material with hydroxide sheets, where a net positive charge is developed on the layer because trivalent cations partially substitute divalent cations. Unfortunately, the anion adsorption capacity of LDH is greatly influenced by the calcination process during the synthesis of LDH, whereby calcined LDH generally exhibits a higher adsorption capacity than uncalcined LDH [11,12]. Moreover, a high

temperature, which requires additional energy, is needed both for the synthesis process and for the reuse of the material. In this study, a new composite of LDH is explored to eliminate the high-temperature requirement during the synthesis process.

Many researchers have reported that the functionalization of zirconium (hydr)oxide, an eco-friendly compound, markedly enhanced the phosphate adsorption ability of adsorbents [13–15]. This clearly relates to the fact that Zr(IV) is easily hydrolyzed to form tetranuclear ions or octanuclear species, thus producing a large number of hydroxyl ions and water molecules, which are involved in the exchange of ligands with phosphate ions in solution [16]. However, the application of pure zirconia is relatively high cost and requires a combination with other low-cost materials to make it more cost-effective. Since LDH is a bio-safe, low-cost, and environmentally friendly [17], combining zirconia with LDH is an attractive approach to lower the cost of zirconia application and produce an environment-friendly adsorbent. Moreover, enabling crystallization of zirconium (hydr)oxides on the LDH matrix can suppress the crystal growth resulting in nanosized particles, in which nanosized adsorbents are preferable because the crystal has a large number of adsorption sites.

Several studies have investigated the adsorption of phosphate by Zr modified LDH [18–20]. However, the type of modification of Zr to LDH remains unclear, as research is inconclusive over whether the Zr ions are distributed in the octahedral sites of the LDH layer, or if the growth of zirconium (hydr)oxides occurs separately and they form a composite with LDH. As reported by Tichit et al. (2002) and Velu et al. (1998), the mixing of solutions simultaneously containing LDH and Zr ions by a simple coprecipitation method resulted in the modification and incorporation of Zr into the LDH layers [21,22]. Although the uptake properties of phosphate by Zr modified MgFe layered double hydroxides (MgFe-LDH), which was synthesized with the coprecipitation method, were studied by Chitrakar et al. (especially in seawater) [18], the effect of zirconium (hydr)oxide on the adsorption stability of composites at low pH, as well as the adsorption kinetics and thermodynamics of composites, have not yet been explained.

In this study, a composite of amorphous zirconium (hydr)oxide (am-Zr) and MgFe-LDH was synthesized, and its application for phosphate removal was systematically examined. The synthesis of the LDH and the addition of Zr to the LDH were performed separately into two stages to minimize the possibility of the LDH structural layer being modified by Zr ions. This new preparation method implies further investigation of phosphate adsorption characteristics of the composite, whereas a different preparation method could change the phosphate adsorption property of the same materials [19]. The characteristics of the composite at different Zr:Fe molar ratios were investigated, and their effect on the phosphate adsorption capacity was evaluated. The effect of pH and competing anions on

phosphate adsorption to the composite were also examined. Furthermore, adsorption kinetics, isotherm, and thermodynamic models were applied to explain the properties of phosphate adsorption. Meanwhile, the reusability of the composite as phosphate adsorbent was also considered.

3.2 Materials and methods

3.2.1 Materials

All the chemicals used in this study ($\text{FeCl}_3 \cdot 6\text{H}_2\text{O}$, $\text{MgCl}_2 \cdot 6\text{H}_2\text{O}$, $\text{ZrOCl}_2 \cdot 8\text{H}_2\text{O}$, Na_2CO_3 , K_2HPO_4 , NaOH , and HCl) were analytical pure-grade reagents that acquired from FUJIFILM Wako Pure Chemical Corporation, and used in their conditions as received without further purification. Deionized (DI) water was used for the preparation of the metal salt solutions.

3.2.2 Preparation of am-Zr/MgFe-LDH

The composites were synthesized in two stages by the combination of coprecipitation and hydrothermal methods. For the first stage, a solution containing FeCl_3 and MgCl_2 with an $\text{Mg}^{2+}:\text{Fe}^{3+}$ molar ratio of 3:1 and a solution containing 1 M NaOH and 1 M Na_2CO_3 with a 3:1 volume ratio were added dropwise into 200 mL DI water under vigorous stirring. A pH of 10 was maintained under continuous stirring at room temperature (~ 298 K) for 30 min. The obtained gel was filtered and washed five times with DI water. For the second stage, the fresh LDH gel was dissolved into 500 mL of DI water. Different volumes of 1 M ZrOCl_2 were added to obtain various Zr contents in the composites (0.5, 1.0, 1.5, and 2.0 Zr/Fe molar ratios). Concurrently, a 25% NaOH solution was added to precipitate out the zirconium (hydr)oxide until a pH of ~ 10 was reached, and was then stirred continuously for 30 min. The resultant precipitates were aged at 353 K for 24 h, whereby the gel was left in solution as a means of improving its crystallization. They were then separated and washed by DI water until the filtrate pH was ~ 7 before being dried in an oven at 353 K for 24 h. As a comparison, MgFe-LDH (hereafter LDH) and am-Zr were also synthesized separately under the same conditions as those used for the composite synthesis. Calcined samples were obtained by heating at 573 K for 3 h.

3.2.3 Characterization of am-Zr/MgFe-LDH

X-ray diffraction (XRD) patterns were recorded on Rigaku Ultima IV Protectus diffractometer using $\text{Cu-K}\alpha$ radiation at 40 kV, with a scanning speed of 1°min^{-1} and 2θ angle ranging from 5° to 70° . Fourier-transform infrared (FTIR) spectra of the samples were recorded on a Jasco FT/IR-4600 spectrophotometer within the range of 4000 to 600 cm^{-1} .

Scanning electron microscopy (SEM) images were collected by using a JEOL JSM-7600F field emission SEM at an accelerating voltage of 5 kV, in which the powdered samples were prepared on a carbon tape coated with a platinum film. X-ray photoelectron spectroscopy (XPS) spectra were obtained using a Thermo Scientific K-alpha X-ray photoelectron spectrometer.

3.2.4 Batch adsorption experiments

K₂HPO₄ (99.0%) was used to prepare a stock of phosphate solution, which was then diluted to the desired concentration using DI water to obtain the working solution. The solution was adjusted to the desired pH by using diluted HCl and NaOH. The sample (0.01 g) was shaken in 100 mL of the K₂HPO₄ solution (10 mg-P L⁻¹) at 140 rpm for 24 h. The supernatant was collected using a syringe and filtered through a 0.45 µm filter. The residual phosphate concentration was analyzed in triplicate using the ascorbic acid method and a Hitachi U-1800 UV/vis spectrophotometer at a wavelength of 880 nm. The phosphate adsorption capacity was calculated using Equation (3.1):

$$q_e = \frac{C_0 - C}{m} \times V \quad (3.1)$$

where q_e is the amount of adsorbed phosphate (mg-P g⁻¹), C_0 and C are the initial and residual phosphate concentrations (mg L⁻¹), respectively, m is the weight of the adsorbent (g), and V is the volume of the solution (L).

The effects of pH and competing anions on the adsorption capacity were investigated by shaking 0.01 g of sample in 100 mL of 3 mg-P L⁻¹ phosphate solution at different pH (2–10) and concentrations (0.005 M and 0.01 M) of anions (Cl⁻, NO₃⁻, SO₄²⁻, and HCO₃⁻), respectively. The adsorption kinetics was investigated by shaking a 0.01 g sample in 100 mL of 10 mg-P L⁻¹ phosphate solution. At various intervals between 0.5 h to 36 h, supernatants were collected for the determination of their phosphate concentration. The adsorption thermodynamics and adsorption isotherm were studied by different initial phosphate concentrations (1–50 mg L⁻¹) at three different temperatures (290, 307, and 324 K) for 24 h.

3.2.5 Desorption experiments

The desorption ability of the adsorbent was investigated using NaOH (0.01, 0.1, 1, and 2 N) solutions at time intervals between 1 and 60 min. After the adsorption of 0.1 g of each sample in 10 mg-P L⁻¹ of phosphate solution, the phosphate-loaded samples were filtered and dried at 373 K for 24 h. The dried samples were subsequently dispersed in 50 mL of each NaOH solution and shaken at 150 rpm. The phosphate concentration in the

supernatants was measured as previously described in Section 2.4. The reusability of the adsorbent was examined by reusing the desorbed adsorbent in a seven-cycle adsorption-desorption experiment and measuring the adsorption performance at the end of each cycle. In each re-adsorption experiment, the sample was dried at 373 K for 24 h prior to the subsequent adsorption. The desorption efficiency (%) was calculated using Equation (3.2):

$$\% \text{Desorption} = \frac{CV}{qm} \times 100 \quad (3.2)$$

where C is the phosphate concentration (mg L^{-1}) after the desorption process, V is the volume of solution (L), q is the amount of phosphate adsorbed before the desorption process (mg-P g^{-1}), and m is the weight of adsorbent (g).

3.3 Results and discussion

3.3.1 Effect of Zr molar ratio and calcination

Figure 3.1a shows the phosphate adsorption ability of the LDH, am-Zr, and the composites both before and after calcination at 573 K. The composites are denoted as Zr(x)/LDH, where x stands for the Zr/Fe molar ratio in the composite. Calcination caused a significant increase in the phosphate adsorption of the LDH. This was due to the surface adsorption and memory effect (layered structure reconstruction) phenomena in the calcined LDH, while in the uncalcined LDH, most of the phosphate adsorption was only caused by anion exchange [23]. The addition of am-Zr to the LDH matrix in the calcined samples markedly decreased the adsorption capacity. The calcination process crystallized am-Zr to tetragonal ZrO_2 by eliminating the hydroxyl groups that were involved in the adsorption of phosphate as active sites, thus resulting in a significant reduction in phosphate adsorption.

The introduction of am-Zr in the LDH matrix in the uncalcined samples increased the adsorption capacity as the Zr content increased. In particular, a significant increase in the adsorption capacity occurred as the Zr/Fe molar ratio increased from 0 to 1.5 (from $30.40 \text{ mg-P g}^{-1}$ to $35.40 \text{ mg-P g}^{-1}$); however, only a slight increase was observed (to $35.70 \text{ mg-P g}^{-1}$) when the molar ratio was further increased to 2. The composites, except Zr(0.5)/LDH, had much higher adsorption capacities than the LDH ($17.99 \text{ mg-P g}^{-1}$) and am-Zr ($32.00 \text{ mg-P g}^{-1}$) samples individually.

The feasibility of adsorbents to economically adsorb phosphate based on the adsorption capacity obtained from the batch studies is shown in Figure 3.1b. The figure shows the cost of each adsorbent necessary to remove 1 mg-P of phosphate from a solution

derived from the use of chemicals in the preparation and energy in calcination. The figure specifies that the cost associated with the uncalcined composite with Zr/Fe molar ratio of 1.5 was found to be less than other studied adsorbents, except for the ratio of 2.0 that shows the same cost. The cost was not effectively decreased by further increasing the Zr/Fe molar ratio from 1.5 to 2.0. The price for removing phosphorus by am-Zr(1.5)/LDH was about half less in comparison to the calcined LDH. The elimination of the calcination process during the LDH synthesis by combining it with am-Zr can produce an economically feasible adsorbent. Moreover, the costs for phosphate removal by uncalcined composites are lower than am-Zr, indicating that the price of fully am-Zr usage as an adsorbent can be reduced by composite synthesis. Based on this result, the uncalcined Zr(1.5)/LDH sample was chosen for the following adsorption study, and the term ‘composite’ is used hereafter to refer specifically to this sample.

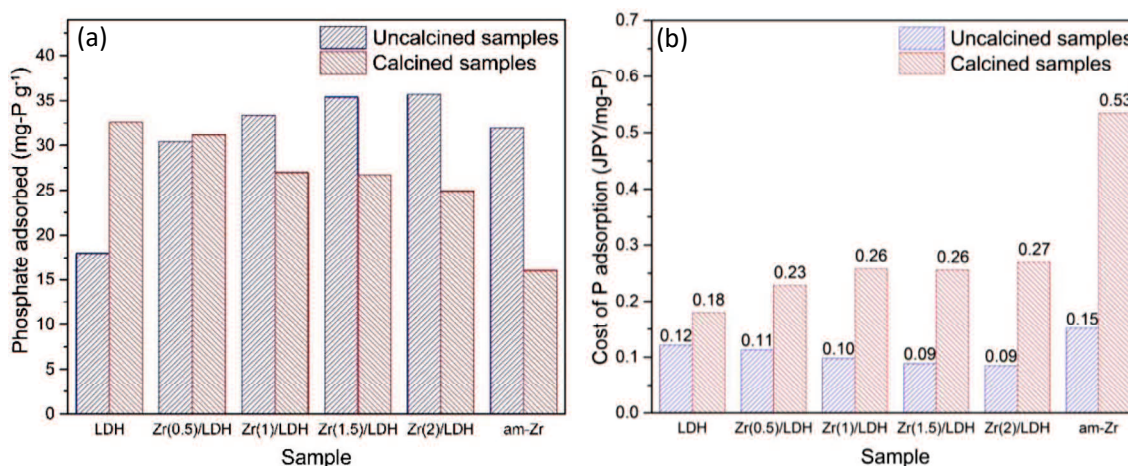


Figure 3.1 – (a) Phosphate adsorption on LDH, composites, and am-Zr, before and after calcination (Phosphate concentration: 10 mg-P L⁻¹; Dosage: 0.01 g; Volume: 100 mL; T = ~298 K; pH = 7; t = 24 h), and (b) Comparative cost for the removal of 1 mg-P of phosphate using studied adsorbents.

3.3.2 Characterization

The XRD patterns of the uncalcined LDH, am-Zr, composites are illustrated in Figure 3.2a. A broad halo around 20–40° of 2θ was observed in am-Zr, which is the typical pattern of amorphous zirconium (hydr)oxide [20]. The uncalcined LDH exhibited sharp peaks at 2θ of 11.6°, 23.14°, 34.24°, 38.46°, 45.64°, 59.64°, and 60.92°, which correlated with planes (003), (006), (009), (015), (018), (110), and (113) of LDH, respectively [24]. These typical peaks of LDH were also observed in the composites. The lattice parameters *c* and *a* of the LDH, which are related to the distance between two neighboring LDH layers and mean cation–cation space, respectively, were calculated using $c = d_{003} + 2d_{006} + 3d_{009}$ and $a = 2d_{110}$ [25]. These parameters were approximately the same between the LDH ($c = 23.16$ Å and a

= 3.08 Å) and the Zr(1.5)/LDH ($c = 23.20$ Å and $a = 3.10$ Å), thus indicating that the LDH layers were not modified by Zr atoms. In addition, the broad halo of the am-Zr was also observed in all of the composites, which indicates that they were the combination of the LDH and am-Zr with no other observed phase. With a lowering of the crystallinity, the adsorption capacity of the composite increased. This signifies that the lowering of the crystallinity corresponded to an increased specific surface area of the composite and an increased amount of hydroxyl groups that acted as active sites [26].

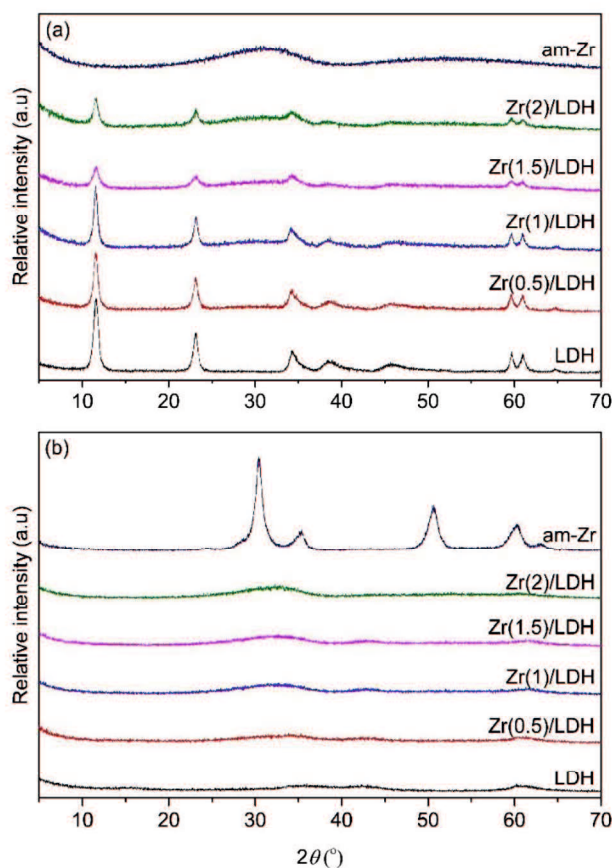


Figure 3.2 – X-ray powder diffraction patterns of LDH, composites, and am-Zr (a) before calcination, and (b) after calcination.

Figure 3.2b displays the XRD patterns of samples after calcination at 573 K for 3 hours. The am-Zr showed the typical diffraction peaks for tetragonal ZrO_2 . However, none of the composites exhibited diffraction peaks for crystalline ZrO_2 , thus indicating that zirconium hydroxide remained amorphous and had just started to be crystallized and had a very small tetragonal crystal, which was due to the interference of the LDH structure that collapsed during the calcination process. The patterns for the LDH and composite indicate that the

layered structure of the LDH completely collapsed due to the removal of structural water and carbonate anions from the interlayer.

The FTIR spectra of the LDH, composite, and am-Zr samples before calcination in the range of 4000–600 cm^{-1} is shown in Figure 3.3a. The OH stretching vibration and LDH interlayer carbonate regions can be found in this region. The intense and broad absorption band centered at around $\sim 3430 \text{ cm}^{-1}$ and the band at $\sim 1640 \text{ cm}^{-1}$ in all spectra could be attributed to the O-H stretching and bending vibrations caused by hydroxyl groups and physically adsorbed water molecules in the samples, respectively [27]. By comparing the FTIR spectrum of the composite with that of LDH and am-Zr, the bands of the Zr-OH bending vibration were observed at around $\sim 1353 \text{ cm}^{-1}$ and $\sim 1565 \text{ cm}^{-1}$, and the band indicating CO_3^{2-} antisymmetric stretching in the interlayer was detected at $\sim 1358 \text{ cm}^{-1}$ [28,29].

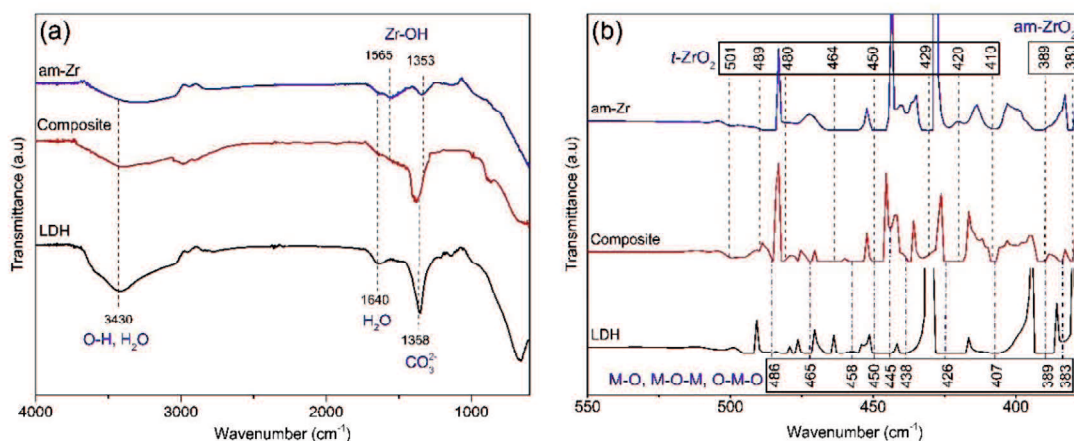


Figure 3.3 – FTIR spectra of LDH, composite (Zr(1.5)/LDH), and am-Zr before calcination in the range of (a) 4000–600 cm^{-1} , and (b) 550–350 cm^{-1} .

The lattice vibrations for all samples can be observed in the range of 550–350 cm^{-1} in the FTIR spectra, as shown in Figure 3.3b. All the bands marked for the LDH reference sample in Figure 3.3b represent the bending and stretching vibration of M–O, M–O–M, and O–M–O (M = Mg and Fe) [30–36]. The as-prepared am-Zr sample shows strong absorption bands $\sim 380 \text{ cm}^{-1}$ and $\sim 389 \text{ cm}^{-1}$ which are indicative for amorphous zirconia [37,38]. Moreover, the tetragonal zirconia ($t\text{-ZrO}_2$) bands [37,39–44] are also found in the am-Zr sample, as shown in Figure 3.3b, which demonstrate that the nucleation of the metastable $t\text{-ZrO}_2$ phase occurred at a few favored points inside the amorphous phase of the am-Zr sample during synthesis. This was predictable since the amorphous zirconium hydroxide has a similar structure with $t\text{-ZrO}_2$, and consequently it promotes the crystallization of $t\text{-ZrO}_2$ nanocomposite from amorphous structure [45]. All the observed bands in am-Zr and LDH

samples are found in the spectra of the composite sample, which signifies that the composite comprises the two primary components, i.e. am-Zr and MgFe-LDH.

The SEM images of the LDH, am-Zr, and composite are presented in Figure 3.4a–3.4c. The image of the LDH shows the formation of a platelet-like layered structure, which is characteristic of LDH materials, while the image of am-Zr appears to show nanosized particles agglomerated to a coral-like shape. The micrograph of the as-prepared composite reveals that the platelet-like structure of the LDH was demolished and broke into smaller nanoparticles with many pores. This combination suppressed the growth of the crystal size and reduced the agglomeration of ultrafine-sized zirconium (hydr)oxide. The morphology of the composite after adsorption (Figure 3.4d) was changed by the formation of a phosphate substance layer on its surface. From the typical XPS spectra shown in Figure 3.4e, the adsorption of phosphate onto the composite surface was confirmed by the appearance of the P 2p peak at 134.08 eV after adsorption [46].

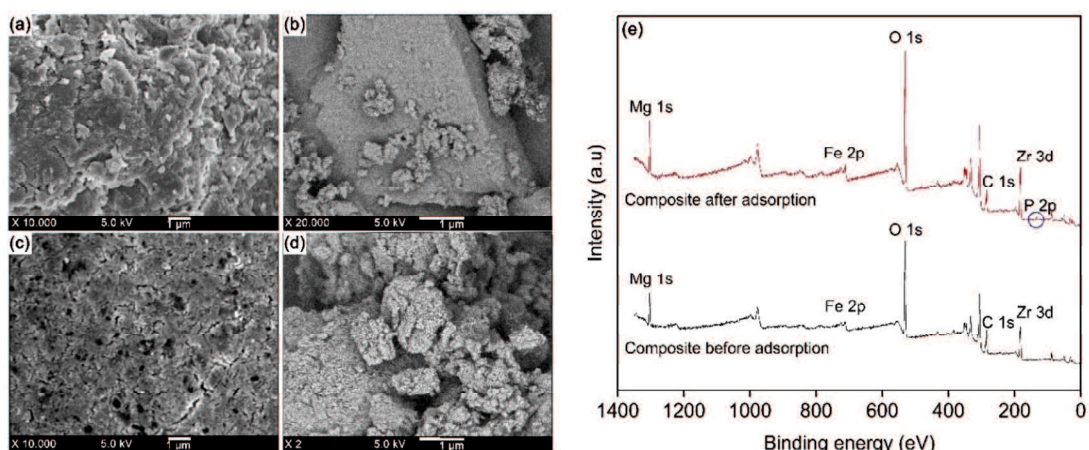


Figure 3.4 – Scanning electron micrographs of (a) LDH, (b) am-Zr, (c) composite before adsorption, and (d) composite after adsorption, and (e) XPS spectra of the composite before and after phosphate adsorption.

3.3.3 Effect of solution pH

The initial pH dependence graph of phosphate adsorption on the adsorbents is displayed in Figure 3.5. The composite and am-Zr exhibited a high phosphate adsorption capacity in very acidic conditions ($\text{pH} \leq 3$), while the adsorption ability of the LDH decreased sharply, which was possibly due to the potential dissolution of Fe and Mg in the LDH at very low pH [47]. The composite could maintain its adsorption ability at pH 2, which was mainly due to the high chemical inertness of zirconium (hydr)oxide even though the LDH could not preserve its structure at such low pH.

The high phosphate adsorption at low pH was primarily caused by the positively charged adsorbent surface due to protonated hydroxyl groups (OH_2^+), which strongly attracted phosphate anions (Li et al., 2016). On the other hand, the decreased removal efficiency at high pH was attributable to the adsorbent surface, which gradually became more negative due to the increased OH^- ions at higher pH. This led to a higher competition with phosphate ions for binding sites on the surface [49]. Moreover, H_2PO_4^- exists at low pH (2.1–7.2) and is more easily adsorbed on hydrated metal oxides than HPO_4^{2-} that exists at pH 7.2–12.36, thus resulting in a lower adsorption capacity at high pH [50].

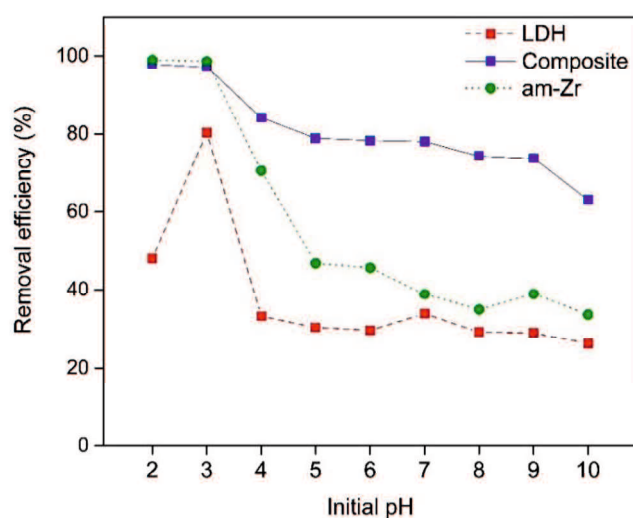


Figure 3.5 – Effect initial pH on phosphate adsorption. (Phosphate concentration: 3 mg-P L^{-1} ; Dosage: 0.01 g ; Volume: 100 mL ; $T = \sim 298 \text{ K}$; $t = 24 \text{ h}$).

The composite showed the highest adsorption over a wide initial pH range of 4–10, thereby indicating that adsorption on the composite was less dependent on the surface charge in comparison to the LDH and am-Zr. The am-Zr on the surface of the LDH likely increased the number of active sites and surface area, which minimized the competition of OH^- ions at high pH. The Lewis acid-base reaction was involved in adsorption under alkaline conditions and was intensified at high pH [46]. The active sites of the adsorbent acted as the Lewis acid, especially Zr atoms that have empty d-orbitals, whereas phosphate anions acted as the Lewis base and donated electrons to form a bond. This result implied that the composite has a wide applicable scope of the pH ranging from 2 to 10, which is suitable for practical utilization, considering that some adsorbents are susceptible to a wide pH range and become a serious problem for wastewater treatment applications that require a long contact time.

3.3.4 Effect of competing anions

Some anions, such as chloride (Cl^-), nitrate (NO_3^-), sulfate (SO_4^{2-}), and bicarbonate (HCO_3^-), exist along with phosphate ions in water bodies and wastewater and compete for adsorption sites on adsorbents. The phosphate removal efficiency in some ion solutions was measured to examine the selectivity of phosphate adsorption on the composite. The results are shown in Figure 3.6, which illustrates that the coexistence of Cl^- , NO_3^- , and SO_4^{2-} ions had no significant effect on phosphate adsorption, whereas the presence of HCO_3^- considerably decreased the removal efficiency. The HCO_3^- ion at a high concentration (high ratio of CO_3/PO_4) and $\text{pH} > 7$ has been found to generate a highly competitive effect with phosphate [51], whereby HCO_3^- also forms inner-sphere complexation with metal hydroxide surfaces [52]. The strong pentacyclic complex formed between Zr_4^+ and HCO_3^- in the surface of the composite greatly inhibited the adsorption of phosphate on the composite [53]. Moreover, the addition of HCO_3^- would be expected to raise the original solution pH to a basic condition which would, in turn, also decrease adsorption capacity. The results indicate that the composite is unsuitable for remediating phosphate from wastewater with a high HCO_3^- concentration.

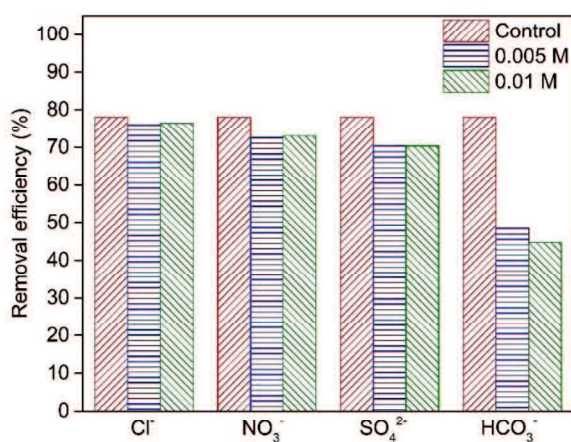


Figure 3.6 – Effect of common competing anions Cl^- , NO_3^- , SO_4^{2-} , and HCO_3^- on the phosphate removal efficiency. (Phosphate concentration: 3 mg-P L^{-1} ; Dosage: 0.01 g ; Volume: 100 mL ; $T = \sim 298 \text{ K}$; $t = 24 \text{ h}$).

3.3.5 Adsorption kinetics

The phosphate adsorption kinetics of the synthesized LDH, composite, and am-Zr are presented in Figure 3.7a. A rapid phosphate adsorption onto the composite was observed within the initial 6 hours, which then became slower until reaching equilibrium. This

adsorption rate was faster than that of am-Zr, which became slower and reached equilibrium after 9 hours. The LDH reached equilibrium for ~3 hours, but the adsorption capacity was markedly lower than that of the other samples.

To investigate the phosphate adsorption characteristics of the composite, the adsorption kinetics were analyzed using pseudo-first-order and pseudo-second-order models. These models are given by Equation (3.3) and (3.4), respectively:

$$\ln(q_e - q_t) = \ln(q_e) - k_1 t \quad (3.3)$$

$$\frac{t}{q_t} = \frac{1}{k_2 q_e^2} + \frac{1}{q_e} t \quad (3.4)$$

where q_e and q_t (mg g^{-1}) are the amount of adsorbed phosphate at equilibrium and time t , respectively; k_1 (h^{-1}) and k_2 ($\text{g mg}^{-1} \text{h}^{-1}$) are the rate constant of the pseudo-first-order model and pseudo-second-order model, respectively.

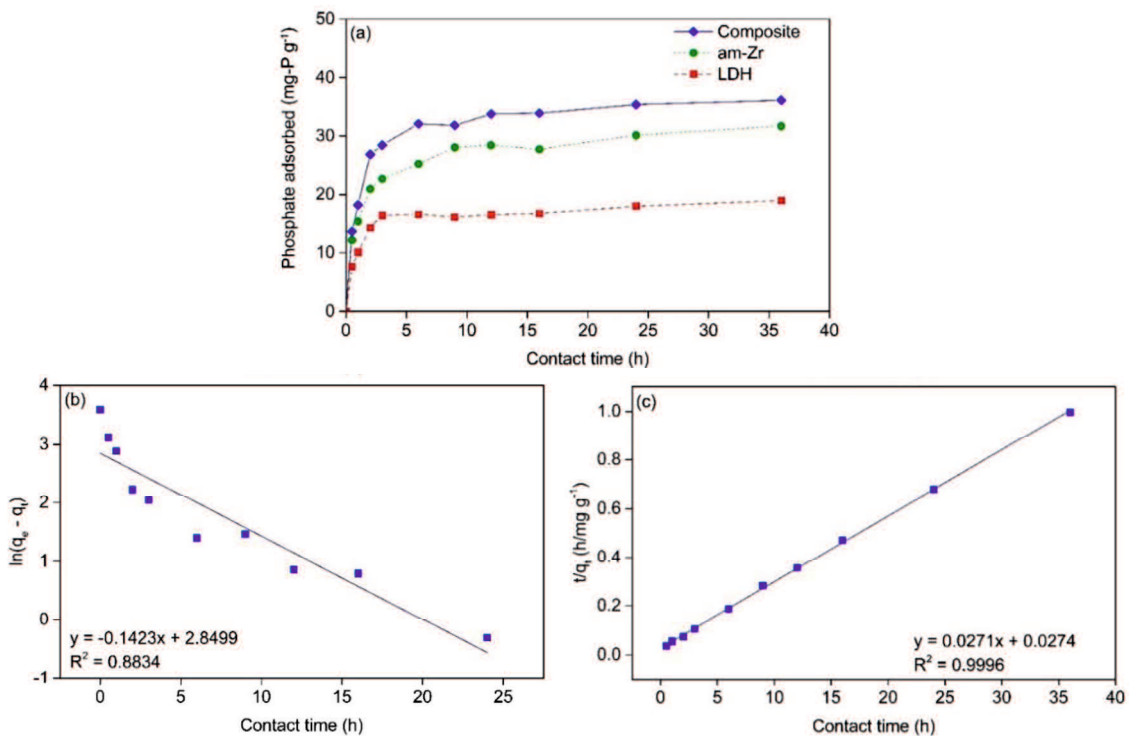


Figure 3.7 – The plots of: (a) phosphate adsorption capacity of LDH, composite, and am-Zr vs. contact time, (b) pseudo-first-order model of composite, and (c) pseudo-second-order model of composite. (Phosphate concentration: 10 mg-P L^{-1} ; Dosage: 0.01 g ; Volume: 100 mL ; $T \sim 298 \text{ K}$; $\text{pH} = 7$).

The linear regressions of the pseudo-first-order and pseudo-second-order models are presented in Figure 3.7b and 3.7c, respectively, and the detailed parametric data are shown

in Table 3.1. The correlation coefficient (R^2) of the pseudo-second-order model was higher than that of the pseudo-first-order model, and the calculated value of q_c (36.90 mg g⁻¹) obtained from the pseudo-second-order model was close to the experimental value of q_e (36.13 mg-P g⁻¹). This indicates that the phosphate adsorption process by the am-Zr/MgFe-LDH followed the pseudo-second-order model and chemisorption took control of the adsorption [54].

Table 3.1 – Kinetic model parameters for phosphate adsorption by am-Zr/MgFe-LDH.

Kinetics model	Parameter	Value
Pseudo-first-order model	q_e (mg-P g ⁻¹)	36.13
	q_c (mg g ⁻¹)	17.29
	k_1 (h ⁻¹)	0.3277
	R^2	0.8834
Pseudo-second-order model	q_e (mg-P g ⁻¹)	36.13
	q_c (mg g ⁻¹)	36.90
	k_2 (g mg ⁻¹ ·h ⁻¹)	0.0268
	R^2	0.9996

3.3.6 Adsorption isotherm

To understand the type of phosphate adsorption onto the composite, the adsorption isotherm was calculated using Langmuir, Freundlich, Temkin, and Dubinin–Radushkevich (D-R) isotherm models, which are defined by Equation (3.5), (3.6), (3.7), and (3.8) respectively:

$$q_e = \frac{q_m k_l C_e}{1 + k_l C_e} \quad (3.5)$$

$$q_e = k_f C_e^{\frac{1}{n}} \quad (3.6)$$

$$q_e = \frac{RT}{bt} \ln(k_t C_e) \quad (3.7)$$

$$q_e = q_m e^{-[RT \ln(1+1/C_e)]^2/2E^2} \quad (3.8)$$

where C_e (mg-P L⁻¹) is the phosphate equilibrium concentration; q_e (mg-P g⁻¹) is the equilibrium adsorption capacity of the adsorbent; q_m (mg g⁻¹) is the theoretical maximum adsorption capacity of the adsorbent; k_l (L g⁻¹) is the Langmuir adsorption constant associated with the adsorption energy; k_f (mg g⁻¹) is the Freundlich adsorption constant associated with the adsorption capacity; n is a constant related to adsorption intensity or

surface heterogeneity; k_t ($L\ mg^{-1}$) and b_t ($J\ mol^{-1}$) are an equilibrium binding constant and a constant related to the heat of adsorption, respectively; E ($kJ\ mol^{-1}$) is the mean free energy of adsorption; R is the universal gas constant ($8.314\ J\ K^{-1}\ mol^{-1}$); and T (K) is the absolute temperature.

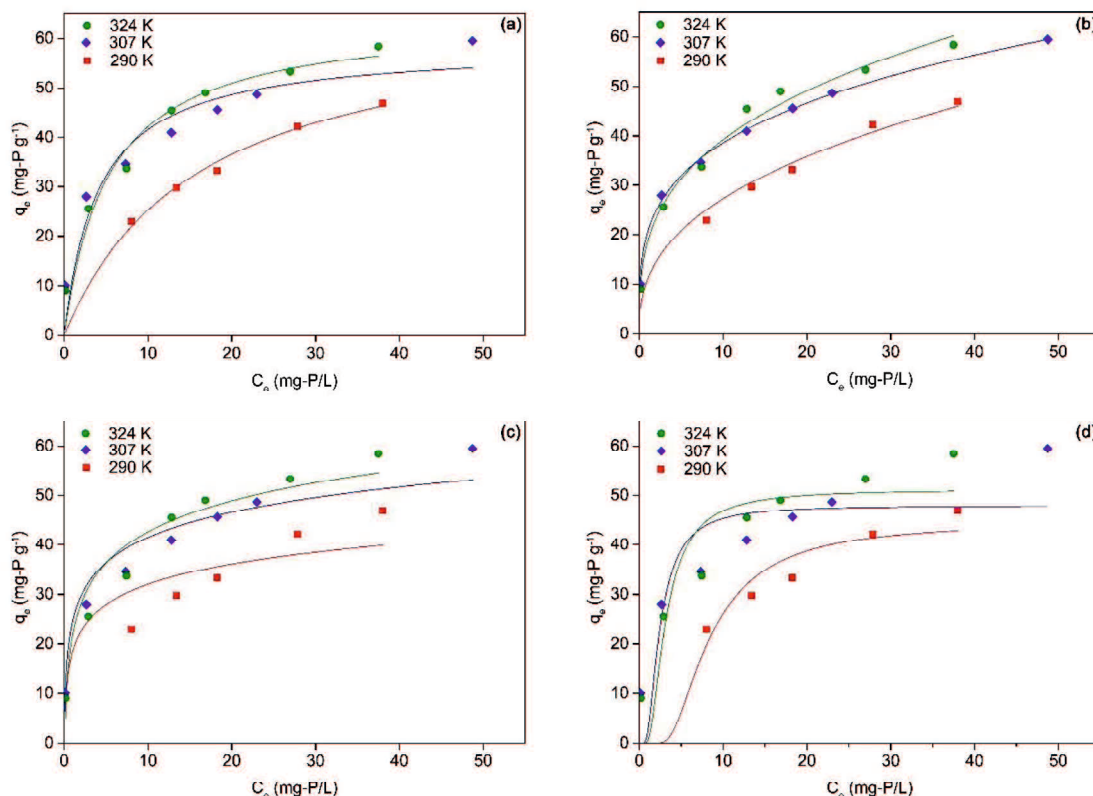


Figure 3.8 – The non-linear fitting plots of adsorption using the (a) Langmuir, (b) Freundlich, (c) Temkin, and (d) D-R isotherm equations at different treatment temperatures. (Dosage: 0.01 g; Volume: 100 mL; pH = 7; t = 24 h).

As shown in Figure 3.8, the amount of phosphate adsorbed increased by increasing the initial concentration of the phosphate solution and the surrounding temperature. This was due to the increased collision probability and frequency between phosphate ions and composite active sites. The non-linear fitting plots of adsorption using the Langmuir, Freundlich, Temkin, and D-R equations are shown in Figure 3.8a–3.8d, and the relative parameters of the models are summarized in Table 3.2. The R^2 values of the Freundlich model (0.9688–0.9984) were greater than those of the other isotherm models for all observed temperatures. This indicates that the Freundlich model was the best model to

describe the adsorption of phosphate onto the am-Zr/MgFe-LDH. This suggests that adsorption might have taken place on the surface containing heterogeneous binding sites with different energies, and that adsorption was generated in multilayers on the surface [3,55]. This type of adsorption involves both physical and chemical adsorption [56]. The values of $1/n$ were lower than 0.4, which signified that the adsorption of phosphate onto the composite was essentially favorable.

Table 3.2 – Isotherm relative parameters for phosphate adsorption by am-Zr/MgFe-LDH.

Isotherm	Isotherm constant	Temperature		
		290 K	307 K	324 K
Langmuir	k_l (L mg ⁻¹)	0.062	0.243	0.189
	q_m (mg g ⁻¹)	66.08	58.59	64.49
	R^2	0.9113	0.8960	0.9568
Freundlich	k_f (L g ⁻¹)	11.07	20.56	18.59
	$1/n$	0.39	0.27	0.32
	R^2	0.9688	0.9984	0.9865
Temkin	k_t (L g ⁻¹)	22.90	28.16	11.00
	b_t (J mol ⁻¹)	409.43	347.22	297.33
	R^2	0.8285	0.9387	0.9407
D-R	E (kJ mol ⁻¹)	4.53	14.30	11.21
	q_m (mg g ⁻¹)	44.56	47.94	51.14
	R^2	0.8449	0.7704	0.8500

3.3.7 Adsorption thermodynamics

The thermodynamic parameters of phosphate adsorption can be calculated from the adsorption isotherm at different temperatures by using Equation (3.9)–(3.11):

$$K_d = \frac{q_e}{C_e} \quad (3.9)$$

$$\Delta G^0 = -RT \ln K_d \quad (3.10)$$

$$\ln K_d = \frac{\Delta S^0}{R} - \frac{\Delta H^0}{RT} \quad (3.11)$$

where K_d is the distribution coefficient, ΔG^0 (kJ mol⁻¹) is the change of Gibbs energy, and ΔS^0 (kJ mol⁻¹ K⁻¹) and ΔH^0 (kJ mol⁻¹) are the change of entropy and enthalpy, respectively. The values of ΔS^0 and ΔH^0 were determined by the plot of $\ln k_d$ and $1/T$, where the intercept and the slope of the plot correspond to $\Delta S^0/R$ and $\Delta H^0/R$, respectively.

According to Equation (3.9)–(3.11), the thermodynamic parameters were determined from the slope of $\ln K_d$ and T^{-1} (Figure 3.9). The detailed thermodynamic parameter values are listed in Table 3.3. The calculated ΔG^0 values were negative, which indicates that the adsorption at all observed temperatures occurred spontaneously. This value decreased with increased temperature, thus indicating that adsorption was more feasible at higher temperatures. The positive value of ΔH^0 reveals that the adsorption process was endothermic. Furthermore, the positive value of ΔS^0 suggests increasing randomness at the solid-solution interface during the adsorption process.

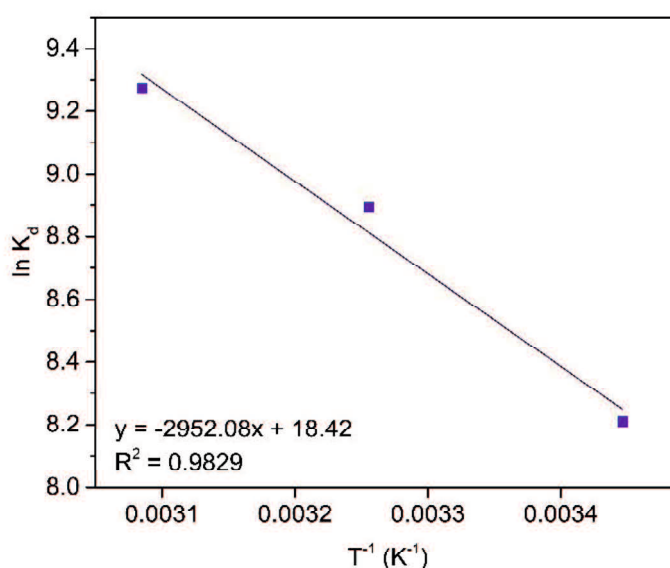


Figure 3.9 – The plot of the relationship between $\ln K_d$ and T^{-1} for the calculation of thermodynamic parameters of phosphate adsorption.

Table 3.3 – Thermodynamic parameters for phosphate adsorption by am-Zr/MgFe-LDH.

Temperature (K)	K_d	ΔG^0 (kJ mol ⁻¹)	ΔH^0 (kJ mol ⁻¹)	ΔS^0 (kJ mol ⁻¹)
290	3679.46	-19.81		
307	7282.72	-22.71	24.54	0.1532
324	10648.85	-24.99		

3.3.8 Phosphate desorption and adsorbent reusability

The recycling performance of the composite was highly affected by phosphate desorption from the composite. Figure 3.10a shows the results of the phosphate desorption in NaOH solutions of different concentrations and shaking times, whereby the desorption

percentage increased remarkably from 0.1 N to 1 N of NaOH. The optimum desorption of 87.37% was achieved at 2 N of NaOH solution for 40 minutes desorption time. This optimum desorption time was applied for the adsorbent reusability experiments. Despite the fact that 2 N of NaOH yielded higher desorption than did 1 N, the use of 2 N NaOH is expected to be higher in cost than 1 N NaOH. In order to find an economical method for the adsorbent regeneration, the use of 1 N NaOH and reused 2 N NaOH (using the same NaOH solution for each desorption cycle) were compared in the reusability experiments.

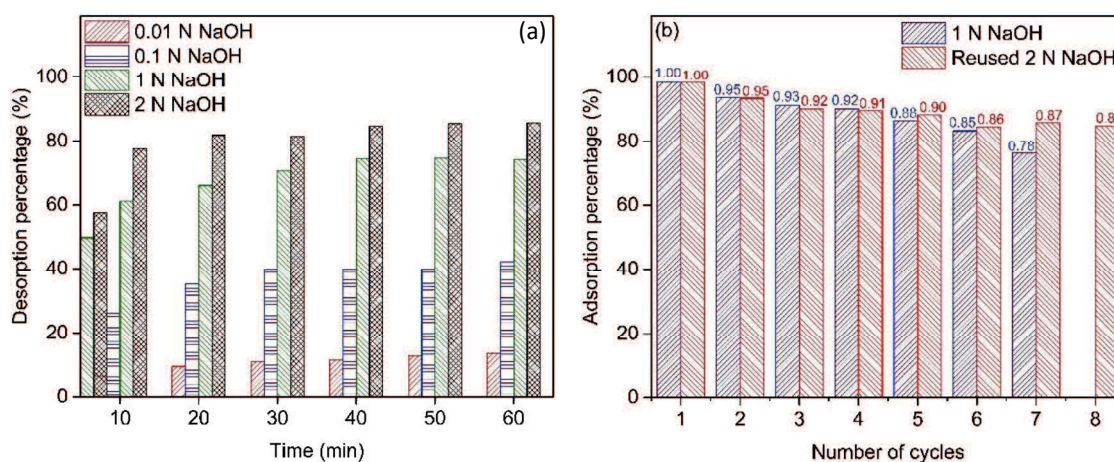


Figure 3.10 – (a) Phosphate desorption by different concentrations of NaOH solution, and (b) the reusability of composite for phosphate adsorption with desorption solution of 1 N NaOH and reused 2 N NaOH (the numbers above the bar are adsorption retain ratio of phosphate adsorption by the composite).

Figure 3.10b displays the reusability of the composite during seven cycles by 1 N NaOH and eight cycles by reused 2 N NaOH. After the first cycle, the composite retained 95% of the adsorption ability of the fresh composite for both desorption solutions. Subsequently, its adsorption ability gradually declined continuously to 78% after the seventh regeneration cycle by 1 N NaOH and 86% after the eighth regeneration cycle by reused 2 N NaOH. The decreasing adsorption ability of the composite reflects the decreasing availability of binding sites on the composite surface after each previous adsorption. The results of the reusability study demonstrated that the composite desorbed by reused 2 N NaOH in the desorption process could hold a higher adsorption efficiency than that desorbed by 1 N NaOH. A high removal efficiency retainment of composite over eight regeneration cycles by 2 N NaOH emphasizes the practicality and stability of the composite in adsorbent reusability and phosphorus recovery. In addition, by comparing with the chemical cost for the synthesis of 0.1 g composite (~31.5 JPY), a reusability cycle by 1 N NaOH (~28.8 JPY) only reduced ~9%

of the new composite synthesis with a 5% performance decrease. Therefore, a further increase in the number of cycles is not adequate to reduce the cost of synthesizing the new composite. However, the use of reused 2 N NaOH during eight cycles (~57.6 JPY) costs 4.4 times lower than the eight-time synthesis of the new composite. Therefore, the use of reused 2 N NaOH solution is an economical alternative for the reuse of am-Zr/MgFe-LDH.

The major problem of the regeneration process by 2 N NaOH in the actual wastewater treatment plant is the disposal of the high alkaline solution regenerated which contains a high concentration of phosphate. To comply with pH discharge limits, which range between 6 and 9, wastewater treatment plants are required to implement a wastewater pretreatment [57]. One of the effective methods to tackle this issue is the precipitation of phosphate to hydroxyapatite (HAP). The HAP has been shown to be effective as phosphate fertilizer for agriculture [58]. Du et al. (2013) precipitated HAP by adding CaCl_2 to a phosphate solution at pH 10–11 [59]. Before the precipitation process, the desorption solution pH (~14) needs to be reduced by dosing acid until the typical pH required for phosphate precipitation. The HAP precipitation by CaCl_2 is followed by the decrease of pH solution to the range of discharge standard ($6 < \text{pH} < 9$) [60]. In this way, the pH of the desorption solution can be reduced, and the phosphate can be recovered to valuable compounds simultaneously.

3.4 Summary

The composite of am-Zr/MgFe-LDH was successfully prepared and used for phosphate removal from aqueous solutions. The XRD analysis showed that the modification of Zr on the LDH layers was eliminated by a two-staged synthesis, which confirmed that the synthesized adsorbent was purely composite. The uncalcined composite with a Zr/Fe ratio of 1.5 at pH 7 had a phosphate adsorption capacity of $35.40 \text{ mg-P g}^{-1}$, which was higher than the uncalcined LDH ($17.99 \text{ mg-P g}^{-1}$) and am-Zr ($32.00 \text{ mg-P g}^{-1}$). It was also much higher than the calcined samples, which demonstrated that the requirement of calcination in the LDH for phosphate adsorption could be eliminated as a means of reducing energy consumption. The adsorption ability of the composite was considerably stable over a wide pH range and significantly increased at $\text{pH} \leq 3$, which is suitable for practical application. However, this composite may not be applicable to wastewater that contains a high HCO_3^- concentration. On the other hand, this study elucidates the effect of zirconium (hydr)oxide on the adsorption ability of composites at low pH, as well as the adsorption kinetics and thermodynamics of the adsorbent which was previously unexplained. The regeneration study showed that the synthesized composite is a potential adsorbent for phosphate

removal and recovery from water. Ongoing research aims to explain the adsorption mechanism of phosphate on the composite surface and will also test the composite using real wastewater to validate our experimental findings.

Acknowledgments

The first author gratefully acknowledges the support of the Indonesian Ministry of Research, Technology, and Higher Education (RISTEK-DIKTI), as well as the Project Implementation Unit (PIU) of the Islamic Development Bank (IsDB) 4in1 Project of Mulawarman University for providing the scholarship. The authors would also like to thank Prof. Tasuma Suzuki for his valuable assistance with FTIR analysis.

References

- [1] Y. Deng, T. Zhang, B.K. Sharma, H. Nie, Optimization and mechanism studies on cell disruption and phosphorus recovery from microalgae with magnesium modified hydrochar in assisted hydrothermal system, *Sci. Total Environ.* 646 (2019) 1140–1154. <https://doi.org/https://doi.org/10.1016/j.scitotenv.2018.07.369>.
- [2] M. Le Moal, C. Gascuel-Oudou, A. Ménesguen, Y. Souchon, C. Étrillard, A. Levain, F. Moatar, A. Pannard, P. Souchu, A. Lefebvre, G. Pinay, Eutrophication: A new wine in an old bottle?, *Sci. Total Environ.* 651 (2019) 1–11. <https://doi.org/10.1016/j.scitotenv.2018.09.139>.
- [3] Y. Hu, Y. Du, G. Nie, T. Zhu, Z. Ding, H. Wang, L. Zhang, Selective and efficient sequestration of phosphate from waters using reusable nano-Zr(IV) oxide impregnated agricultural residue anion exchanger, *Sci. Total Environ.* 700 (2019) 134999. <https://doi.org/https://doi.org/10.1016/j.scitotenv.2019.134999>.
- [4] X. Huang, X. Liao, B. Shi, Adsorption removal of phosphate in industrial wastewater by using metal-loaded skin split waste, *J. Hazard. Mater.* 166 (2009) 1261–1265. <https://doi.org/10.1016/j.jhazmat.2008.12.045>.
- [5] W. Huang, Y. Zhang, D. Li, Adsorptive removal of phosphate from water using mesoporous materials: A review, *J. Environ. Manage.* 193 (2017) 470–482. <https://doi.org/https://doi.org/10.1016/j.jenvman.2017.02.030>.
- [6] K. Zhou, B. Wu, L. Su, W. Xin, X. Chai, Enhanced phosphate removal using nanostructured hydrated ferric-zirconium binary oxide confined in a polymeric anion exchanger, *Chem. Eng. J.* 345 (2018) 640–647. <https://doi.org/10.1016/j.cej.2018.01.091>.

- [7] Y. Makita, A. Sonoda, Y. Sugiura, A. Ogata, C. Suh, J. Lee, K. Ooi, Phosphorus removal from model wastewater using lanthanum hydroxide microcapsules with poly(vinyl chloride) shells, *Sep. Purif. Technol.* 241 (2020) 116707. <https://doi.org/https://doi.org/10.1016/j.seppur.2020.116707>.
- [8] S. Daneshgar, A. Callegari, A. Capodaglio, D. Vaccari, The Potential Phosphorus Crisis: Resource Conservation and Possible Escape Technologies: A Review, *Resources*. 7 (2018) 37. <https://doi.org/10.3390/resources7020037>.
- [9] H. Qiu, W. Ni, H. Zhang, K. Chen, J. Yu, Fabrication and evaluation of a regenerable HFO-doped agricultural waste for enhanced adsorption affinity towards phosphate, *Sci. Total Environ.* 703 (2020) 135493. <https://doi.org/https://doi.org/10.1016/j.scitotenv.2019.135493>.
- [10] H. Hatami, A. Fotovat, A. Halajnia, Comparison of adsorption and desorption of phosphate on synthesized Zn-Al LDH by two methods in a simulated soil solution, *Appl. Clay Sci.* 152 (2018) 333–341. <https://doi.org/10.1016/j.clay.2017.11.032>.
- [11] X. Sun, T. Imai, M. Sekine, T. Higuchi, K. Yamamoto, K. Akagil, Adsorption of Phosphate by Calcinated Mg-Fe Layered Double Hydroxide, *J. Water Environ. Technol.* 11 (2013) 111–120. <https://doi.org/10.2965/jwet.2013.111>.
- [12] S. Iftekhhar, M.E. Küçük, V. Srivastava, E. Repo, M. Sillanpää, Application of zinc-aluminium layered double hydroxides for adsorptive removal of phosphate and sulfate: Equilibrium, kinetic and thermodynamic, *Chemosphere*. 209 (2018) 470–479. <https://doi.org/10.1016/j.chemosphere.2018.06.115>.
- [13] W. Wang, H. Zhang, L. Zhang, H. Wan, S. Zheng, Z. Xu, Adsorptive removal of phosphate by magnetic Fe₃O₄@C@ZrO₂, *Colloids Surfaces A Physicochem. Eng. Asp.* 469 (2015) 100–106. <https://doi.org/10.1016/j.colsurfa.2015.01.002>.
- [14] F. Long, J.L. Gong, G.M. Zeng, L. Chen, X.Y. Wang, J.H. Deng, Q.Y. Niu, H.Y. Zhang, X.R. Zhang, Removal of phosphate from aqueous solution by magnetic Fe-Zr binary oxide, *Chem. Eng. J.* 171 (2011) 448–455. <https://doi.org/10.1016/j.cej.2011.03.102>.
- [15] X. Luo, X. Wang, S. Bao, X. Liu, W. Zhang, T. Fang, Adsorption of phosphate in water using one-step synthesized zirconium-loaded reduced graphene oxide, *Sci. Rep.* 6 (2016) 39108. <https://doi.org/10.1038/srep39108>.
- [16] J. Wang, Y. Liu, P. Hu, R. Huang, Adsorption of phosphate from aqueous solution by Zr(IV)-crosslinked quaternized chitosan/bentonite composite, *Environ. Prog. Sustain. Energy*. 37 (2018) 267–275. <https://doi.org/10.1002/ep.12667>.

- [17] S. Mallakpour, M. Hatami, An effective, low-cost and recyclable bio-adsorbent having amino acid intercalated LDH@Fe₃O₄/PVA magnetic nanocomposites for removal of methyl orange from aqueous solution, *Appl. Clay Sci.* 174 (2019) 127–137. <https://doi.org/https://doi.org/10.1016/j.clay.2019.03.026>.
- [18] R. Chitrakar, S. Tezuka, J. Hosokawa, Y. Makita, A. Sonoda, K. Ooi, T. Hirotsu, Uptake properties of phosphate on a novel Zr-modified MgFe-LDH(CO₃), *J. Colloid Interface Sci.* 349 (2010) 314–320. <https://doi.org/10.1016/j.jcis.2010.05.068>.
- [19] H. Miyauchi, T. Yamamoto, R. Chitrakar, Y. Makita, Z. Wang, J. Kawai, T. Hirotsu, Phosphate adsorption site on zirconium ion modified MgAl-layered double hydroxides, *Top. Catal.* 52 (2009) 714–723. <https://doi.org/10.1007/s11244-009-9209-1>.
- [20] R. Chitrakar, S. Tezuka, A. Sonoda, K. Sakane, K. Ooi, T. Hirotsu, Synthesis and phosphate uptake behavior of Zr⁴⁺ incorporated MgAl-layered double hydroxides, *J. Colloid Interface Sci.* 313 (2007) 53–63. <https://doi.org/10.1016/j.jcis.2007.04.004>.
- [21] S. Velu, D.P. Sabde, N. Shah, S. Sivasanker, New Hydrotalcite-like Anionic Clays Containing Zr⁴⁺ in the Layers: Synthesis and Physicochemical Properties, *Chem. Mater.* 10 (1998) 3451–3458. <https://doi.org/10.1021/cm980185x>.
- [22] D. Tichit, N. Das, B. Coq, R. Durand, Preparation of Zr-Containing Layered Double Hydroxides and Characterization of the Acido-Basic Properties of Their Mixed Oxides, *Chem. Mater.* 14 (2002) 1530–1538. <https://doi.org/10.1021/cm011125l>.
- [23] R. Elmoubarki, F.Z. Mahjoubi, A. Elhalil, H. Tounsadi, M. Abdennouri, M. Sadiq, S. Qourzal, A. Zouhri, N. Barka, Ni/Fe and Mg/Fe layered double hydroxides and their calcined derivatives: preparation, characterization and application on textile dyes removal, *J. Mater. Res. Technol.* 6 (2017) 271–283. <https://doi.org/10.1016/J.JMRT.2016.09.007>.
- [24] T.-T.H. Nguyen, X.-T.T. Nguyen, C.Q. Nguyen, P.H. Tran, Porous metal oxides derived from Cu–Al layered double hydroxide as an efficient heterogeneous catalyst for the Friedel–Crafts alkylation of indoles with benzaldehydes under microwave irradiation, *Heliyon.* 4 (2018) e00966. <https://doi.org/https://doi.org/10.1016/j.heliyon.2018.e00966>.
- [25] E. Herald, K.D. Nugrahaningtyas, Heriyanto, X-ray Diffraction Analysis on Post Treatment of Ca-Mg-Al-Layered Double Hydroxide Slurry, *IOP Conf. Ser. Mater. Sci. Eng.* 176 (2017) 12020. <https://doi.org/10.1088/1757-899x/176/1/012020>.
- [26] Y. Seida, Y. Nakano, Removal of phosphate in dissolution-coagulation process of

- layered double hydroxide, *J. Chem. Eng. Japan.* 34 (2001) 906–911. <https://doi.org/10.1252/jcej.34.906>.
- [27] Y. Su, H. Cui, Q. Li, S. Gao, J.K. Shang, Strong adsorption of phosphate by amorphous zirconium oxide nanoparticles, *Water Res.* 47 (2013) 5018–5026. <https://doi.org/10.1016/j.watres.2013.05.044>.
- [28] X. Dou, D. Mohan, C.U. Pittman, S. Yang, Remediating fluoride from water using hydrous zirconium oxide, *Chem. Eng. J.* 198–199 (2012) 236–245. <https://doi.org/10.1016/j.cej.2012.05.084>.
- [29] V.R. Magri, A. Duarte, G.F. Perotti, V.R.L. Constantino, Investigation of Thermal Behavior of Layered Double Hydroxides Intercalated with Carboxymethylcellulose Aiming Bio-Carbon Based Nanocomposites, *ChemEngineering.* 3 (2019) 55. <https://doi.org/10.3390/chemengineering3020055>.
- [30] P. Samoila, C. Cojocar, I. Cretescu, C.D. Stan, V. Nica, L. Sacarescu, V. Harabagiu, Nanosized spinel ferrites synthesized by sol-gel autocombustion for optimized removal of azo dye from aqueous solution, *J. Nanomater.* 2015 (2015) 713802. <https://doi.org/10.1155/2015/713802>.
- [31] B.P. Jacob, A. Kumar, R.P. Pant, S. Singh, E.M. Mohammed, Influence of preparation method on structural and magnetic properties of nickel ferrite nanoparticles, *Bull. Mater. Sci.* 34 (2011) 1345–1350. <https://doi.org/10.1007/s12034-011-0326-7>.
- [32] K. Rybka, J. Matusik, A. Kuligiewicz, T. Leiviskä, G. Cempura, Surface chemistry and structure evaluation of Mg/Al and Mg/Fe LDH derived from magnesite and dolomite in comparison to LDH obtained from chemicals, *Appl. Surf. Sci.* 538 (2021) 147923. <https://doi.org/10.1016/j.apsusc.2020.147923>.
- [33] T.N. Brusentsova, R.E. Peale, D. Maukonen, G.E. Harlow, J.S. Boesenberg, D. Ebel, Far infrared spectroscopy of carbonate minerals, *Am. Mineral.* 95 (2010) 1515–1522. <https://doi.org/10.2138/am.2010.3380>.
- [34] P.A. Schroeder, Infrared Spectroscopy in Clay Science, in: A.C. Rule, S. Guggenheim (Eds.), *Teach. Clay Sci., Clay Minerals Society, Aurora, CO, 2002: pp. 182–205.* <https://doi.org/10.1346/CMS-WLS-11.11>.
- [35] P. Marzbani, H. Resalati, A. Ghasemian, A. Shakeri, Surface Modification of Talc Particles with Phthalimide: Study of Composite Structure and Consequences on Physical, Mechanical, and Optical Properties of Deinked Pulp, *BioResources.* 11 (2016) 8720–8738. <https://doi.org/10.15376/biores.11.4.8720-8738>.

- [36] R.C. Zeng, Z.G. Liu, F. Zhang, S.Q. Li, H.Z. Cui, E.H. Han, Corrosion of molybdate intercalated hydrotalcite coating on AZ31 Mg alloy, *J. Mater. Chem. A*. 2 (2014) 13049–13057. <https://doi.org/10.1039/c4ta01341g>.
- [37] T. Ivanova, A. Harizanova, T. Koutzarova, N. Krins, B. Vertruyen, Electrochromic TiO₂, ZrO₂ and TiO₂-ZrO₂ thin films by dip-coating method, *Mater. Sci. Eng. B Solid-State Mater. Adv. Technol.* 165 (2009) 212–216. <https://doi.org/10.1016/j.mseb.2009.07.013>.
- [38] H.J. Quah, Z. Hassan, W.F. Lim, Passivation of silicon substrate using two-step grown ternary aluminium doped zirconium oxide, *Appl. Surf. Sci.* 493 (2019) 411–422. <https://doi.org/10.1016/j.apsusc.2019.07.023>.
- [39] N.S. Hassan, A.A. Jalil, F.F.A. Aziz, A.A. Fauzi, M.S. Azami, N.W.C. Jusoh, Tailoring the Silica Amount in Stabilizing the Tetragonal Phase of Zirconia for Enhanced Photodegradation of 2-Chlorophenol, *Top. Catal.* 63 (2020) 1145–1156. <https://doi.org/10.1007/s11244-020-01274-3>.
- [40] M. Ranjbar, M. Yousefi, M. Lahooti, A. Malekzadeh, Preparation and Characterization of Tetragonal Zirconium Oxide Nanocrystals from Isophthalic Acid-Zirconium(IV) Nanocomposite As a New Precursor, *Int. J. Nanosci. Nanotechnol.* 8 (2012) 191–196.
- [41] F. Monte, W. Larsen, J.D. Mackenzie, Stabilization of Tetragonal ZrO₂ in ZrO₂-SiO₂ Binary Oxides, *J. Am. Ceram. Soc.* 83 (2004) 628–634. <https://doi.org/10.1111/j.1151-2916.2000.tb01243.x>.
- [42] A. Arjun, A. Dharr, T. Raguram, K.S. Rajni, Study of Copper Doped Zirconium Dioxide Nanoparticles Synthesized via Sol–Gel Technique for Photocatalytic Applications, *J. Inorg. Organomet. Polym. Mater.* 30 (2020) 4989–4998. <https://doi.org/10.1007/s10904-020-01616-4>.
- [43] W. Li, X. Liu, A. Huang, P.K. Chu, Structure and properties of zirconia (ZrO₂) films fabricated by plasma-assisted cathodic arc deposition, *J. Phys. D: Appl. Phys.* 40 (2007) 2293–2299. <https://doi.org/10.1088/0022-3727/40/8/S08>.
- [44] F. Bollino, E. Armenia, E. Tranquillo, Zirconia/hydroxyapatite composites synthesized via sol-gel: Influence of hydroxyapatite content and heating on their biological properties, *Materials (Basel)*. 10 (2017) 757. <https://doi.org/10.3390/ma10070757>.
- [45] J. Li Vage, K. Doi, C. Maziers, Nature and Thermal Evolution of Amorphous Hydrated Zirconium Oxide, *J. Am. Ceram. Soc.* 51 (1968) 349–353. <https://doi.org/10.1111/j.1151-2916.1968.tb15952.x>.

- [46] S. Dong, Q. Ji, Y. Wang, H. Liu, J. Qu, Enhanced phosphate removal using zirconium hydroxide encapsulated in quaternized cellulose, *J. Environ. Sci.* 89 (2020) 102–112. <https://doi.org/10.1016/j.jes.2019.10.005>.
- [47] H. Zhou, Z. Jiang, S. Wei, A new hydrotalcite-like absorbent FeMnMg-LDH and its adsorption capacity for Pb²⁺ ions in water, *Appl. Clay Sci.* 153 (2018) 29–37. <https://doi.org/10.1016/j.clay.2017.11.033>.
- [48] R. Li, J.J. Wang, B. Zhou, M.K. Awasthi, A. Ali, Z. Zhang, L.A. Gaston, A.H. Lahori, A. Mahar, Enhancing phosphate adsorption by Mg/Al layered double hydroxide functionalized biochar with different Mg/Al ratios, *Sci. Total Environ.* 559 (2016) 121–129. <https://doi.org/10.1016/j.scitotenv.2016.03.151>.
- [49] K. Dox, M. Everaert, R. Merckx, E. Smolders, Optimization of phosphate recovery from urine by layered double hydroxides, *Sci. Total Environ.* 682 (2019) 437–446. <https://doi.org/10.1016/j.scitotenv.2019.05.181>.
- [50] J. Li, B. Li, H. Huang, X. Lv, N. Zhao, G. Guo, D. Zhang, Removal of phosphate from aqueous solution by dolomite-modified biochar derived from urban dewatered sewage sludge, *Sci. Total Environ.* 687 (2019) 460–469. <https://doi.org/10.1016/j.scitotenv.2019.05.400>.
- [51] J.C. Mendez, T. Hiemstra, Carbonate Adsorption to Ferrihydrite: Competitive Interaction with Phosphate for Use in Soil Systems, *ACS Earth Sp. Chem.* 3 (2019) 129–141. <https://doi.org/10.1021/acsearthspacechem.8b00160>.
- [52] R.B. Balow, J.G. Lundin, G.C. Daniels, W.O. Gordon, M. McEntee, G.W. Peterson, J.H. Wynne, P.E. Pehrsson, Environmental Effects on Zirconium Hydroxide Nanoparticles and Chemical Warfare Agent Decomposition: Implications of Atmospheric Water and Carbon Dioxide, *ACS Appl. Mater. Interfaces.* 9 (2017) 39747–39757. <https://doi.org/10.1021/acsami.7b10902>.
- [53] Q. Dong, S. Shi, Y. Xie, Y. Wang, X. Zhang, X. Wang, S. Guo, L. Zhu, G. Zhang, D. Xu, Preparation of mesoporous zirconia ceramic fibers modified by dual surfactants and their phosphate adsorption characteristics, *Ceram. Int.* 46 (2020) 14019–14029. <https://doi.org/10.1016/j.ceramint.2020.02.201>.
- [54] W. Gu, X. Li, M. Xing, W. Fang, D. Wu, Removal of phosphate from water by amine-functionalized copper ferrite chelated with La(III), *Sci. Total Environ.* 619–620 (2018) 42–48. <https://doi.org/10.1016/j.scitotenv.2017.11.098>.
- [55] N. Tahir, H.N. Bhatti, M. Iqbal, S. Noreen, Biopolymers composites with peanut hull waste biomass and application for Crystal Violet adsorption, *Int. J. Biol. Macromol.*

94 (2017) 210–220. <https://doi.org/10.1016/j.ijbiomac.2016.10.013>.

- [56] X. Zhang, H. Han, X. Zheng, T. Yu, Y. Chen, Tetracycline-induced effects on the nitrogen transformations in sediments: Roles of adsorption behavior and bacterial activity, *Sci. Total Environ.* 695 (2019) 133811. <https://doi.org/10.1016/j.scitotenv.2019.133811>.
- [57] Y. Lei, J.C. Remmers, M. Saakes, R.D. van der Weijden, C.J.N. Buisman, Is There a Precipitation Sequence in Municipal Wastewater Induced by Electrolysis?, *Environ. Sci. Technol.* 52 (2018) 8399–8407. <https://doi.org/10.1021/acs.est.8b02869>.
- [58] T. Guan, Y. Kuang, X. Li, J. Fang, W. Fang, D. Wu, The recovery of phosphorus from source-separated urine by repeatedly usable magnetic Fe₃O₄@ZrO₂ nanoparticles under acidic conditions, *Environ. Int.* 134 (2020) 105322. <https://doi.org/https://doi.org/10.1016/j.envint.2019.105322>.
- [59] L.-W. Du, S. Bian, B.-D. Gou, Y. Jiang, J. Huang, Y.-X. Gao, Y.-D. Zhao, W. Wen, T.-L. Zhang, K. Wang, Structure of Clusters and Formation of Amorphous Calcium Phosphate and Hydroxyapatite: From the Perspective of Coordination Chemistry, *Cryst. Growth Des.* 13 (2013) 3103–3109. <https://doi.org/10.1021/cg400498j>.
- [60] M. Hermassi, C. Valderrama, J. Dosta, J.L. Cortina, N.H. Batis, Evaluation of hydroxyapatite crystallization in a batch reactor for the valorization of alkaline phosphate concentrates from wastewater treatment plants using calcium chloride, *Chem. Eng. J.* 267 (2015) 142–152. <https://doi.org/10.1016/j.cej.2014.12.079>.

CHAPTER 4

APPLICATION OF AMORPHOUS ZIRCONIUM (HYDR)OXIDE/MgFe LAYERED DOUBLE HYDROXIDES COMPOSITE IN FIXED-BED COLUMN FOR PHOSPHATE REMOVAL FROM WATER

4.1. Introduction

Phosphates are vital for the sustainability of organisms and several industrial activities. However, their widespread use, along with the increase in population, has induced superfluous levels of phosphates in the aquatic environment, leading to water eutrophication [1]. Thus, it is essential to minimize or eliminate phosphorus contaminations from wastewater prior to its discharge into the receiving water body to maintain water quality and improve human health. Additionally, the global increase in food demand and the limited carrying capacity of the land has increased the dependence on phosphorus, which is used to increase agricultural productivity to fulfil human and livestock needs [2]. As phosphorus is a non-renewable natural resource and cannot be substituted by other resources [3], the recovery of phosphates from wastewater is important for the sustainability of global phosphorus reserves.

In the last decade, numerous phosphate removal techniques have been designed, ranging from adsorption and chemical precipitation to the application of polyphosphate-accumulating organisms (PAOs) [4]. Among these techniques, adsorption is constantly gaining popularity owing to its simplicity and the possibility of phosphorus recovery from wastewater [5]. However, the cost-effectiveness depends on the reusability of the adsorbent [6]. Consequently, adsorbents with high chemical stability are being preferred for phosphorus adsorption because of their stability during the desorption process under various stripping agent chemistry conditions, which usually use a solution with extreme acidity or alkalinity.

In previous study, a composite of amorphous zirconium (hydr)oxide/MgFe layered double hydroxides (am-Zr/MgFe-LDH) was synthesized using a novel two-stage synthesis. A series of batch experiments showed that the uncalcined am-Zr/MgFe-LDH with a Zr:Fe ratio of 1:5 showed a high adsorption performance towards phosphates and retained good removal efficiency over eight adsorption-desorption cycles. The high adsorption capacity is related to the high surface area and a large number of hydroxyl groups on the composite as a consequence of small crystal size and agglomeration of amorphous zirconium (hydr)oxide (am-Zr) in the composite. However, batch settings are not suitable for large-scale applications and continuously generated wastewater [7]. Therefore, it is important to

understand the application of the composite in continuous fixed-bed column adsorption to investigate its performance in practical applications. Fixed-bed column adsorption is very popular in wastewater treatment because of its continuous, high yield, simple, and economical operation and the ability to be scaled up from the laboratory scale [8,9]. Sun *et al.* (2014) found that MgFe-LDH in a fixed-bed column had a high phosphate adsorption capacity and acceptable desorption efficiency [10]. However, no studies have been conducted on the phosphate removal performance of the am-Zr/MgFe-LDH in a fixed-bed column.

Following the previous study, the phosphate adsorption performance and reusability of a fixed-bed column filled with the am-Zr/MgFe-LDH were investigated. The effects of design parameters essential for practical applications, such as flow rate, bed height, influent phosphate concentration, pH, and adsorbent particle size, on the composite performance, were examined. Furthermore, the three most widely used models, Thomas, Yoon-Nelson, and modified dose-response (MDR) models, were applied to interpret the phosphate adsorption breakthrough data. The applicability of the composite for real anaerobic sludge and phosphate-enriched seawater and its reusability were also evaluated.

4.2 Materials and methods

4.2.1 Adsorbent and adsorbate preparation

Analytical grade $\text{FeCl}_3 \cdot 6\text{H}_2\text{O}$ (99.0% pure), $\text{MgCl}_2 \cdot 6\text{H}_2\text{O}$ (98.0% pure), $\text{ZrOCl}_2 \cdot 8\text{H}_2\text{O}$ (99.0% pure), Na_2CO_3 (99.8% pure), NaOH (97.0% pure) were purchased from FUJIFILM Wako Pure Chemical Corporation, Japan. for preparing the am-Zr/MgFe-LDH and used directly in this study without further purification. A composite with a Zr:Fe molar ratio of 1.5:1 was synthesized using an established method [11]. Briefly, a solution containing Mg^{2+} and Fe^{3+} ions with a molar ratio of 3:1 was poured into 200 mL of deionized (DI) water. The solution pH was maintained at ~ 10 using a solution of 1 M NaOH and 1 M Na_2CO_3 with a 3:1 volume ratio under vigorous stirring for 30 min. The separated and neutralized gel obtained was then mixed with $\text{ZrOCl}_2 \cdot 8\text{H}_2\text{O}$ (Zr to Fe molar ratio of 1.5:1) in 500 mL of DI water. Simultaneously, a 25% NaOH solution was used to precipitate the am-Zr under constant stirring until a pH of ~ 10 was obtained. After ageing at 353 K for 24 h, the composite was filtered, washed with DI water for neutralization, and then dried in an oven at 353 K for 24 h. The dried composite was ground in a mortar and sieved to the desired particle size.

K_2HPO_4 (99.0% pure) was obtained from FUJIFILM Wako Pure Chemical Corporation, Japan. A phosphate stock solution (500 mg-P/L) was prepared by dissolving an appropriate amount of K_2HPO_4 in 1 L of DI water. The stock solution was diluted to the desired working

solution using DI water. The pH of the working solution was adjusted using 0.1 M HCl and NaOH solutions and monitored using a pH meter (Horiba, LAQUA SS131 D-71).

4.2.2 Adsorption experiments

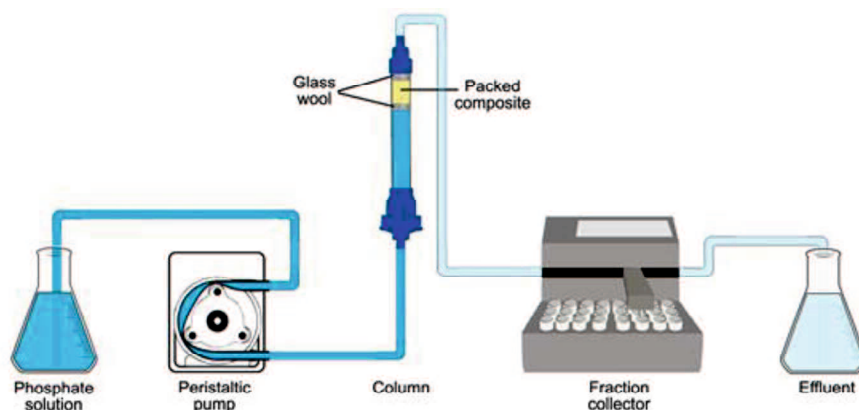


Figure 4.1 – Schematic diagram of lab-scale fixed-bed column adsorption system.

Continuous fixed-bed column adsorption experiments were conducted at room temperature (~ 298 K) using a non-jacketed liquid chromatography column (Sigma-Aldrich, Co.) with an inner diameter of 1.0 cm and a length of 10 cm. Figure 4.1 shows a schematic diagram of the fixed-bed column system used in this study. A 1 cm thick glass wool was placed on the top and bottom of the sample to prevent the adsorbent from being washed out by the liquid flow. A particular weight (0.7, 1.0, and 1.4 g) of the composite with a maximum particle size of $106 \mu\text{m}$ was packed into the column to attain the desired bed height (h) (1.0, 1.5, and 2.0 cm). The artificial influent phosphate solution with various concentrations (C_0) (5 mg-P/L, 12 mg-P/L, and 20 mg-P/L) at pH 7 was pumped in an up-flow configuration through the packed composite inside the column at varying flow rates (Q) (1.5, 2.5, and 3.5 mL/min) using a peristaltic pump (EYELA MP-1000). The effects of phosphate solution pH (4, 7, and 10) and composite particle size (d) (≤ 0.1 , 0.1–0.5, and 0.5–1.0 mm) on phosphate adsorption were examined. To obtain the breakthrough curves, the effluent solutions were automatically collected at specified intervals using a fraction collector (Advantec SF-3120) for measuring phosphate concentrations. In this study, the breakthrough time was assigned when the ratio of effluent to influent phosphate concentration (C/C_0) was 10%. An exhaustion time is a time when the influent solution passes through the adsorbent without any significant decrease in concentration [13]. A preliminary experiment showed that the breakthrough curves became relatively flat after C/C_0 reached approximately 85% and the phosphate adsorption became insignificant.

Therefore, the exhausted time in this study was determined to be the time when C/C_0 reached 85%.

Breakthrough curves of phosphate adsorption were constructed by plotting the ratio of effluent phosphate concentration at an interval time to influent phosphate concentration (C/C_0) as a function of time (t). The breakthrough curves demonstrate the mass transfer characteristics of phosphate onto the packed composite. The total amount of adsorbed phosphate, $q_{adsorbed}$ (mg), during adsorption and the equilibrium adsorption capacity, q_e (mg/g), were calculated as follows (Equation 4.1 and 4.2, respectively) [14].

$$q_{adsorbed} = \frac{QC_0}{1000} \int_{t=0}^{t=t_e} \left(1 - \frac{C}{C_0}\right) dt \quad (4.1)$$

$$q_e = \frac{q_{adsorbed}}{m} \quad (4.2)$$

where Q is the flow rate (mL/min), C_0 and C are the influent and effluent phosphate concentrations (mg/L), respectively, t_e is the time required to reach exhaustion time (min), and m is the weight of the composite packed inside the column (g).

4.2.3 Regeneration and reusability experiments

Before the regeneration experiment, the exhausted bed in the column was washed with DI water at a flow rate of 2.5 mL/min for 1 h to remove residual phosphorus. Subsequently, 0.1 M NaOH was pumped in the opposite direction to desorb the adsorbed phosphate. In this study, regeneration was done until the effluent concentration reached approximately 0.5 mg-P/L, and it was assumed that the column had been regenerated. In the first cycle of desorption, the desorption effluent solutions were collected at the pre-determined intervals to obtain the desorption curve. The amount of phosphorus eluted from the composite (EAP) (mg/g) was calculated using the following equations (Equation 4.3 and 4.4) [15]:

$$EAP = \frac{1}{m} q_{desorbed} \quad (4.3)$$

$$q_{desorbed} = \sum_{q=1}^{n2} CV_q \quad (4.4)$$

where m is the weight of adsorbent in the column (g), $q_{desorbed}$ is the total amount of desorbed phosphate (mg), V_q is the effluent volume of the q -th fraction (L), and $n2$ is the number of the last fraction in the desorption operation. Desorption and regeneration experiments were conducted for eight cycles of the adsorption-desorption process.

4.3 Results and discussion

4.3.1 Fixed-bed column adsorption

The effect of phosphate solution flow rate on the phosphate adsorption on the composite in the column was investigated at three different flow rates (1.5, 2.5, and 3.5 mL/min), where the bed height (1.5 cm) and the influent phosphate concentration (12 mg-P/L) were kept constant. Figure 4.2a shows the effect of the flow rate on the breakthrough curve of phosphate adsorption on the composite. The increase in flow rate from 1.5 to 3.5 mL/min resulted in a reduction in the breakthrough time from 14.9 to 5.5 h and in the exhaustion time from 24.0 to 8.9 h. The increase in the flow rate led to an increase in the volume speed, leading to a reduction in the time required to reach breakthrough and exhaustion states. The amount of adsorbed phosphate calculated using Equation 4.2, decreased from 20.40 to 18.23 mg-P/g as the flow rate increased from 1.5 to 3.5 mL/min (Table 4.1). At a high flow rate, the phosphate anions have a short residence time in the bed, where composite particles in the fixed-bed column have a short contact time with the phosphate anions as the solution flows through the bed [14]. Consequently, the possibility of phosphate anions passing through the column before being completely adsorbed increased because of the insufficient contact time for adsorption equilibrium. In addition, the steepness of the breakthrough curves increased with the increase in flow rate. The different slope of the breakthrough curves was due to the retention process. A high flow rate led to an increase in mass transfer rate, increasing the amount of phosphate captured onto the adsorbent surface at the beginning of the operation. This caused an early saturation with a steeper slope given in the breakthrough curves.

Breakthrough curves resulting from fixed-bed column experiments at different bed heights (1.0, 1.5, and 2.0 cm) with a constant flow rate (2.5 mL/min) and influent phosphate concentration (12 mg-P/L) are depicted in Figure 4.2b. The figure demonstrates that the breakthrough and exhaustion times were extended when the bed height increased. Table 4.1 shows that the adsorbed phosphate increased from 18.75 to 19.56 mg-P/g as the bed height increased from 1.0 to 2.0 cm. This was predictable as there were more active binding sites at a higher bed height, and these increased the adsorption areas [16]. Furthermore, a higher bed height provides a longer packed composite through which the phosphate anions pass, which allows a longer residence time of phosphate, enabling it to be deeply adsorbed within the composite. The bed height of 2.0 cm had a flatter breakthrough curve than the lower bed height, which might be due to a broad mass transfer zone provided by a high bed height.

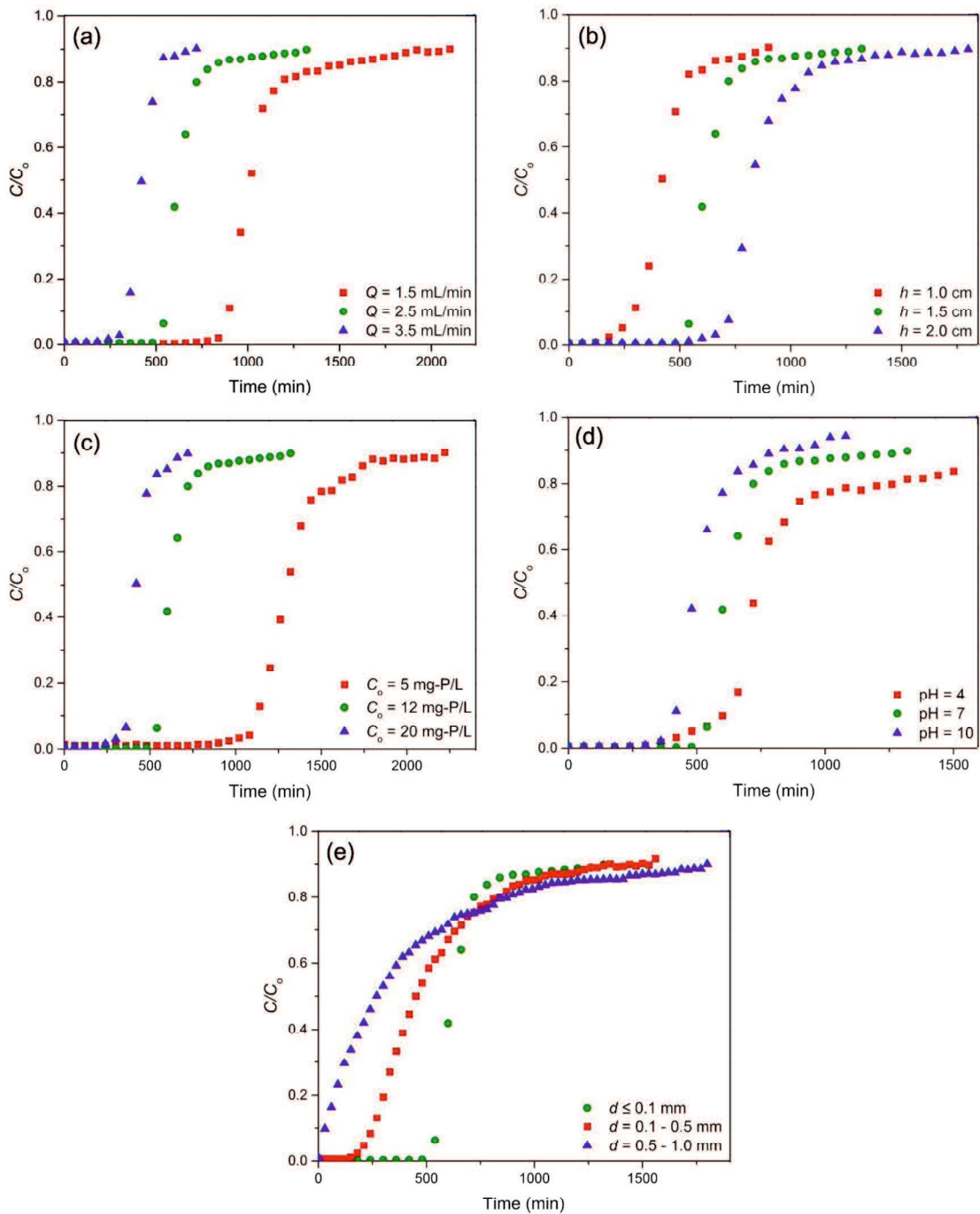


Figure 4.2 – The Effect of (a) flow rate ($h = 1.5$ cm, $C_0 = 12$ mg-P/L, $pH = 7$, and $d \leq 0.1$ mm), (b) bed height ($Q = 2.5$ mL/min, $C_0 = 12$ mg-P/L, $pH = 7$, and $d \leq 0.1$ mm), (c) influent phosphate concentration ($h = 1.5$ cm, $Q = 2.5$ mL/min, $pH = 7$, and $d \leq 0.1$ mm), (d) solution pH ($h = 1.5$ cm, $Q = 2.5$ mL/min, $C_0 = 12$ mg-P/L, and $d \leq 0.1$ mm), and (e) composite particle size ($m = 1.01$ g cm, $Q = 2.5$ mL/min, $C_0 = 12$ mg-P/L, and $pH = 7$), on the fixed-bed column studies.

Figure 4.2c shows the adsorption curves of various influent phosphate concentrations (5, 12, and 20 mg-P/L) at a constant bed height (1.5 cm) and flow rate (2.5 mL/min). An increase in influent phosphate concentration from 5 to 20 mg-P/L decreased the breakthrough time from 18.7 to 4.4 h and exhaustion time from 28.7 to 7.8 h. The concentration gradient between the solution and adsorbent surface increased at high phosphate concentrations, which increased the driving force for phosphate adsorption [17]. Under these conditions, the limited active binding sites in the column were inhibited rapidly, and saturated conditions were achieved in a short period. This led to a steeper breakthrough curve at higher influent phosphate concentrations. This steeper curve at the high load of phosphate anions signifies that the am-Zr/MgFe-LDH is likely favorable for phosphate adsorption. The amount of phosphate adsorbed increased from 17.08 to 19.13 mg-P/g when the influent phosphate concentration was raised from 5 to 20 mg-P/L. A higher influent concentration of phosphate can deliver more phosphate anions into the outer and inner surface of the composite to attach with the adsorption sites, which is possibly the reason for an increase in equilibrium adsorption capacity with influent concentration increasing. In addition, a high concentration gradient at high influent phosphate concentration can overcome the mass transfer resistance in the adsorbent surface, leading to an increase in the amount of adsorbed phosphate.

Table 4.1 – Fixed-bed column parameters for phosphate adsorption on am-Zr/MgFe-LDH.

No.	Q (mL/min)	h (cm)	C_o (mg-P/L)	m (g)	pH	d (mm)	t_b (h)	τ (h)	t_e (h)	q_e (mg-P/g)
1	1.5	1.5	12	1.01	7	≤ 0.1	14.9	17.33	24.0	20.40
2	2.5	1.5	12	1.01	7	≤ 0.1	9.1	10.65	13.5	19.04
3	3.5	1.5	12	1.01	7	≤ 0.1	5.5	7.19	8.9	18.23
4	2.5	1.0	12	0.68	7	≤ 0.1	4.8	7.24	10.7	18.75
	2.5	1.5	12	1.01	7	≤ 0.1	9.1	10.65	13.5	19.04
5	2.5	2.0	12	1.36	7	≤ 0.1	12.1	14.48	19.0	19.56
6	2.5	1.5	5	1.01	7	≤ 0.1	18.7	22.28	28.7	17.08
	2.5	1.5	12	1.01	7	≤ 0.1	9.1	10.65	13.5	19.04
7	2.5	1.5	20	1.01	7	≤ 0.1	4.4	6.04	7.8	19.13
8	2.5	1.5	12	1.01	4	≤ 0.1	10.0	12.82	25.0	25.15
	2.5	1.5	12	1.01	7	≤ 0.1	9.1	10.65	13.5	19.04
9	2.5	1.5	12	1.01	10	≤ 0.1	6.9	8.63	11.5	15.73
	2.5	1.5	12	1.01	7	≤ 0.1	9.1	10.65	13.5	19.04
10	2.5	1.8	12	1.01	7	0.1–0.5	4.2	7.51	16.0	15.80
11	2.5	2.0	12	1.01	7	0.5–1	0.5	4.49	19.0	12.45

Another important parameter that affects the dynamic phosphate adsorption process in a fixed-bed column is the pH solution. Figure 4.2d shows the effect of phosphate solution

pH (4, 7, and 10) on phosphate adsorption breakthrough curves while maintaining a constant bed height (1.5 cm), flow rate (2.5 mL/min), and influent phosphate concentration (12 mg-P/L). It can be seen clearly that the breakthrough time was reached in a longer time at a lower pH. The breakthrough time increased from 6.9 to 10.0 h with decreasing pH from 10 to 4. As shown in Table 4.1, a higher amount of adsorbed phosphate (25.15 mg-P/g) was obtained at a lower pH (acidic solution). The adsorbed phosphate decreased significantly when the influent pH increased from 4 to 10, signifying that pH played a key role that affected the physical-chemical interaction between the phosphate and composite surface. The adsorbent surface was positively charged at low pH, attracting the negatively charged phosphate anions. Conversely, the number of hydroxyl ions (OH^-) increased at higher pH, which competed with phosphate anions to occupy more active binding sites on the adsorbent surface and led to the reduction of phosphate adsorption onto the composite surface [18]. The lower pH showed a broader tailing edge in the breakthrough curve shape, reflecting that the phosphate adsorption onto the composite bed in lower pH was extended with slow adsorption.

The effect of composite particle size on the breakthrough curve of phosphate adsorption was investigated by isolating the composite into three groups of particle sizes using sieves with apertures of different sizes (≤ 0.1 mm, 0.1–0.5 mm, and 0.5–1.0 mm). The bed height (1.5 cm), flow rate (2.5 mL/min), and influent phosphate concentration (12 mg-P/L) were kept constant. Figure 4.2e shows the breakthrough curves of phosphate adsorption resulting from different composite particle sizes. The bed performance of the smallest particle size (≤ 0.1 mm) was better than that of the larger particle sizes, particularly for the initial part of the curve. The reduction in particle size led to a longer breakthrough time but a shorter exhaustion time. As the particle size of the composite increased, the surface area per unit volume decreased. Consequently, the number of active binding sites on the surface that directly interact with the phosphate ions in the solution, smaller than the composite with smaller particle size, resulted in an earlier breakthrough time corresponding to the completion of surface adsorption. However, after the breakthrough point was achieved in the large particle composite, the pore adsorption continued at a lower rate, which resulted in a delayed exhaustion time. Additionally, for smaller particle sizes with a higher surface area [19], phosphate adsorption mostly occurred on the surface of the composite with a large number of exposed active binding sites. A decrease in particle size appears to have increased the sharpness of the breakthrough curves and delayed the breakthrough time.

Table 4.2 summarizes the equilibrium phosphate adsorption capacity of am-Zr/MgFe-LDH in this study and calcined MgFe-LDH as well as other Zr-based adsorbents in fixed-bed

column adsorption. It was demonstrated that am-Zr/MgFe-LDH was found to have higher equilibrium adsorption capacity than calcined MgFe-LDH and positively comparable to most of the Zr-based adsorbents reported in the literature. This result confirmed that the combination of am-Zr and MgFe-LDH resulted in favorable modification in the adsorbent surface for effective phosphate adsorption. The high equilibrium phosphate adsorption capacity of am-Zr/MgFe-LDH can be associated with the development of a high amount of hydroxyl groups in the adsorbent surface by am-Zr, where the hydroxyl groups act as the effective binding sites for phosphate anions.

Table 4.2 – Comparison of the equilibrium phosphate adsorption capacity of am-Zr/MgFe-LDH with various adsorbents in a fixed-bed column.

Adsorbent	Experimental condition					q_e (mg-P/g)	Reference
	Q (mL/min)	h (cm)	C_o (mg-P/L)	pH	d (mm)		
Zr-FPS	1.77	1.6	0.411	2.01	-	1.73	[20]
Zirconium ferrite	0.083	-	20	7	0.7	2.6	[21]
A-Zr-NP	6	4.8	20	5.4	-	5.59	[22]
Zr-loaded SOW gel	0.083	-	20	7	0.075–0.15	10	[21]
Zr-loaded okara	12	9	5.5	7.6	0.3–0.15	14.97	[15]
Zr-loaded okara	12	23	5.6	3	1–0.6	16.43	[15]
Calcined MgFe-LDH	0.4	12	20	-	0.075–0.028	21.09	[10]
CS-Zr-PEPA	6	12	2.4	6.5	-	32.50	[23]
Am-Zr/MgFe-LDH	2.5	1.5	12	4	≤ 0.1	25.15	Present study
Am-Zr/MgFe-LDH	2.5	1.5	12	7	≤ 0.1	19.04	Present study

4.3.2 Breakthrough curve modelling

Generally, the modelling of breakthrough curves resulting from fixed-bed column adsorption is essential for designing a column adsorption system for practical applications. To describe the behavior of dynamic phosphate adsorption onto the am-Zr/MgFe-LDH in a fixed-bed column system, three nonlinear mathematical models, Yoon-Nelson (Equation 4.5) [24], Thomas (Equation 4.6) [25], and MDR models (Equation 4.7) [26] were used.

$$\ln\left(\frac{C}{C_o - C}\right) = k_{YN}t - \tau k_{YN} \quad (4.5)$$

$$\ln\left(\frac{C_o}{C} - 1\right) = \frac{k_{Th}q_{Th}m}{Q} - k_{Th}C_o t \quad (4.6)$$

$$\ln\left(\frac{C}{C_o - C}\right) = a \ln\left(\frac{C_o Q t}{1000}\right) - a \ln q_{mdr} m \quad (4.7)$$

where, k_{Th} and k_{YN} are the Thomas kinetic coefficient (L/mg min) and the Yoon-Nelson kinetic coefficient (1/min), respectively, q_{Th} and q_{mdr} are the predicted adsorption capacities (mg/g), τ is the time required for 50% phosphate adsorption breakthrough (min), and a is an MDR model parameter.

The main parameters of each mathematical model obtained by nonlinear fitting of the breakthrough data under different experimental conditions are presented in Table 4.3. A simple Yoon-Nelson model was applied to examine the phosphate adsorption behavior of the packed composite. This model assumes that the decrease in the adsorption probability of each molecule is proportional to the adsorption probability of the molecule and the probability of molecule breakthrough on the adsorbent [27]. Although this model is based on the adsorption probability, the R^2 (0.864–0.984) values showed a good fit with the experimental data. Additionally, the predicted values of τ were similar to those obtained from experiments (Table 4.1), except for d values of 0.1–0.5 and 0.5–1.0 mm, where the breakthrough curves deviated from the ideal adsorption system with an S-shaped profile characteristic. The τ values decreased with increasing flow rate, influent phosphate concentration, pH, and adsorbent particle size, and by reducing the bed height. Conversely, the k_{YN} values indicated opposite trends in τ values. For instance, increasing the flow rate or decreasing the bed height resulted in an increase in phosphate ions passing the packed adsorbent for a given period of time. Consequently, k_{YN} increased and τ decreased.

Table 4.3 – Yoon-Nelson, Thomas, and MDR model parameters for phosphate adsorption by am-Zr/MgFe-LDH in a fixed-bed column at various experimental conditions.

Experimental conditions No.	Yoon-Nelson			Thomas			MDR		
	k_{YN} ($\times 10^{-2}$)	τ	R^2	k_{Th} ($\times 10^{-3}$)	q_{Th}	R^2	q_{mdr}	a	R^2
1	0.96	17.33	0.958	0.76	19.91	0.958	19.94	8.157	0.966
2	1.59	10.65	0.962	1.29	19.02	0.962	19.01	8.583	0.969
3	1.92	7.19	0.984	1.55	18.44	0.984	18.31	7.796	0.990
4	1.82	7.11	0.961	1.01	19.10	0.972	18.79	4.845	0.985
5	0.95	14.48	0.960	0.76	19.49	0.960	19.45	6.987	0.970
6	0.70	22.28	0.974	1.33	17.16	0.974	17.10	8.693	0.981
7	2.19	6.21	0.968	0.81	19.05	0.964	19.05	6.980	0.975
8	0.81	12.83	0.916	0.48	24.67	0.926	24.66	4.418	0.953
9	1.89	8.40	0.974	1.16	15.84	0.978	15.73	6.840	0.986
10	0.52	8.66	0.943	0.42	15.61	0.943	15.33	2.516	0.985
11	0.25	5.78	0.864	0.21	10.21	0.864	10.80	1.370	0.931

The Thomas and MDR models were also applied to the experimental phosphate adsorption curves to depict the entire breakthrough curve. The Thomas model is based on

the assumption that adsorption is only controlled by the surface reaction between the adsorbate and adsorbent surface, where the effects of intra-particle diffusion and external film resistances are neglected [28]. The MDR model was developed based on mathematical issues to reduce the error resulting from the Thomas model [29]. The values of predicted q_{Th} and q_{mdr} were close to the experimental q values (percentage errors < 3%), except for d values of 0.5–1.0 mm. Additionally, their trends in response to various experimental conditions were similar to those of the experimental q . However, the Thomas model was not completely fit with the experimental curves as the phosphate adsorption on the am-Zr/MgFe-LDH involved intra-particle diffusion as the rate-limiting step. The slow intra-particle diffusion of phosphate on the composite pores was signified by the considerably slow adsorption from the C/C_0 ratio of 0.85 to reach 1 [30]. As can be seen from Table 4.3, the MDR model showed larger R^2 values than those of the Yoon-Nelson and Thomas models for all experimental conditions. This indicates that the phosphate adsorption behavior of the packed am-Zr/MgFe-LDH in a fixed-bed column system was better described by the MDR model in each experimental condition. As the MDR model based on the Thomas model, the results suggest that adsorption follows the Langmuir isotherm, which suggests that the driving forces obey second-order reversible reaction kinetics with no axial dispersion in the column [29].

4.3.3 Phosphate adsorption from real municipal anaerobic sludge filtrate and synthetic seawater

The anaerobic sludge used in this study was collected from an eastern municipal wastewater treatment plant in Ube, Japan. Before use in the column adsorption test, the sludge was allowed to stand for 24 h for deposition, and the supernatant was filtered using a 0.45 μm filter membrane. The effect of seawater ions on phosphate adsorption in seawater was also investigated using synthetic phosphate-containing seawater (P seawater). As 99% of the seawater electrolyte concentration consists of NaCl, Na_2SO_4 , KCl, MgCl_2 , and CaCl_2 , synthetic seawater was prepared using these salts, corresponding to a salinity of 15 PSU [31]. The 15 PSU salinity was chosen to represent the salinity of the mesohaline estuary (salinity ranges from 5 to 18 PSU), an area that has great potential to be eutrophic and needs attention [32]. For comparison, phosphate adsorption was also conducted in synthetic phosphate-containing water (P water). The details of the sludge, synthetic P seawater, and P water are listed in Table 4.4. In this experiment, an adsorbent particle size range of 0.1–0.5 mm was used to prevent column clogging by extremely small particles present in the

sludge filtrate. Each water sample was pumped through the 1.0 g of adsorbent column at flow rate of 2.5 mL/min.

Table 4.4 – The details of anaerobic sludge filtrate, synthetic P water, and synthetic P seawater used in fixed-bed column phosphate adsorption.

Anaerobic sludge filtrate		Synthetic P seawater		Synthetic P water	
Parameter	Value	Parameter	Value	Parameter	Value
pH	8.5	pH	8.1	pH	8.5
Phosphate (PO ₄ -P)	14.2 mg/L	Phosphate (PO ₄ -P)	14.6 mg/L	Phosphate (PO ₄ -P)	14.2 mg/L
TSS	169 mg/L	NaCl	10519 mg/L		
COD	400 mg/L	MgCl ₂	2095 mg/L		
Chloride (Cl ⁻)	575 mg/L	Na ₂ SO ₄	1705 mg/L		
Nitrate (NO ₃ ⁻ -N)	14.6 mg/L	CaCl ₂	488.31 mg/L		
Alkalinity (CaCO ₃)	110 mg/L	KCl	298.21 mg/L		

Figure 4.3 shows a comparison of the breakthrough curves for phosphate adsorption onto the composite-packed column using real anaerobic sludge filtrate, synthetic P water, and seawater. The earlier breakthrough of phosphate adsorption in anaerobic sludge might be due to the high concentration of carbonate (CO₃²⁻), which is signified by high alkalinity (Table 4.4). In the previous study, it was found that CO₃²⁻ (or bicarbonate) was highly competitive with phosphate for the active binding sites on the adsorption surface [11]. Furthermore, the presence of extremely fine suspended solids that passed through the filter during filtration in the filtrate could interfere with the transfer of phosphate from the bulk liquid to the am-Zr/MgFe-LDH surface [10]. The equilibrium adsorption capacity in the sludge filtrate (8.99 mg-P/L) was lower than that in synthetic P water (13.12 mg-P/L). However, phosphate adsorption was not negatively affected by the seawater ions but was enhanced after the breakthrough point passed. The equilibrium adsorption capacity in synthetic P seawater was 19.99 mg-P/L. The positively charged seawater ions (such as Na⁺, Mg²⁺, Ca²⁺, and K⁺) in the solution were easily attracted by an adsorbent surface that became more negatively charged after initial phosphate adsorption. This increased positive charge on the adsorbent surface and promoted subsequent phosphate adsorption. According to the results, the equilibrium adsorption capacity of composite reduced due to the highly carbonated wastewater in the continuous adsorption system. However, it exhibited more favorable phosphate adsorption in synthetic seawater.

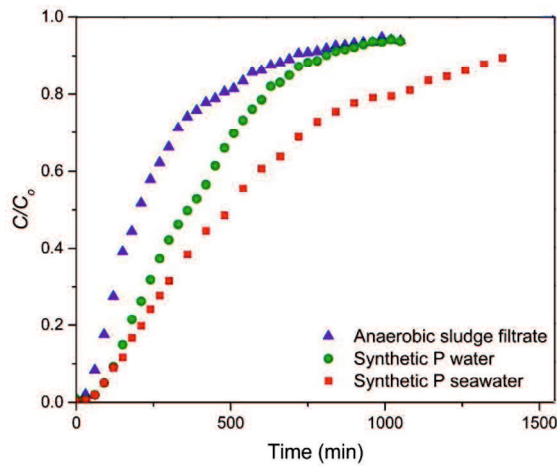


Figure 4.3 – Breakthrough curves for phosphate adsorption from anaerobic sludge filtrate, synthetic P water, and synthetic P seawater ($m = 1.01$ g, $Q = 2.5$ mL/min, $d = 0.1$ - 0.5 mm).

4.3.4 Column regeneration and reusability

The effectiveness of the adsorbent for practical applications depends on the equilibrium adsorption capacity and efficiency of adsorbent regeneration and reusability. However, the reuse of an adsorbent requires a desorption agent to desorb phosphate from the adsorbent for regeneration. To ensure that the adsorbent was saturated with phosphate before the regeneration study, a phosphate solution ($C_0 = 12$ mg-P/L, $\text{pH} = 7$) was pumped ($Q = 2.5$ mL/min) to the column ($h = 1.5$ cm, $d \leq 0.1$ mm) for 24 h. The exhausted composite was regenerated with 0.1 N NaOH at a flow rate of 2.5 mL/min. The effluent phosphate concentrations in a continuous desorption curve of phosphate at particular time points were determined and are shown in Figure 4.4.

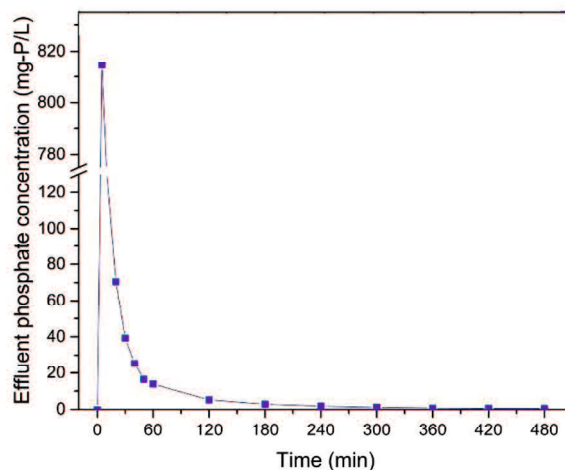


Figure 4.4 – Continuous phosphate desorption curve on am-Zr/MgFe-LDH column by 0.1 N NaOH ($h = 1.5$ cm and $Q = 2.5$ mL/min).

The desorption curve was an asymmetrically shaped curve with significantly high desorption at the beginning, followed by a flattened decline. The regeneration study was conducted for 8 h when the effluent concentration was 0.51 mg-P/L. Figure 4.4 shows that the maximum phosphate concentration was obtained within 5–10 min, indicating that the majority of the phosphate amount desorbed during this period. The flattened curve was observed after one-hour desorption, indicating that almost complete desorption was achieved after 1 h with a desorption efficiency ($100 \% \times q_{desorbed}/q_{adsorbed}$) of 91.7% and an effluent concentration of 13.82 mg-P/L. However, a total regeneration of 98.8% was achieved after an eight-hour operation.

The regenerated column was reused for subsequent adsorption to assess the reusability of the column, and its breakthrough curves and regeneration equilibrium adsorption capacity after eight adsorption-desorption cycles are shown in Figure 4.5. A significant decrease in the equilibrium adsorption capacity ($\sim 8.0\%$) was observed in the second cycle, as depicted by the earlier breakthrough point after the first cycle (Figure 4.5a). These breakthrough points appeared to shift slowly to an earlier time, signifying a slow decrease in the equilibrium adsorption capacity after the second cycle (Figure 4.5b). The gradual decrease in adsorption performance is attributed to the loss of active binding sites from the previous adsorption process, particularly in the first cycle, by strongly attached phosphate, which is difficult to desorb. The decrease in the equilibrium adsorption capacity from the first to the eighth cycle was approximately 17%, indicating that the composite may be suitable for practical applications.

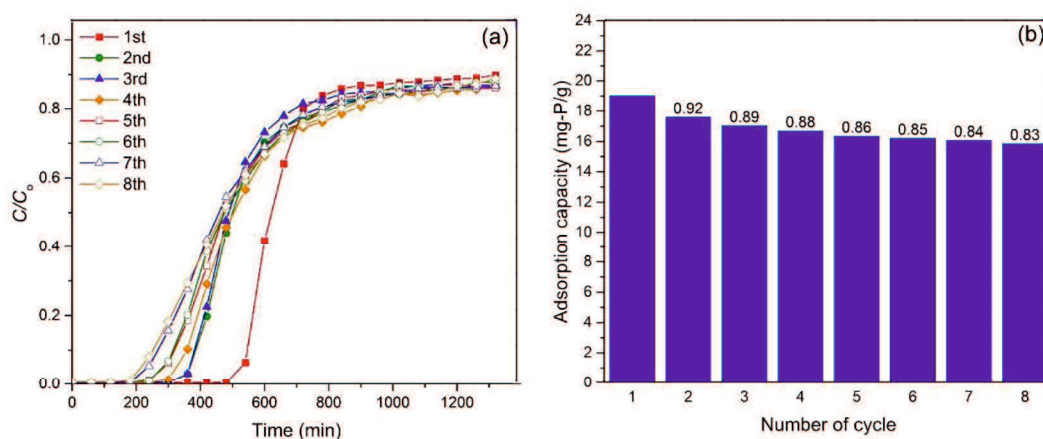


Figure 4.5 – Column reusability study: (a) phosphate adsorption breakthrough curve on am-Zr/MgFe-LDH for each consecutive eight adsorption-desorption cycles at a flow rate 2.5 mL/min, and (b) equilibrium adsorption capacity of column calculated for each adsorption cycle (the numbers above the bar are adsorption retain ratio of equilibrium phosphate adsorption capacity).

4.4 Summary

This study involves the application of a synthesized am-Zr/MgFe-LDH as a phosphate sorbent in a continuous fixed-bed column system, as well as the investigation of the feasibility of its reusability using NaOH solution in the regeneration process. The results of the column experiments showed that the equilibrium phosphate adsorption capacity of the composite was affected by the flow rate, bed height, influent phosphate concentration, influent pH, and composite particle size. The increase in the flow rate, pH, and adsorbent particle size, decreased the amount of adsorbed phosphate onto the composite. Contrarily, the adsorbed phosphate onto the composite increased with increasing bed height and influent phosphate concentration in the fixed-bed column system. The highest equilibrium adsorption capacity of 25.15 mg-P/L was obtained when the influent pH was 4, indicating that the adsorption of phosphate onto the composite surface is favorable in acidic. From the nonlinear fitting of the breakthrough data, the MDR model was found to be the best model for predicting the experimental phosphate adsorption behavior of a packed composite in a fixed-bed column system, as compared to the Yoon-Nelson and Thomas models. The amount of adsorbed phosphate on the composite decreased when it was used in wastewater with a high (bi)carbonate concentration. However, it exhibited more effective phosphate adsorption in synthetic seawater. The column regeneration studies revealed that 91.7 % of adsorbed phosphorus was desorbed during the one-hour desorption, and 83% of the fresh composite adsorption ability could be retained even after eight adsorption-desorption cycles. The am-Zr/MgFe-DH has the potential to be utilized as an adsorbent for phosphorus removal from aqueous solutions as it has high equilibrium phosphate adsorption capacity and reusability. Although this study provides helpful information for the design of a practical system for phosphorus removal and recovery, some considerations should be taken to improve the performance of the composite adsorption system in future work. First, the application of economical pretreatment to reduce (bi)carbonate from wastewater before process, such as chemical precipitation, since (bi)carbonate is the most competitive anion for phosphate adsorption onto the composite. Second, the use of adsorption byproduct to create an economic adsorption system, such as the processing of desorbed phosphorus in the regeneration process to a valuable product like hydroxyapatite, or the application of saturated composite as the slow-release phosphate fertilizer.

Acknowledgements

The first author expresses his gratitude to the support of the Indonesian Ministry of Research, Technology, and Higher Education (RISTEK-DIKTI), as well as the Project Implementation Unit (PIU) of the Islamic Development Bank (IsDB) 4in1 Project of Mulawarman University for providing the scholarship.

References

- [1] S. Dash, S.S. Borah, A.S. Kalamdhad, Study of the limnology of wetlands through a one-dimensional model for assessing the eutrophication levels induced by various pollution sources, *Ecol. Modell.* 416 (2020) 108907. <https://doi.org/https://doi.org/10.1016/j.ecolmodel.2019.108907>.
- [2] M.D. March, L. Toma, A.W. Stott, D.J. Roberts, Modelling phosphorus efficiency within diverse dairy farming systems – pollutant and non-renewable resource?, *Ecol. Indic.* 69 (2016) 667–676. <https://doi.org/https://doi.org/10.1016/j.ecolind.2016.05.022>.
- [3] X. Wang, J. Miao, S. You, N. Ren, Statistical entropy analysis as a proxy method for quantitative evaluation of phosphorus of a food-based bioethanol system, *Resour. Conserv. Recycl.* 164 (2021) 105125. <https://doi.org/https://doi.org/10.1016/j.resconrec.2020.105125>.
- [4] S.K. Ramasahayam, L. Guzman, G. Gunawan, T. Viswanathan, A Comprehensive Review of Phosphorus Removal Technologies and Processes, *J. Macromol. Sci. Part A.* 51 (2014) 538–545. <https://doi.org/10.1080/10601325.2014.906271>.
- [5] Y. Zou, R. Zhang, L. Wang, K. Xue, J. Chen, Strong adsorption of phosphate from aqueous solution by zirconium-loaded Ca-montmorillonite, *Appl. Clay Sci.* 192 (2020) 105638. <https://doi.org/https://doi.org/10.1016/j.clay.2020.105638>.
- [6] P.S. Kumar, L. Korving, M.C.M. van Loosdrecht, G.J. Witkamp, Adsorption as a technology to achieve ultra-low concentrations of phosphate: Research gaps and economic analysis, *Water Res.* X. 4 (2019) 100029. <https://doi.org/10.1016/j.wroa.2019.100029>.
- [7] A.L. Taka, M.J. Klink, X.Y. Mbianda, E.B. Naidoo, Chitosan Nanocomposites for Water Treatment by Fixed-Bed Continuous Flow Column Adsorption: A Review, *Carbohydr. Polym.* (2020) 117398. <https://doi.org/https://doi.org/10.1016/j.carbpol.2020.117398>.

- [8] D. Jiang, B. Chu, Y. Amano, M. Machida, Removal and recovery of phosphate from water by Mg-laden biochar: Batch and column studies, *Colloids Surfaces A Physicochem. Eng. Asp.* 558 (2018) 429–437. <https://doi.org/https://doi.org/10.1016/j.colsurfa.2018.09.016>.
- [9] R. Kumar, D. Bhatia, R. Singh, S. Rani, N.R. Bishnoi, Sorption of heavy metals from electroplating effluent using immobilized biomass *Trichoderma viride* in a continuous packed-bed column, *Int. Biodeterior. Biodegradation.* 65 (2011) 1133–1139. <https://doi.org/https://doi.org/10.1016/j.ibiod.2011.09.003>.
- [10] X. Sun, T. Imai, M. Sekine, T. Higuchi, K. Yamamoto, A. Kanno, S. Nakazono, Adsorption of phosphate using calcined Mg₃–Fe layered double hydroxides in a fixed-bed column study, *J. Ind. Eng. Chem.* 20 (2014) 3623–3630. <https://doi.org/https://doi.org/10.1016/j.jiec.2013.12.057>.
- [11] A. Nuryadin, T. Imai, A. Kanno, K. Yamamoto, M. Sekine, T. Higuchi, Phosphate adsorption and desorption on two-stage synthesized amorphous-ZrO₂/Mg–Fe layered double hydroxide composite, *Mater. Chem. Phys.* 266 (2021) 124559. <https://doi.org/10.1016/j.matchemphys.2021.124559>.
- [12] K. Bourikas, J. Vakros, C. Kordulis, A. Lycourghiotis, Potentiometric Mass Titrations: Experimental and Theoretical Establishment of a New Technique for Determining the Point of Zero Charge (PZC) of Metal (Hydr)Oxides, *J. Phys. Chem. B.* 107 (2003) 9441–9451. <https://doi.org/10.1021/jp035123v>.
- [13] M.H. Marzbali, M. Esmaili, Fixed bed adsorption of tetracycline on a mesoporous activated carbon: Experimental study and neuro-fuzzy modeling, *J. Appl. Res. Technol.* 15 (2017) 454–463. <https://doi.org/https://doi.org/10.1016/j.jart.2017.05.003>.
- [14] R. Gouran-Orimi, B. Mirzayi, A. Nematollahzadeh, A. Tardast, Competitive adsorption of nitrate in fixed-bed column packed with bio-inspired polydopamine coated zeolite, *J. Environ. Chem. Eng.* 6 (2018) 2232–2240. <https://doi.org/https://doi.org/10.1016/j.jece.2018.01.049>.
- [15] T.A.H. Nguyen, H.H. Ngo, W.S. Guo, T.Q. Pham, F.M. Li, T. V Nguyen, X.T. Bui, Adsorption of phosphate from aqueous solutions and sewage using zirconium loaded okara (ZLO): Fixed-bed column study, *Sci. Total Environ.* 523 (2015) 40–49. <https://doi.org/https://doi.org/10.1016/j.scitotenv.2015.03.126>.
- [16] R. Mohan, R.K. Dutta, Continuous fixed-bed column assessment for defluoridation of water using HAp-coated-limestone, *J. Environ. Chem. Eng.* 8 (2020) 103840. <https://doi.org/https://doi.org/10.1016/j.jece.2020.103840>.

- [17] S.Y. Lee, J.-W. Choi, K.G. Song, K. Choi, Y.J. Lee, K.-W. Jung, Adsorption and mechanistic study for phosphate removal by rice husk-derived biochar functionalized with Mg/Al-calcined layered double hydroxides via co-pyrolysis, *Compos. Part B Eng.* 176 (2019) 107209. <https://doi.org/https://doi.org/10.1016/j.compositesb.2019.107209>.
- [18] Y. He, H. Lin, Y. Dong, Q. Liu, L. Wang, Simultaneous removal of phosphate and ammonium using salt-thermal-activated and lanthanum-doped zeolite: fixed-bed column and mechanism study, *Desalin. Water Treat.* 57 (2016) 27279–27293. <https://doi.org/10.1080/19443994.2016.1166459>.
- [19] E. Oguz, Fixed-bed column studies on the removal of Fe³⁺ and neural network modelling, *Arab. J. Chem.* 10 (2017) 313–320. <https://doi.org/https://doi.org/10.1016/j.arabjc.2014.10.008>.
- [20] M.R. Awual, A. Jyo, T. Ihara, N. Seko, M. Tamada, K.T. Lim, Enhanced trace phosphate removal from water by zirconium(IV) loaded fibrous adsorbent, *Water Res.* 45 (2011) 4592–4600. <https://doi.org/10.1016/j.watres.2011.06.009>.
- [21] B.K. Biswas, K. Inoue, K.N. Ghimire, H. Harada, K. Ohto, H. Kawakita, Removal and recovery of phosphorus from water by means of adsorption onto orange waste gel loaded with zirconium, *Bioresour. Technol.* 99 (2008) 8685–8690. <https://doi.org/10.1016/j.biortech.2008.04.015>.
- [22] D.Z. Husein, T. Al-Radadi, E.Y. Danish, Adsorption of Phosphate Using Alginate-Zirconium-Grafted Newspaper Pellets: Fixed-Bed Column Study and Application, *Arab. J. Sci. Eng.* 42 (2017) 1399–1412. <https://doi.org/10.1007/s13369-016-2250-z>.
- [23] Z. Chen, H. Luo, H. Rong, Development of polyaminated chitosan-zirconium(IV) complex bead adsorbent for highly efficient removal and recovery of phosphorus in aqueous solutions, *Int. J. Biol. Macromol.* 164 (2020) 1183–1193. <https://doi.org/10.1016/j.ijbiomac.2020.07.218>.
- [24] Y.H.E.E. Yoon, J.H. Nelson, Application of Gas Adsorption Kinetics I. A Theoretical Model for Respirator Cartridge Service Life, *Am. Ind. Hyg. Assoc. J.* 45 (1984) 509–516. <https://doi.org/10.1080/15298668491400197>.
- [25] H.C. Thomas, Heterogeneous Ion Exchange in a Flowing System, *J. Am. Chem. Soc.* 66 (1944) 1664–1666. <https://doi.org/10.1021/ja01238a017>.
- [26] G. Yan, T. Viraraghavan, M. Chen, A New Model for Heavy Metal Removal in a Biosorption Column, *Adsorpt. Sci. Technol.* 19 (2001) 25–43. <https://doi.org/10.1260/0263617011493953>.

- [27] J.L. Sotelo, G. Ovejero, A. Rodríguez, S. Álvarez, J. García, Removal of Atenolol and Isoproturon in Aqueous Solutions by Adsorption in a Fixed-Bed Column, *Ind. Eng. Chem. Res.* 51 (2012) 5045–5055. <https://doi.org/10.1021/ie300334q>.
- [28] B.S. Chittoo, C. Sutherland, Column breakthrough studies for the removal and recovery of phosphate by lime-iron sludge: Modeling and optimization using artificial neural network and adaptive neuro-fuzzy inference system, *Chinese J. Chem. Eng.* 28 (2020) 1847–1859. <https://doi.org/https://doi.org/10.1016/j.cjche.2020.02.022>.
- [29] D. Sana, S. Jalila, A comparative study of adsorption and regeneration with different agricultural wastes as adsorbents for the removal of methylene blue from aqueous solution, *Chinese J. Chem. Eng.* 25 (2017) 1282–1287. <https://doi.org/https://doi.org/10.1016/j.cjche.2017.01.012>.
- [30] K.H. Chu, Improved fixed bed models for metal biosorption, *Chem. Eng. J.* 97 (2004) 233–239. [https://doi.org/10.1016/S1385-8947\(03\)00214-6](https://doi.org/10.1016/S1385-8947(03)00214-6).
- [31] H. Zhang, M. Elskens, G. Chen, C. Snoeck, L. Chou, Influence of seawater ions on phosphate adsorption at the surface of hydrous ferric oxide (HFO), *Sci. Total Environ.* 721 (2020) 137826. <https://doi.org/https://doi.org/10.1016/j.scitotenv.2020.137826>.
- [32] G.S. Brush, Historical Land Use, Nitrogen, and Coastal Eutrophication: A Paleocological Perspective, *Estuaries and Coasts.* 32 (2009) 18–28. <https://doi.org/10.1007/s12237-008-9106-z>.

CHAPTER 5

MECHANISM STUDY OF PHOSPHATE ADSORPTION AND DESORPTION ON AMORPHOUS ZIRCONIUM (HYDR)OXIDE/MgFe LAYERED DOUBLE HYDROXIDES COMPOSITE

5.1. Introduction

Adsorption has found various applications in many industries, especially in environmental technologies. One of the adsorption process applications in environmental protection is the separation of unwanted organic and inorganic pollutants from wastewater, including phosphorus removal [1]. Phosphorus has been known as the primary limiting nutrient in water bodies, and excessive discharge frequently leads to eutrophication problems [2]. Phosphorus eutrophication leads to algal blooms, anoxic events, altering biomass and species composition [3]. Therefore, it is crucial to develop efficient adsorbents with high surface areas and a high amount of active binding sites to improve the adsorption capacity, adsorption rate, and selectivity for decontaminating water from phosphorus.

In particular, previous works done by the authors exhibited that amorphous zirconium (hydr)oxide/MgFe layered double hydroxides composite (am-Zr/MgFe-LDH) has a high adsorption capacity towards phosphate anions in aqueous solution, both by batch and fixed-bed column tests [4,5]. However, to effectively utilize the composite as a phosphate adsorbent, the understanding of phosphate adsorption mechanisms by the composite is essential. Miyauchi *et al.* (2009) synthesized zirconium ion modified MgAl layered double hydroxides for phosphate adsorbent and suggested that the synthesized adsorbent were a nano-composite of binary MgAl layered double hydroxides and amorphous ZrO_2 [6]. They reported that the high phosphate adsorption capacity of the composite was due to the nano-size amorphous ZrO_2 , which has a large surface area. Chitrakar *et al.* (2010) reported that the presence of zirconium hydroxide particles on the LDH sheets greatly enhanced the phosphorus adsorption ability. However, to the best of the author's knowledge, an in-depth study about the mechanism of phosphorus adsorption by amorphous zirconium (hydr)oxide modified layered double hydroxides has not been done.

The applicability of am-Zr/MgFe-LDH depends not only on the adsorption ability but also on its reusability, while reusability is highly determined by the desorption during the regeneration process. Some previous studies indicated that a more effective phosphate desorption rate from LDH was achieved by NaOH solution than NaCl and $NaCO_3$ solution, as well as mixed solution of NaCl and NaOH [7,8]. The use of NaCl is not suitable for exchanging phosphate from exhausted LDH because of the low affinity of Cl^- with LDH, while the use of $NaCO_3$ can negatively affect the adsorption ability of phosphate since carbonate is a highly

competitive anion for phosphate adsorption [7]. A comprehensive understanding of the phosphate adsorption mechanism by am-Zr/MgFe-LDH is essential for the consideration of an appropriate reagent for composite regeneration.

In the present study, the possible adsorption mechanisms of phosphate by am-Zr/MgFe-LDH were carefully investigated by means of X-ray diffraction (XRD), Fourier transform infrared (FTIR), X-ray photoelectron spectroscopy (XPS), and pH at the point of zero charge (pH_{PZC}) analyses. The adsorption mechanisms were proposed for consideration in designing a practical system for the removal and recovery of phosphorus by am-Zr/MgFe-LDH. Moreover, the desorption mechanism of phosphate by NaOH solution was tried to explain at the molecular scale to gain a complete understanding of the release of phosphate from the composite surface.

5.2 Materials and methods

5.2.1 Materials

Synthesized amorphous zirconia/MgFe layered double hydroxide composite (am-Zr/MgFe-LDH) was prepared using two-stage synthesis with the combination of coprecipitation hydrothermal method as described in Chapter III. Before characterization, the size of composite particles was isolated by using a sieve with apertures size of $d \leq 0.1$ mm and kept in a desiccator. The phosphate-loaded samples were prepared by conducting batch adsorption. After 24 h adsorption in 10 mg-P L^{-1} of phosphate solution, the samples were separated by vacuum filtration and dried at 373 K for 24 h.

5.2.2 X-ray diffraction (XRD) analysis

The XRD spectra of the composite for the crystallinity analysis was recorded on a Rigaku Ultima IV Protectus diffractometer using Cu-K α radiation at 40 kV at a scanning rate of 1°min^{-1} in the 2θ angle range from 5° to 70° . The XRD patterns were analyzed by using Match! Software version 2.

5.2.3 Fourier transform infrared (FTIR) analysis

The FTIR spectra of the composites before and after adsorption were recorded on a Jasco FT/IR-4600 spectrophotometer. The spectra were recorded in the region of $4000\text{--}600 \text{ cm}^{-1}$.

5.2.4 X-ray photoelectron spectroscopy (XPS) analysis

The XPS spectra were obtained using a Thermo Scientific K-alpha X-ray photoelectron spectrometer. The experimental data were fitted with XPSPEAK41 and Origin 9.4 software for analysis. The high-resolution scans in this study focused on Mg, Fe, Zr, C, and O.

5.2.5 pH at the point of zero charge (pH_{pzc}) analysis

The pH at the point of zero charge (pH_{pzc}) of the composite was investigated using potentiometric mass titration (PMT), as described by Bourikas *et al.* (2003) [9]. Three different doses of the composite (5, 15, and 25 g/L) were immersed in Erlenmeyer flasks containing 100 mL of 0.03 M KNO_3 and shaken under an N_2 atmosphere at 200 rpm for 24 h. In each flask, 0.5 mL of 1 M KOH was added to deprotonate sites in the composite surface, and the shaken samples were titrated using a 0.1 M HNO_3 solution. The titration curve was constructed by plotting the pH value as a function of HNO_3 volume.

5.3 Results and discussion

5.3.1 FTIR spectra and XRD patterns analysis

The functional groups of the composite before and after adsorption were identified using FTIR spectroscopy, and the spectra are shown in Figure 5.1a. The intense and broadband centered at 3430 cm^{-1} and the band at 1640 cm^{-1} could be attributed to strong OH stretching and structural OH bending vibrations due to the presence of structural hydroxyl groups and physically adsorbed water molecules in the samples, respectively [10,11]. The bands of the Zr-OH bending vibration were observed at approximately 1353 cm^{-1} and 1565 cm^{-1} , and the band of CO_3^{2-} antisymmetric stretching in the interlayer was detected at 1358 cm^{-1} [12–14]. These bands were weakened after phosphate adsorption, indicating that phosphate anions were successfully adsorbed by replacing hydroxyl bonds and exchanging some carbonate anions in the LDH interlayer. In addition, phosphate adsorption in the composite was confirmed by the appearance of a new peak near 1057 cm^{-1} after the adsorption process, which could be attributed to the P=O bond [15].

Figure 5.1b shows a comparison between the XRD patterns of the composite, before and after phosphate adsorption. The patterns exhibited the presence of an LDH structure with a typical halo pattern of amorphous zirconium hydroxide. There was no significant change in the structure, and no additional characteristic peak was observed in the patterns after the adsorption process. However, the structure showed a lower crystallinity. The

decrease in crystallinity confirmed the occurrence of phosphate adsorption, which caused a disordered structure in the composite surface.

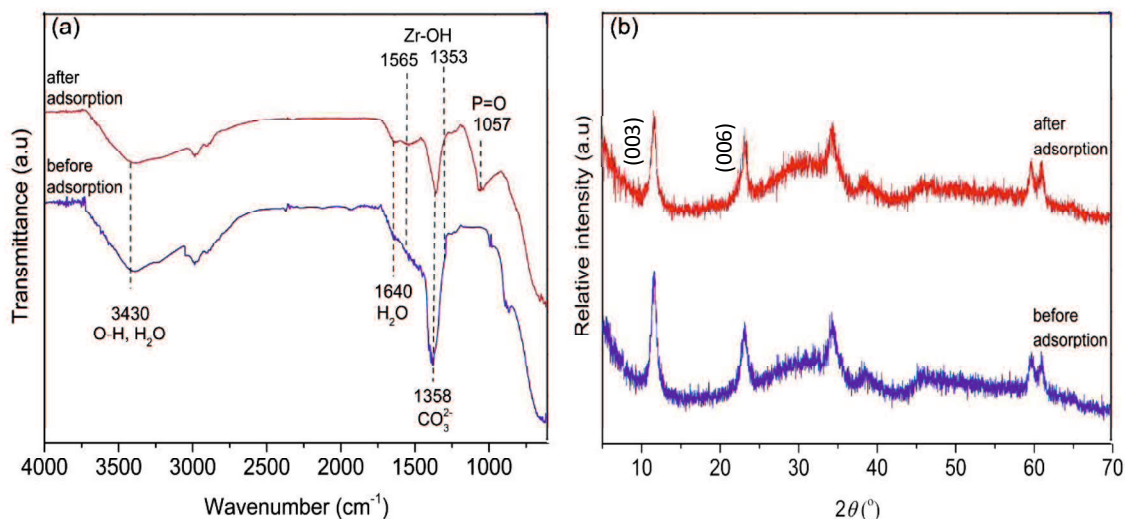


Figure 5.1 – (a) FTIR spectra and (b) XRD patterns of am-Zr/MgFe-LDH before and after adsorption.

5.3.2 XPS spectra analysis

The phosphate adsorption mechanism was further evaluated by deconvolution of the XPS spectra. The Mg 1s and Fe 2p spectra of am-Zr/MgFe-LDH are depicted in Figure 5.2a and Figure 5.2b, respectively. As illustrated in the figures, the Mg 1s and Fe 2p spectra peaks shifted to higher binding energies after phosphate adsorption by about 0.2 eV for Mg 1s, 0.4 eV for Fe 2p₁, and 0.2 eV for Fe 2p₃. This enhancement of binding energy values was caused by electron withdrawal from the negatively charged O atoms of the phosphate species to the valence band of Mg s₁ and Fe 2p and the formation of Mg-O-P and Fe-O-P through surface complexation [16,17]. This indicated that the surface of LDH in the composite was also involved in the phosphate adsorption process.

Figure 5.2c shows the Zr 3d spectra of am-Zr/MgFe-LDH. As presented in the figure, the two peaks centered at 181.85 eV and 184.20 eV were assigned to Zr-O-Zr bonds of Zr 3d_{5/2} and Zr 3d_{3/2} in the composite, respectively. The main peaks of Zr 3d were shifted to a higher binding energy of approximately 0.2 eV after phosphate adsorption, indicating that electron transfer occurred in the valence band, and Zr-O-P inner-sphere complexation was formed by substituting the hydroxyl groups of am-Zr [18]. This shift can also be attributed to the overlap from two new Zr-O-P peaks in higher binding energies (182.35 eV and 184.79 eV) formed through ligand exchange [19]. These indicated that phosphate was adsorbed chemically on the composite surface.

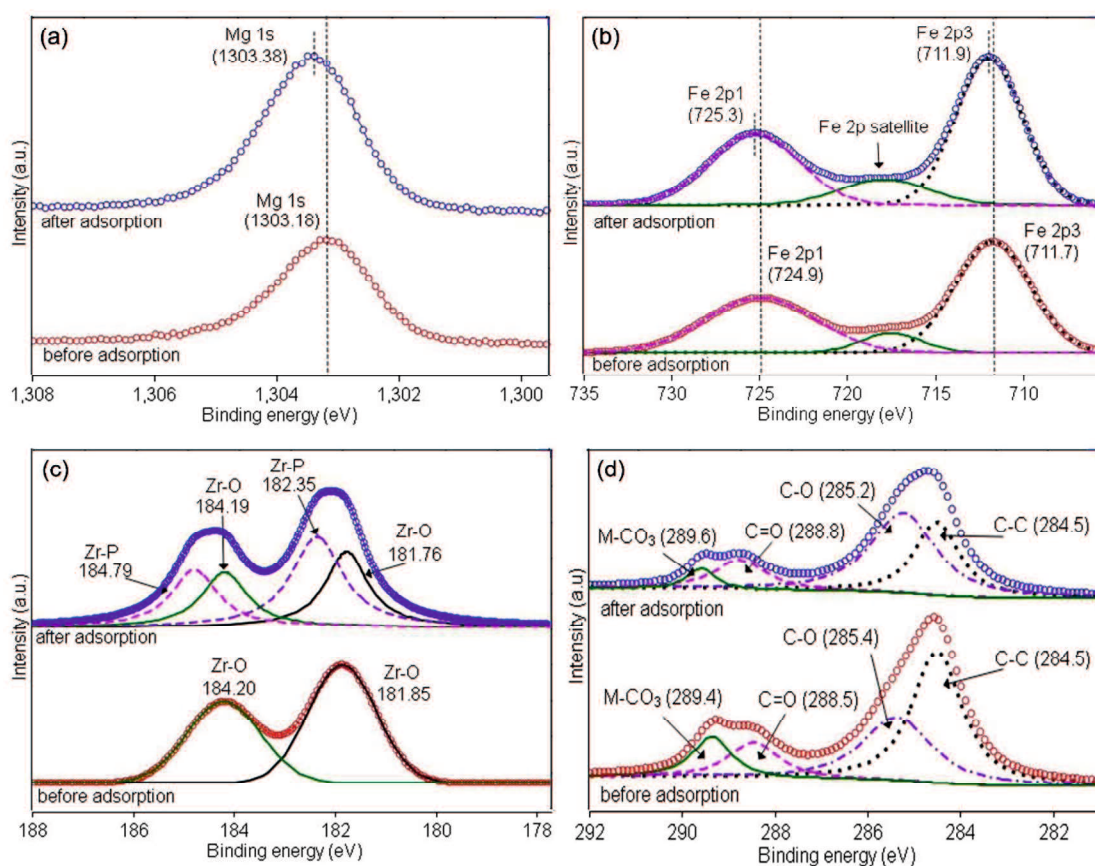


Figure 5.2 – XPS analysis of am-Zr/MgFe-LDH before and after phosphate adsorption: (a) Mg 1s, (b) Fe 2p, (c) Zr 3d, and (d) C 1s.

Figure 5.2d shows the C 1s spectra of the am-Zr/MgFe-LDH. As shown in the figure, the C 1s spectra can be divided into four different peaks: C-C (284.5 eV), C-O (285.2 eV), C=O (288.8 eV), and metal carbonate (M-CO₃) (289.6 eV) [20]. After phosphate adsorption, the relative area of the metal carbonate decreased from 14.7% to 5.2%. This signified that the carbonate in the LDH interlayer took part in the phosphate adsorption process via ion and ligand exchange.

5.3.3 pH_{pzc} analysis

As explained in Chapter III, the adsorption was high at low pH (particularly at pH 2 and 3) and decreased at higher pH (notably at pH 10) [4]. To explain this condition, the pH_{pzc} of the composite was investigated by PMT, and the plotted experimental curves are shown in Figure 5.3. The curves show an intersection point at a pH of approximately 9.7, which was identified as the pH_{pzc} of the composite. This indicates that the negatively charged

composite surface triggered a significant decrease in adsorption efficiency at pH 10 as the solution pH was higher than pH_{pzc} . This result suggests that the electrostatic bond also contributed to the phosphate adsorption mechanism between the composite surface and phosphate anions, particularly at pH values lower than 9.7.

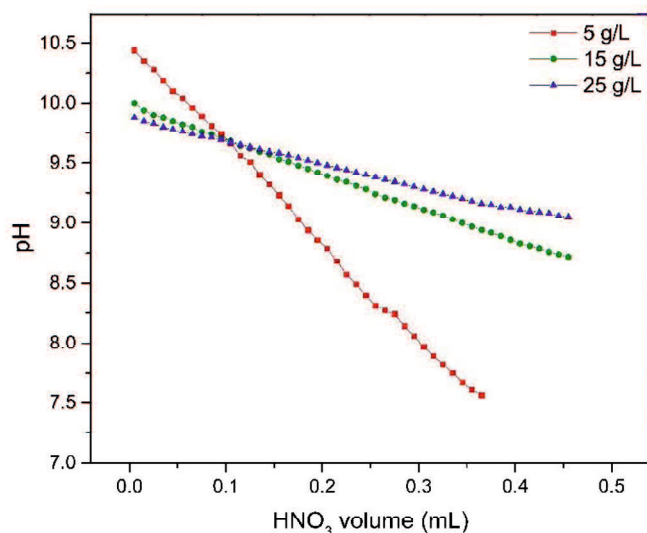


Figure 5.3 – Potentiometric mass titration curves of am-Zr/MgFe-LDH samples using 0.1 M HNO₃.

5.3.4 Proposed phosphate adsorption and desorption mechanisms

Based on the analysis of adsorption in varying pH solutions, FTIR spectra, XRD patterns, and XPS spectra, the potential adsorption mechanisms involved in the composite during the adsorption process were found to mainly consist of electrostatic attraction between the positively charged adsorbent surface and phosphate anions (particularly at low pH), inner-sphere complex formation between metal hydroxides and phosphate anions on the adsorbent surface, and exchange of carbonate anions in the LDH interlayer. The proposed phosphate-adsorption mechanism is illustrated in Figure 5.4. The presence of am-Zr on the surface of the LDH likely increased the adsorption capacity of the composite. The zirconium species, which is in amorphous form, have a massive number of hydroxyl groups as the active binding sites for the phosphate anions. As shown in Figure 3.2a, the introduction of am-Zr to the LDH lowered the crystallinity of LDH, indicating a high number of hydroxyl groups in the adsorbent surface as active binding sites for phosphate. Moreover, the crystallization of am-Zr on the LDH matrix was presumably suppressed during synthesis, leading to the formation of nanosized am-Zr [4], as confirmed by the SEM images in Figure 3.4c. The nanosized materials are preferable for adsorbents because they have a large surface area for adsorption sites. Therefore, we suggest that the high phosphate adsorption

of the composite is mainly associated with the presence of highly hydrated am-Zr collaborated with the ability of MgFe-LDH for adsorbing phosphate by anion exchange and surface adsorption.

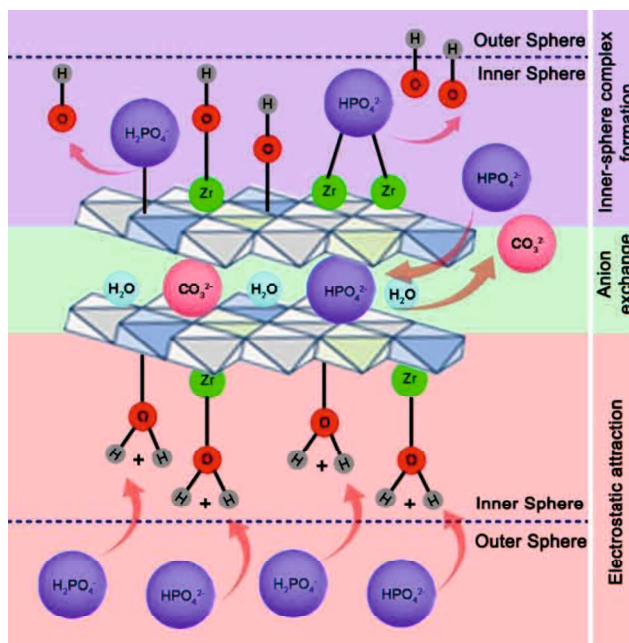


Figure 5.4 – Proposed mechanism of phosphate adsorption on am-Zr/MgFe-LDH.

In XRD patterns of LDH, the intercalation of phosphate anions into the LDH interlayer is characterized by the shift (003) reflection to a lower 2θ angle, which is corresponding to the enlargement of the basal distance d_{003} compared to the host LDH [21]. As shown in Figure 5.1b, no obvious displacement on the (003) diffraction plane was observed after the phosphate adsorption process suggesting that the anion exchange is not the main mechanism during the phosphate adsorption process. Most of the phosphate was adsorbed on the composite surface through surface adsorption, both electrostatic attraction and inner-sphere complexation than via anion exchange. This implies that the desorption process is better performed by stripping adsorbed phosphate on the adsorbent surface rather than exchanging phosphate intercalated in the LDH interlayer. Moreover, regenerating composite by NaCO_3 solution, to replace back phosphate anion in the LDH interlayer by carbonate anion, can negatively affect subsequent phosphate adsorption. As previously revealed that carbonate anion is the most competitive anion for phosphate adsorption onto the composite surface. On the other hand, the carbonate anion on the desorption solution makes it difficult to recover phosphorus as calcium phosphate because of the calcium carbonate formation [7].

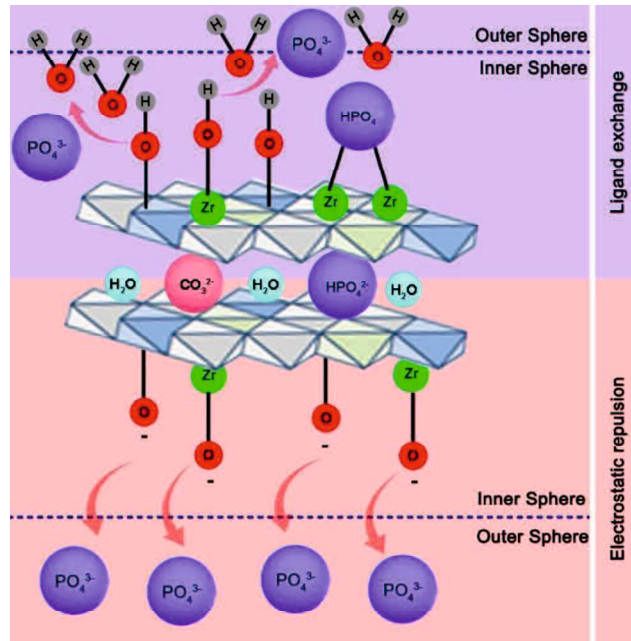
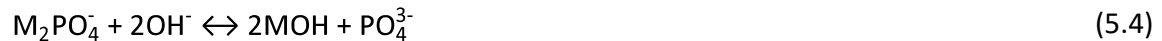


Figure 5.5 – Proposed mechanism of phosphate desorption from am-Zr/MgFe-LDH by NaOH solution.

Desorption of adsorbed phosphate from the composite by NaOH solution can be described as the reverse process of the phosphate uptake by surface adsorption as shown in Figure 5.5. High NaOH concentration and low phosphate concentration promote the phosphate desorption process by ligand exchange between adsorbed phosphate species and hydroxyl groups, which can be expressed as following reactions [22]:



where M stands for metal atom and OH is the hydroxyl group. Furthermore, high concentration of OH^- results in the deprotonation of hydroxyl groups in the composite surface which can be expressed as [22]:



This reaction causes a negatively charged composite surface, which then creates the repulsion of phosphate adsorbed by electrostatic attraction, and subsequently shields phosphate re-adsorption during desorption process. However, desorption experiment results showed that the phosphate adsorption process was not fully reversible. The loss of

efficiency might be attributed to the strongly bound phosphates with metal oxy-hydroxides on the composite surface, as well as to other interfering parameters, such as the partial destruction of adsorption sites during the regeneration process. Electrostatically bound phosphates are easier to desorb than inner-sphere complex bound phosphates. The irreversible phosphates mostly come from inner-sphere complex bound phosphates which are bound by bidentate ligands. Bidentate phosphates are strongly attached to the composite surface because they are chemically bound by two bonds, compared to monodentate phosphates that are attached by a single bond.

5.4 Summary

In this study, the possible mechanisms of phosphate adsorption onto am-Zr/MgFe-LDH were analyzed employing pH_{pzc} , FTIR, XRD, and XPS analyses, and the desorption mechanism of phosphate by NaOH solution was tried to elucidate. The results showed that electrostatic attraction, inner-sphere complexation, and anion exchange played an important role in phosphate adsorption. The high phosphate adsorption of the composite is primarily related to the introduction of highly hydrated am-Zr, cooperated with the ability of MgFe-LDH for adsorbing phosphate by anion exchange and surface adsorption. Phosphate desorption was focused on stripping adsorbed phosphate on the composite surface since most phosphates are adsorbed by surface adsorption. Therefore, the phosphate desorption mechanisms from the composite surface by NaOH solution were the reverse process of the phosphate uptake by surface adsorption, which were electrostatic repulsion and ligand exchange between adsorbed phosphates and hydroxyl groups. This study provides insights to assist in designing practical systems for removing and recovering phosphorus by using am-Zr/MgFe-LDH.

Acknowledgements

The first author expresses his gratitude to the support of the Indonesian Ministry of Research, Technology, and Higher Education (RISTEK-DIKTI), as well as the Project Implementation Unit (PIU) of the Islamic Development Bank (IsDB) 4in1 Project of Mulawarman University for providing the scholarship. The authors would also like to thank T. Suzuki for valuable assistance with FTIR analysis.

References

- [1] M. Wiśniewska, T. Urban, S. Chibowski, G. Fijałkowska, M. Medykowska, A. Nosal-Wiercińska, W. Franus, R. Panek, K. Szewczuk-Karpisz, Investigation of adsorption mechanism of phosphate(V) ions on the nanostructured Na-A zeolite surface

modified with ionic polyacrylamide with regard to their removal from aqueous solution, *Appl. Nanosci.* 10 (2020) 4475–4485. <https://doi.org/10.1007/s13204-020-01397-9>.

- [2] M. Le Moal, C. Gascuel-Oudou, A. Ménesguen, Y. Souchon, C. Étrillard, A. Levain, F. Moatar, A. Pannard, P. Souchu, A. Lefebvre, G. Pinay, Eutrophication: A new wine in an old bottle?, *Sci. Total Environ.* 651 (2019) 1–11. <https://doi.org/10.1016/j.scitotenv.2018.09.139>.
- [3] L. Ngatia, R. Taylor, Phosphorus Eutrophication and Mitigation Strategies, in: R.T.E.-T. Zhang (Ed.), *Phosphorus - Recover. Recycl.*, IntechOpen, Rijeka, 2019: p. Ch. 4. <https://doi.org/10.5772/intechopen.79173>.
- [4] A. Nuryadin, T. Imai, A. Kanno, K. Yamamoto, M. Sekine, T. Higuchi, Phosphate adsorption and desorption on two-stage synthesized amorphous-ZrO₂/Mg–Fe layered double hydroxide composite, *Mater. Chem. Phys.* 266 (2021) 124559. <https://doi.org/10.1016/j.matchemphys.2021.124559>.
- [5] A. Nuryadin, T. Imai, Application of amorphous zirconium (hydr)oxide/MgFe layered double hydroxides composite in fixed-bed column for phosphate removal from water, *Glob. J. Environ. Sci. Manag.* 7 (2021) 485–502. <https://doi.org/10.22034/GJESM.2021.04.01>.
- [6] H. Miyauchi, T. Yamamoto, R. Chitrakar, Y. Makita, Z. Wang, J. Kawai, T. Hirotsu, Phosphate adsorption site on zirconium ion modified MgAl-layered double hydroxides, *Top. Catal.* 52 (2009) 714–723. <https://doi.org/10.1007/s11244-009-9209-1>.
- [7] X. Cheng, X. Huang, X. Wang, B. Zhao, A. Chen, D. Sun, Phosphate adsorption from sewage sludge filtrate using zinc–aluminum layered double hydroxides, *J. Hazard. Mater.* 169 (2009) 958–964. <https://doi.org/10.1016/j.jhazmat.2009.04.052>.
- [8] X. Sun, T. Imai, M. Sekine, T. Higuchi, K. Yamamoto, K. Akagil, Adsorption of Phosphate by Calcinated Mg-Fe Layered Double Hydroxide, *J. Water Environ. Technol.* 11 (2013) 111–120. <https://doi.org/10.2965/jwet.2013.111>.
- [9] K. Bourikas, J. Vakros, C. Kordulis, A. Lycourghiotis, Potentiometric Mass Titrations: Experimental and Theoretical Establishment of a New Technique for Determining the Point of Zero Charge (PZC) of Metal (Hydr)Oxides, *J. Phys. Chem. B.* 107 (2003) 9441–9451. <https://doi.org/10.1021/jp035123v>.
- [10] Y. Su, H. Cui, Q. Li, S. Gao, J.K. Shang, Strong adsorption of phosphate by amorphous zirconium oxide nanoparticles, *Water Res.* 47 (2013) 5018–5026.

<https://doi.org/10.1016/j.watres.2013.05.044>.

- [11] N. Tang, T. He, J. Liu, L. Li, H. Shi, W. Cen, Z. Ye, New Insights into CO₂ Adsorption on Layered Double Hydroxide (LDH)-Based Nanomaterials, *Nanoscale Res. Lett.* 13 (2018). <https://doi.org/10.1186/s11671-018-2471-z>.
- [12] X. Dou, D. Mohan, C.U. Pittman, S. Yang, Remediating fluoride from water using hydrous zirconium oxide, *Chem. Eng. J.* 198–199 (2012) 236–245. <https://doi.org/10.1016/j.cej.2012.05.084>.
- [13] V.R. Magri, A. Duarte, G.F. Perotti, V.R.L. Constantino, Investigation of Thermal Behavior of Layered Double Hydroxides Intercalated with Carboxymethylcellulose Aiming Bio-Carbon Based Nanocomposites, *ChemEngineering.* 3 (2019) 55. <https://doi.org/10.3390/chemengineering3020055>.
- [14] Q. Zhang, Q. Du, T. Jiao, B. Pan, Z. Zhang, Q. Sun, S. Wang, T. Wang, F. Gao, Selective removal of phosphate in waters using a novel of cation adsorbent: Zirconium phosphate (ZrP) behavior and mechanism, *Chem. Eng. J.* 221 (2013) 315–321. <https://doi.org/10.1016/j.cej.2013.02.001>.
- [15] Z. Zha, Y. Ren, S. Wang, Z. Qian, L. Yang, P. Cheng, Y. Han, M. Wang, Phosphate adsorption onto thermally dehydrated aluminate cement granules, *RSC Adv.* 8 (2018) 19326–19334. <https://doi.org/10.1039/c8ra02474j>.
- [16] X. Hong, E. Zhu, Z. Ye, K.S. Hui, K.N. Hui, Enhanced phosphate removal under an electric field via multiple mechanisms on MgAl-LDHs/AC composite electrode, *J. Electroanal. Chem.* 836 (2019) 16–23. <https://doi.org/https://doi.org/10.1016/j.jelechem.2019.01.046>.
- [17] R. Liu, L. Chi, X. Wang, Y. Wang, Y. Sui, T. Xie, H. Arandiyani, Effective and selective adsorption of phosphate from aqueous solution via trivalent-metals-based amino-MIL-101 MOFs, *Chem. Eng. J.* 357 (2019) 159–168. <https://doi.org/https://doi.org/10.1016/j.cej.2018.09.122>.
- [18] L. Zhang, Z. Wang, X. Xu, C. Chen, B. Gao, X. Xiao, Insights into the phosphate adsorption behavior onto 3D self-assembled cellulose/graphene hybrid nanomaterials embedded with bimetallic hydroxides, *Sci. Total Environ.* 653 (2019) 897–907. <https://doi.org/https://doi.org/10.1016/j.scitotenv.2018.11.030>.
- [19] E. Zong, X. Liu, J. Jiang, S. Fu, F. Chu, Preparation and characterization of zirconia-loaded lignocellulosic butanol residue as a biosorbent for phosphate removal from aqueous solution, *Appl. Surf. Sci.* 387 (2016) 419–430. <https://doi.org/https://doi.org/10.1016/j.apsusc.2016.06.107>.

- [20] Y.T. Lai, Y.S. Huang, C.H. Chen, Y.C. Lin, H.T. Jeng, M.C. Chang, L.J. Chen, C.Y. Lee, P.C. Hsu, N.H. Tai, Green Treatment of Phosphate from Wastewater Using a Porous Bio-Templated Graphene Oxide/MgMn-Layered Double Hydroxide Composite, *IScience*. 23 (2020) 101065. <https://doi.org/10.1016/j.isci.2020.101065>.
- [21] C. Novillo, D. Guaya, A. Allen-Perkins Avendaño, C. Armijos, J.L. Cortina, I. Cota, Evaluation of phosphate removal capacity of Mg/Al layered double hydroxides from aqueous solutions, *Fuel*. 138 (2014) 72–79. <https://doi.org/https://doi.org/10.1016/j.fuel.2014.07.010>.
- [22] T. Guan, Y. Kuang, X. Li, J. Fang, W. Fang, D. Wu, The recovery of phosphorus from source-separated urine by repeatedly usable magnetic Fe₃O₄@ZrO₂ nanoparticles under acidic conditions, *Environ. Int.* 134 (2020) 105322. <https://doi.org/https://doi.org/10.1016/j.envint.2019.105322>.

CHAPTER 6

CONCLUSIONS AND FUTURE WORKS

6.1 Conclusions

The conclusions gathered from this study are as follows:

1. The composite of am-Zr/MgFe-LDH was successfully prepared, and the uncalcined composite with a Zr/Fe ratio of 1.5 had a higher phosphate adsorption capacity ($35.40 \text{ mg-P g}^{-1}$) than the uncalcined MgFe-LDH ($17.99 \text{ mg-P g}^{-1}$) and am-Zr ($32.00 \text{ mg-P g}^{-1}$).
2. The adsorption ability of the composite was considerably stable over a wide pH range that is suitable for practical application. However, this composite may not apply to wastewater that contains a high HCO_3^- concentration. The adsorption kinetics and isotherm of the composite were approved to follow the pseudo-second-order and Freundlich model, respectively. The adsorption thermodynamics showed that the phosphate adsorption was more feasible at high temperature, occurred spontaneously, and endothermic process.
3. The increased bed height and phosphate concentration; and reduced flow rate, pH, and adsorbent particle size in the fixed-bed column study were found to increase the column adsorption capacity. The optimum adsorption capacity of 25.15 mg-P/g was obtained at pH 4. The non-linear fitting of the breakthrough data showed that the MDR model was found to be the best model for predicting the experimental phosphate adsorption behavior as compared to the Yoon-Nelson and Thomas models.
4. The phosphate adsorption capacity of composite reduced when it was used in wastewater with a high (bi)carbonate concentration, the most competitive anion for phosphate adsorption on the composite surface. However, it exhibited more favorable phosphate adsorption in the coexistence of seawater ions.
5. The results of the reusability studies demonstrated that the composite could hold its removal efficiency at approximately 86% after eight cycles in batch test by reused 2 N NaOH and 83% after eight cycles in column desorption by 0.1 N NaOH, emphasizing the practicality and stability of the composite in adsorbent regeneration and phosphorus recovery processes.
6. Based on the analysis of adsorption in varying pH solutions, FTIR spectra, XRD patterns, and XPS spectra, the potential adsorption mechanisms involved in the composite during the adsorption process were found to mainly consist of electrostatic attraction between the positively charged adsorbent surface and phosphate anions (particularly at low pH), inner-sphere complex formation between metal hydroxides and phosphate anions on

the adsorbent surface, and exchange of carbonate anions in the LDH interlayer. On the other hand, the desorption of adsorbed phosphate from the composite by NaOH solution can be described as the reverse process of the phosphate uptake by surface adsorption.

6.2 Future works

Suggestions for future research topics concerning the application of am-Zr/MgFe-LDH for phosphate adsorption are listed below:

1. The application of economical pretreatment to reduce (bi)carbonate from wastewater before process, such as chemical precipitation, since (bi)carbonate is the most competitive anion for phosphate adsorption onto the composite.
2. The use of adsorption byproduct to create an economic adsorption system, such as the processing of desorbed phosphorus in the regeneration process to a valuable product like hydroxyapatite, or the application of saturated composite as a slow-release phosphate fertilizer.
3. Further study for the effective adsorbent dose for desorption using NaOH solution to effectively reduce desorption cost.

APPENDIX

LIST OF PUBLICATIONS

1. **Nuryadin A.** & Imai T. (2021). Application of amorphous zirconium (hydr)oxide/MgFe layered double hydroxides composite in fixed-bed column for phosphate removal from water. *Global Journal of Environmental Science and Management*, **7**(4), 485-502.
2. **Nuryadin A.**, Imai T., Kanno A., Yamamoto K., Sekine M., Higuchi T. (2021). Phosphate adsorption and desorption on two-stage synthesized amorphous-ZrO₂/Mg-Fe layered double hydroxide composite. *Material Chemistry and Physics*, **266**, 124559.

LIST OF PRESENTATIONS

1. **Nuryadin A.** & Imai T. The Application of Amorphous-ZrO₂/Mg-Fe Layered Double Hydroxide Composite in Phosphate Wastewater Treatment: Desorption, Reusability, and Phosphorus Recovery. *Water and Environment Technology Conference 2020-online*. Online Meeting. November 7-8, 2020. (Oral and poster presentation)
2. **Nuryadin A.** & Imai T. Study on the regeneration of amorphous-ZrO₂/Mg-Fe layered double hydroxide composite for phosphate adsorption by NaOH solution and phosphorus recovery from the regenerating solution. *The 17th Young Scientist Seminar "Establishment of International Research Network for Bioresources and Their Utilization"*. Online Meeting. December 28-29, 2020. (Oral presentation)
3. **Nuryadin A.** & Imai T. Synthesis of amorphous-ZrO₂/Mg-Fe layered double hydroxide (LDH) composite for phosphate adsorption. *The 16th Young Scientist Seminar "Establishment of International Research Network for Tropical Bioresources and Their Utilization"*. Yamaguchi Prefectural Seminar Park, Japan. October 12-13, 2019. (Oral presentation)
4. **Nuryadin A.** & Imai T. Amorphous-ZrO₂/Mg-Fe Layered Double Hydroxide Composite for Phosphate Adsorption. *Water and Environment Technology Conference 2019*. Osaka University, Japan. July 13-14, 2019. (Oral and poster presentation)
5. **Nuryadin A.** & Imai T. Study of Thermal Aging and Calcination Application on The Synthesis of Mg-Fe Layered Double Hydroxide for Phosphate Removal: Capacity and Kinetics of Adsorption. *The 5th International Symposium "Green and Smart*

Technologies for a Sustainable Society". Faculty of Engineering, Yamaguchi University. March 25-27, 2019. (Poster presentation)

6. **Nuryadin A.** & Imai T. The Effect of Thermal Treatment on the Phosphate Adsorption by Calcined Mg-Fe Layered Double Hydroxide. *The 15th Young Scientist Seminar "Establishment of International Research Network for Tropical Bioresources and Their Utilization"*. Yamaguchi Prefectural Seminar Park, Japan. November 13-14, 2018. (Oral presentation)